Preparation of Gold Nanoparticles and Their Surface Modification for Biomedical Applications

Jingchao Li

Doctoral Program in Materials Science and Engineering

Submitted to the Graduate School of

Pure and Applied Sciences

in Partial Fulfillment of the Requirements

for the Degree of Doctor of Philosophy in

Engineering

at the

University of Tsukuba

Content

List of abbreviations

1D	One dimension
2D	Two dimension
3D	Three dimension
AA	Ascorbic acid
AFM	Atomic force microscope
ALP	Alkaline phosphatase
ARS	Alizarin Red S
AuNPs	Gold nanoparticles
AuNSs	Gold nanostars
BSA	Bovine serum albumin
Calcein-AM	Calcein-acetoxymethyl
CEBPA	CCAAT/enhancer binding protein
CTAB	Cetyltrimethylammonium bromide
DAPI	4'-6-diamidino-2-phenylindole
DCFH-DA	2',7'-dichlorofluorescin diacetate
DLS	Dynamic light scattering
DMEM	Dulbecco's modified Eagle's Medium
DMSO	Dimethylsulfoxide
DNA	Deoxyribonucleic acid
ECM	Extracellular matrix
EDC	1-ethyl-3-[3-dimethylaminopropyl] carbodiimide hydrochloride
EMEM	Eagle's Minimun Essential Medium
FA	Folic acid
FABP4	Fatty acid binding protein 4
FASN	Fatty acid synthase
FBS	Fetal bovine serum
GAPDH	Glyceraldehyde 3-phosphate dehydrogenase
hMSCs	Human marrow-derived mesenchymal stem cells
IBSP	Bone sialoprotein 2
ICP-OES	Inductively Coupled Plasma-Optical Emission Spectroscopy
LPL	Lipoprotein lipase
MWCO	Molecular weight cut-off
NHS	N-hydroxysuccinimide

NIR	Near infrared
PBS	Phosphate buffered saline
PCR	Polymerase chain reaction
PDI	Polydispersity index
PEG	Poly(ethylene glycol)
PI	Propidium iodide
PPARG	Peroxisome proliferator-activated receptor gamma
PTT	Photothermal therapy
RGD	Arginine-glycine-aspartate
RNA	Ribonucleic acid
ROS	Reactive oxygen species
Runx2	Runt-related transcription factor 2
S.D.	Standard deviation
SPPI	Secreted phosphoprotein I
TEM	Transmission electron microscope
TGA	Thermal gravimetric analysis
UV-Vis	Ultraviolet-visible
YAP	Yes-associated protein

Chapter 1

General introduction

1.1 Nanomaterials

As the development of nanoscience and nanotechnology, many different kinds of nanoscale materials has emerged to meet the demands of research[1-3]. In general, nanomaterials are defined as the materials have a size between 1 and 100 nm in at least one dimension (1D). Nanomaterials usually have some unique physical and chemical properties that are significantly different from their bulk counterparts, such as small size, vast surface area and high surface atomic insufficiency[4]. The most commonly used nanomaterials include gold (Au) nanoparticles (NPs), iron oxide NPs, graphene, quantum dot, titanium dioxide NPs, silicon NPs and carbon nanotubes. All of them show great potentials in different fields, such as energy storage, sensors, catalyst, environmental monitoring and biomedical engineering.

1.2 Nanomaterials for biomedical applications

Most recently, one of the most important applications of nanomaterials is biomedicine[5]. The nanomaterials in biological systems potential to dramatically change the medical science and technology. Nanomaterials can be used for biomedical applications mainly because their advantages including small size, larger specific surface area, high surface atomic slot insufficiency and relatively low toxicity. Up to date, various nanomaterials have been developed for biomedical applications, such as liposome, micelle, AuNPs, iron oxide NPs, dendrimer, graphene, quantum dot, polymeric NPs and carbon nanotubes (Figure 1.1). Their applications for drug/gene/protein delivery[6-8], molecular imaging[9, 10], cancer therapy[11, 12], biological separation[13] and tissue engineering[14-16] have been presented.

1.2.1 Nanomaterials for delivery

To improve the delivery efficiency of drugs and therapeutic agents into targeting tissues, various nanomaterials are fabricated into vesicles as nanocarriers. These nanocarriers can be applied for targeting delivery of drugs, proteins/peptides, siRNA and genes. In general, these loadings are incorporated into

nanocarriers through entrapping, surface adsorption or encapsulation. These nanoscaled carriers can easily cross different biological barriers (such as blood/brain barrier and gastro/intestinal barrier) and delivery drugs/genes/biomolecules with very high efficiency. Sustained release of drugs can be achieved by using nanocarriers. Therefore, this strategy will significantly improve the therapeutic efficiency as compared with traditional drug delivery systems. In addition, the nanocarriers can provide a protection for loadings from extreme environment to avoid the unwanted loss. The targeting delivery of drugs into located region of disease can also reduce the side effects of drugs to normal tissues.

The unique properties of nanomaterials make them be ideal candidates for cargo delivery. For example, the 3D hyperbranched structure of dendrimer can provide a good locus for drug encapsulation[17]. Mesoporous silica NPs are reported as efficient delivery carriers due to their porosity[18]. The hydrophobic property and larger surface area of carbon nanotubes contribute to their high loading amount and efficiency[19]. AuNPs are also developed as promising nanocarriers for drug/gene delivery because of their easily controlled surface chemistry. In a previous work, a monolayer of folate-modified amphiphilic copolymer stabilized AuNPs were developed for targeting drug delivery into tumors[20]. The doxorubicin (DOX) was loaded into the nanocarriers by covalently conjugation to the hydrophobic inner shell. In another work, AuNPs were capped with polyethyleneimine (PEI) for efficient delivery of siRNA for therapy[21]. The electrostatic interaction between cationic PEI and anionic siRNA enabled the loading and release of gene remarkably efficient.

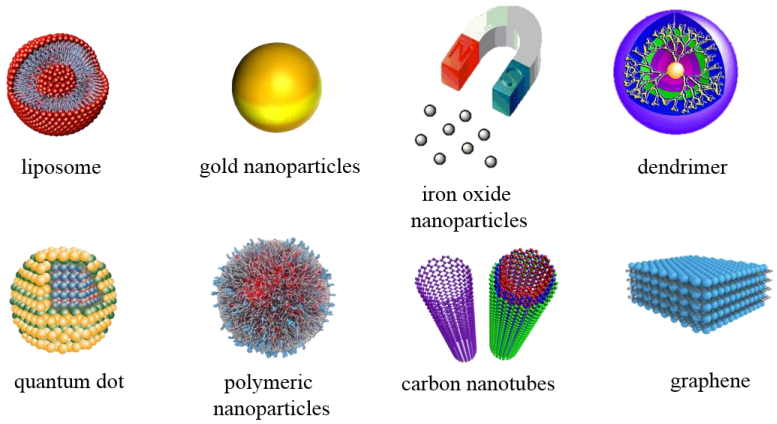

Figure 1.1 Most commonly used nanomaterials for biomedical applications.

1.2.2 Nanomaterials for molecular imaging

To visualize cellular lesions and disease developments in living organisms, some nanomaterials have been developed as contrast agents for molecular imaging. For instance, superparamagnetic iron oxide NPs, manganese oxide NPs and gadolinium-based nanoplatforms are most commonly used probes for magnetic resonance (MR) imaging.[22] Hollow silica nanospheres and quantum dots are generally developed for ultrasound (US) imaging and fluorescence imaging, respectively[23, 24]. In particular, because of the tunable properties, AuNPs also gain more and more attentions to be used for disease diagnosis, including fluorescence imaging, computed tomography (CT) imaging and photoacoustic (PA) imaging[1]. The applications of nanomaterials as contrast agents will be helpful for the location and treatments of diseases.

Because of the intrinsic limitations, sometimes the information of disease cannot be obtained

completely and accurately from single imaging modality. Therefore, dual- or multi-mode imaging techniques are generally need. To achieve this objective, multifunctional nanomaterials containing more than one kinds of imaging agents have been developed for diagnostic applications[25]. As an example, nanocomposites consisting of iron oxide NPs and manganese oxide NPs were synthesized by facile one-pot hydrothermal route for T_1/T_2-weighted dual-mode MR imaging of cancer cells.[26] In another work, AuNPs were coated onto the surface of iron oxide NPs through layer-by-layer self-assembly technique and the fabricated multifunctional composite NPs showed great potential to be used as contrast agents for MR and CT imaging[27]. In addition, iron oxide NPs loaded Au nanostars were also designed and prepared for multi-mode MR/CT/thermal imaging and MR/CT/PA imaging[28, 29].

1.2.3 Nanomaterials for cancer therapy

Recently, nanomaterials have been applied for cancer therapy because they can induce the local temperature increase or free radical generation with the aid of laser or magnetic field. The commonly used approaches for cancer therapy include photothermal therapy, photodynamic therapy and magnetic hyperthermia. Compared with nanomaterial-assisted chemotherapy, these treatments have some apparent advantages, such as focalized therapeutic regions and very low side effects to normal tissues.

Photothermal therapy is considered as an effective method for cancer treatments. For the successful applications, nanomaterials are generally need as photothermal conversion agents. After the internalization, nanomaterials inside the cancer cells can absorb the near infrared (NIR) light and convert it into heat, and the generated heat will help to kill the cancer cells. Many different NPs have been developed for photothermal therapy, for example carbon nanotubes, tungsten oxide, graphene oxide, molybdenum sulfide, Au nanomaterials and so on. In particularly, Au nanomaterials including Au nanocages, Au nanorods, Au nanoshells, Au nanoclusters and Au nanostars have been widely used for photothermal therapy due to their facile large scale preparation and high photothermal conversion efficiency. For example, Li et al. reported the usage of hyaluronic acid-modified iron oxide@Au core/shell structured nanostars for targeting photothermal therapy of human cervical carcinoma (HeLa cells) *in vitro* and xenografted tumor model *in vivo*.

As an emerging modality for cancer treatments, photodynamic therapy has obtained more and more attentions. Nanomaterials can be used as photosensitizers in this process. Under the light irradiation at suitable wavelength, the photosensitizers will be activated and transfer their energy to oxygen. This energy transfer results in the generation of free radical to kill the cancer cells[30]. Upconversion NPs[31], single-walled carbon nanotubes (SWCNTs)[32] and photodynamic agents loaded nanosystems[33] have been widely developed as photosensitizers for photodynamic therapy of cancer cells. In a previous work, AuNPs conjugated with 5-aminolevulinic acid were synthesized for the photodynamic therapy of cancer cells[34].

Under an alternating magnetic field, magnetic NPs can transform the electromagnetic energy to heat and the increase of temperature will destroy the tumors. This is the principle of magnetic hyperthermia. In general, only magnetic NPs can be applied for this hyperthermia, such as iron oxide NPs. For example, bovine serum albumin (BSA)-coated iron oxide NPs were fabricated for their usage as thermal therapeutic agents in a previous work. Being exposed upon alternating magnetic field, these NPs had a rapid temperature increase, thus killing the cancer cells[35].

1.2.4 Nanomaterials for biomedical separation

Beside the MR imaging and magnetic hyperthermia, biomedical separation is another very important application of iron oxide NPs because of their unique magnetic property. Benefited from the development of nanotechnology in the NP size controlling and surface functionalization, a larger number of sensitive and selective nanoplatforms have been structured for the separation of biomolecules, proteins and tumor cells[36]. As an example, Zengin et al. reported the preparation of polymer coated core-shell structured superparamagnetic iron oxide NPs and their usage for rapid enrichment and separation of cholesterol[37]. In another work, it was reported that the surface coating of AuNPs onto iron oxide NPs enabled their further modifications with nitrilotriacetic acid and the resultant bifunctional Au@iron oxide NPs could realize the biological separation of proteins simply with the help of magnetic fields[38]. Wang et al. immobilized anticycline E antibodies on the surface of superparamagnetic cores and CdSe/ZnS quantum dots shell nanocomposite particles, which could be used for the separation of breast cancer cells from serum solutions[39].

1.2.5 Nanomaterials for tissue engineering

Over the past decade, continued progress in nanotechnology contributes to the greatly potential applications of nanomaterials in tissue engineering because of their similar nanostructure with the microenvironment. The internalization of nanomaterials activates the intracellular signaling to regulate the stem cell functions[40]. In addition, the incorporation of nanomaterials into the scaffolds will increase the surface roughness and mechanical property of scaffolds. These nanocomposite scaffolds can well mimic extracellular matrix (ECM) and affect the cell proliferation and functions[41]. Therefore, understanding the roles of nanomaterials on cellular functions is necessary to define their applications for tissue engineering.

Modulating the differentiation of stem cells should be one of the mostly common applications of nanomaterials on cell functions.[42-44] Increasing types of nanomaterials showed the ability to induce the osteogenic differentiation and mineralization of stem cells through activating specific signaling pathway.[45-48] For example, AuNPs were reported to promote osteogenic differentiation of mouse bone marrow-derived mesenchymal stem cells (MSCs) through the p38 mitogen-activated protein kinase (MAPK) pathway.[49] The metallofullerene NPs enhanced osteogenic differentiation of bone marrow stromal cells through activating the intracellular bone morphogenetic proteins (BMP) signaling pathway[50]. More interestingly, bioactive silicate nanoplatelets were found to have the capability to induce osteogenic differentiation of human MSCs even without the osteogenic induction supplement[47].

1.3 Interaction between nanomaterials and cells

For the successful biomedical applications, it is necessary to study the interaction between nanomaterials and cells.[51-53] For example, increasing the accumulation of nanomaterials inside some specific cells and tissues can effectively improve the diagnostic and therapeutic efficiency with low dosage.[54-56] In addition, it has been reported that the internalization of nanomaterials may have a promotive influence on

cell proliferation and differentiation.[57-59] However, the nanomaterials potentially have side effects on cells or living body, such as toxicity, immune response and inflammation.[60, 61] These observations regarding the nanomaterial-cell interaction will provide useful information for the design and development of nanomaterials for different biomedical applications.

Because of the small size, nanomaterials can be easily internalized by cells. The cellular uptake of nanomaterials is an essential prerequisite for their successful applications in biomedicine fields. There are four main mechanisms involved in the cellular uptake of nanomaterials and each of them usually mediate the internalization of nanomaterials with different sizes.[62, 63] Caveolae-mediated endocytosis is responsible for the cellular uptake of nanomaterials with a size smaller than 80 nm. Clathrin-dependent endocytosis generally mediate the internalization of nanomaterials with a size about 120 nm. The cellular uptake of nanomaterials with a size larger than 250 nm is performed in a phagocytosis pathway. Pinocytosis is the mostly common mechanism for larger nanomaterials (about 1 μm).

Cytotoxicity is a non-ignorable side effect of nanomaterials to cells.[64] Nanomaterials inside cells may induce the generation of reactive oxygen species (ROS), thus leading to cell apoptosis or necrosis.[65] It is generally thought that higher concentration of nanomaterials in biological systems leads to higher toxicity to cells. Some nanomaterials have been reported to be low cytotoxic or biocompatible in previous works, but these studies are performed in limited concentration range. More attentions still should be paid onto the potential cytotoxicity of nanomaterials at high concentration range. In addition, due to varying metabolic processes and toleration of different cell types, the potential toxicity of nanomaterials to different cells may be inconsistent.

Beside the toxicity of nanomaterials to cells, their influence on cell proliferation has also been widely studied. The promotive effect on cell proliferation will enable the nanomaterials be used for tissue engineering. For example, it has been reported that silica NPs can enhance the proliferation of stem cells and osteoblast-like cells, so they have greatly potential applications in bone repair.[66, 67] Moreover, some other nanomaterials including AuNPs,[68] silver (Ag) NPs,[42] iron oxide NPs,[69] titanium (TiO_2) NPs[70] are also reported to be conducive to the cell proliferation without obvious cytotoxicity. However, the internalization of nanomaterials may also inhibit signaling pathway inside the cells, thus suppressing the cell proliferation, such as carboxylated-SWCNTs.[71]

The intracellular mechanical property change affected by the nanomaterials should also be considered when study the nanomaterial-cell interaction. The mechanical property has a very important role in regulating cell functions, cell morphology, cell migration and cell metabolism.[72] The internalized nanomaterials may alter the mechanical signal inside the cells to regulate the cytoskeletal reorganization and mechanical property.[73, 74] For example, the treatments of iron-iron oxide core-shell magnetic NPs have been reported to increase the Young's modulus of bovine articular chondrocytes (BACs) and higher concentration of nanomaterials leads to wider Young's modulus distribution and higher Young's modulus.[75] In some other studies, silica NPs, AgNPs and SWCNTs have also been found to reorganize cytoskeleton and enhance the stiffness of cells.[76-79] In addition, the nanomaterials' influence on mechanical property change may be different for different cell types. In a recent study, treatments of SWCNTs at the same concentration induced the smallest, moderate and biggest influence on Young's modulus for MSCs, HeLa cells and BACs, which

may be due to the different interactions dependent on cell types.[80]

Previous studies have indicated that the physical and chemical properties (size, shape and surface chemistry) of nanomaterials have obvious influence on nanomaterial-cell interaction (Figure 1.2).[64, 81] The cellular uptake of nanomaterials is dependent on their size, shape, surface charge, ligand modification, surface hydrophilicity, surface coating, shell structure and protein corona formations. 50-nm AuNPs have the maximum cellular uptake efficiency by mammalian cells as compared with their counterparts of other sizes.[82] The cellular uptake efficiency of spherical polymeric NPs in both MSCs and HeLa cells has been reported to be much higher than that of non-spherical counterparts.[83] The shell structure of nanomaterials also had some influence on their internalization. As shown in a recent study, poly(lactic-co-glycolic acid) (PLGA) core/lipid shell structured NPs with higher rigidity had an obviously higher cellular uptake than the ones with lower rigidity.[84] In another study, silica NPs with a rough surface have been found to exhibit an enhanced uptake amount as compared to similarly sized smooth particles.[85] Recently, surface coating of nanomaterials with stealth molecules or cell membrane has been proposed to reduce their nonspecific macrophage uptake but increase their accumulation in tumors.[86] For the surface charge factor, positively charged nanomaterials in general can enter into cells more efficiently than negatively charged and neutral nanomaterials because of their strong binding affinity to cell membrane.[87] The surface coatings or modifications of nanomaterials usually can improve their hydrophilicity, which is very important to maintain the colloidal stability and dispersibility of nanomaterials in biological medium.[88, 89] But surface hydrophobility is considered as good feature for their internalization into cells because of the abundant hydrophobic tails on cell membrane.[90, 91] Based on this theory, amphiphilic nanomaterials with hydrophilic and hydrophobic tails have been developed to improve their penetration ability.[92] The surface modifications of targeting ligands are a good strategy to enhance the specific accumulation of nanomaterials into cancer cells because of the receptor-mediated endocytosis, which will enable highly efficient diagnosis and therapy of cancers.[93, 94] However, the protein corona formation on the surface potential to build a barrier to cover the ligands of functional nanomaterials, thus leading to the loss of targeting specificity.[95]

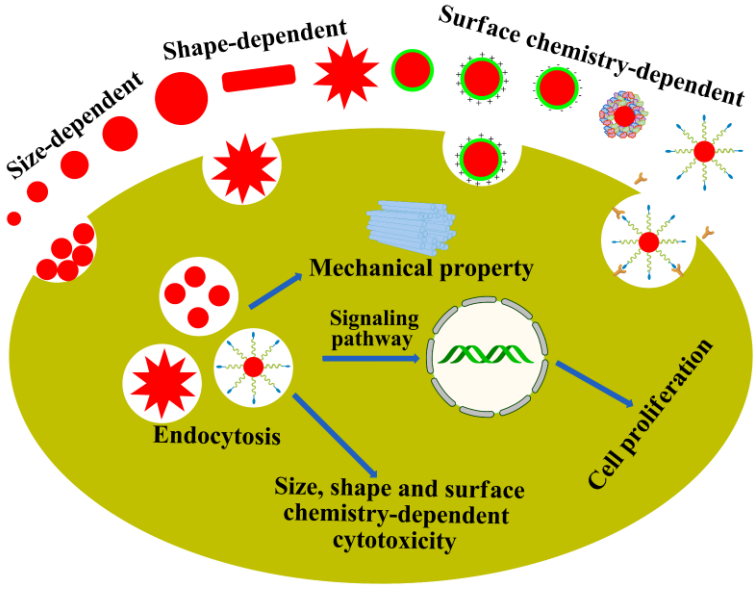

Figure 1.2 Summary of nanomaterial properties influence on nanomaterial-cell interaction.

The size, shape and surface chemistry of nanomaterials also affect their potential toxicity to cells, which may be due to their influence on cellular uptake.[96-98] For example, it has been reported that the cytotoxicity of silica NPs to endothelial cell line (EAHY926 cells) is dependent on their size. Smaller size of NPs results in higher cytotoxicity.[99] The size-dependent trendss in cytotoxicity of nanomaterials are inconsistent in different studies. As shown in another study, cytotoxicity of silica NPs to HepG2 cells increased in the order of 20 nm > 7 nm > 50 nm.[100] The influence of nanomaterial shape on cytotoxicity is very common for AuNPs. It has been reported that Au nanospheres induce higher cytotoxicity to fibroblast cells and endothelial cells than Au nanostars,[101] while Au nanorods have much more obvious toxic effects as compared to Au nanocages and Au nanohexapods.[102] For Au nanorods, the cytotoxicity is also different dependent on their aspect ratio, lower aspect ratio leads to higher cytotoxicity.[103] Surface coatings or modifications of nanomaterials with polymers is a commonly used strategy to improve their biocompatibility but reduce their cytotoxicity.[104] For example, graphene oxide (GO) showed greatly reduced cytotoxicity after being coated with poly(ethylene glycol) (PEG) and BSA.[105] In addition, the surface charge of nanomaterials is thought to have prominent influence on their cytotoxicity. A previous work reported that positively charged NPs display much more obvious cytotoxicity than neutral charged and negatively charged NPs.[106] The difference in cytotoxicity may be because of different locations inside cells. If the NPs are localized in lysosome, significant cytotoxicity will be observed. While the locations of NPs in cytoplasm will not induce any toxic effects to cells. Therefore, many endeavors have been made to reduce the surface charge of nanomaterials to improve their biocompatibility. For example, the totoxicity of PEI-coated multiwalled carbon nanotubes (MWCNTs) and iron oxide NPs is very high, while the cytotoxicity can be obviously attenuated after modifying their surface excessive amine groups with acetic anhydride, succinic anhydride and PEG.[107, 108]

In addition, the functions and biomedical applications of nanomaterials sometimes are decided by their unique properties. For example, Au nanostars and Au nanorods are widely used for photothermal therapy of cancer cells because these shaped-NPs have an obvious absorption in the NIR regions.[102, 109] Cationic NPs are good carriers for gene delivery due to their strong electrostatic adsorption with anionic genes.[110] That is to say, the physical and chemical properties of nanomaterials can not only change their functions, but also affect the nanomaterial-cell interactions and cell functions. As the advance of nanotechnology and nanoscience, these properties can be well controlled during the synthesis of nanomaterials. Therefore, development of functional nanomaterials with suitable properties for different biomedical applications is highly desirable.

1.4 Au nanostructures in nanomedicine

Among of these reported nanomaterials for biomedical applications, AuNPs are considered as one of the mostly promising candidates because of their advantages including facile synthetic methods, well controlled size, shape, surface chemistry and relatively good biocompatibility.[111] Most of the applications of AuNPs are based on their optical properties.[112] Under light irradiation, AuNPs will exhibit strong absorption and scattering, this is the well-known localized surface plasmon resonance (LSPR).[113] More importantly, the LSPR of AuNPs can be tuned by changing their size, shape, surface modification and aggregation state.[114, 115] Up to

date, engineered AuNPs have been used for molecular imaging, photothermal/photodynamic therapy, cargo delivery and biosensing (Figure 1.3).

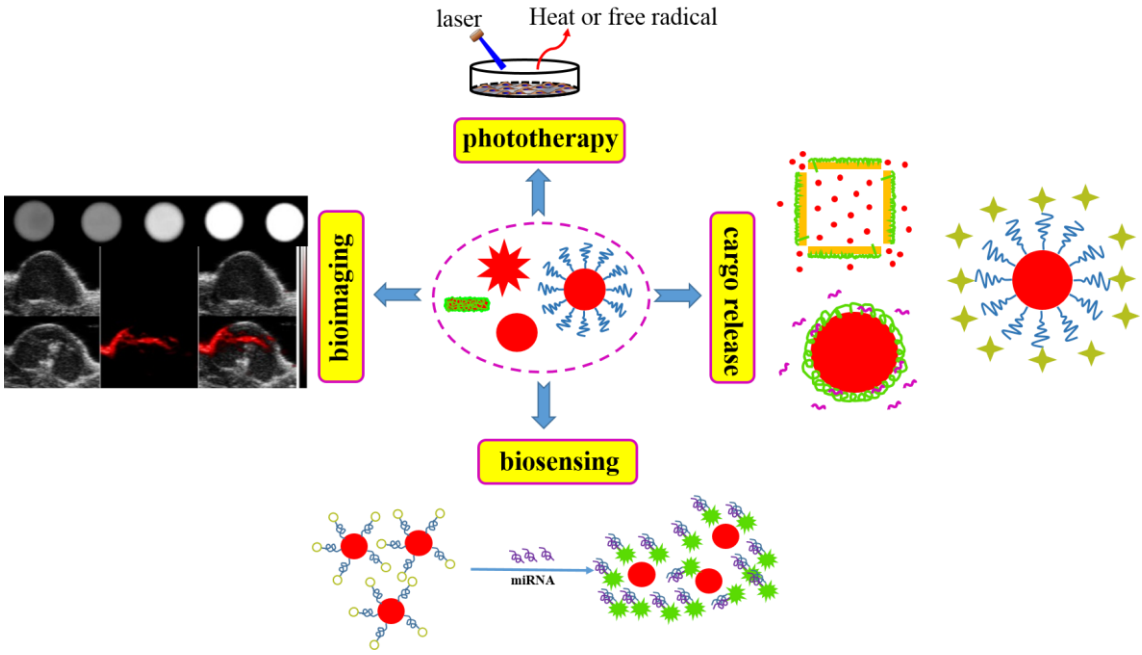

Figure 1.3 Overview of the different biomedical applications of AuNPs.

As-prepared AuNPs easily lose their colloidal stability in biological liquid, so ligand exchange or surface coatings have become indispensable for the biomedical applications.[116] The most commonly used strategy is binding AuNPs with thiol group (-SH) or disulfide group (S-S) to form stable Au-S bonds. In a recent study, PEGylated AuNPs can be formed by adding thiolated PEG into the citrate-capped AuNP solution under stirring.[117] This ligand exchange reaction is very facile and can be conducted under a mild condition. What's more, by changing the terminal functional groups of bounded molecular, it is highly possible to obtain water-dispersed and colloidally stable AuNPs with amines, hydroxyls and carbohydrates on the surface. Surface adsorption of polymer onto AuNPs can also be used to generate desired nanostructures with high stability. For example, transferrin has be successfully attached onto the surface of AuNPs by simply physical absorption.[118] To extend the biomedical applications, some bioactive molecular have also be attached onto the surface of AuNPs by simple ligand exchange processes, such as drugs, proteins, peptides, DNAs, siRNA, targeting ligands, fluorescent dyes, antibodies and so on.[119]

Various Au nanostructures with different morphologies have been developed benefited from the progress of nanotechnology, such as Au nanospheres, Au nanorods, Au nanostars, Au nanoshells, Au nanoclusters, Au nanorices, Au nanobipyramids, Au nanocrescents, Au nanowires, Au nanocubes and Au nanocages.[120] These nanostructures are in general synthesized by different protocols and have discriminative properties and functions. Among of them, Au nanospheres, Au nanorods, Au nanoshells, Au nanostars, Au nanoclusters and Au nanocages represent the mostly common candidates in the fields of nanomedicine.

Au nanospheres: Au nanospheres can be synthesized by simple reduction of Au salts or seed-mediated methods with controlled size. Their absorption peaks are tunable in the wavelength range from 500 nm to 600 nm by changing the size. It is generally considered that Au nanospheres are the most widely used

nanostructures for biomedical applications. Folic acid (FA)-modified Au nanospheres have been reported to be excellent contrast agents for CT imaging of tumors because of their X-ray attenuation property.[121] On another hand, Au nanospheres employed as carriers for the drug delivery facilitates the cancer therapy with high efficient.[20] Although single Au nanosphere fails to generate heat under the laser irradiation, while their aggregations display red-shifted absorption peaks in the NIR regions, enabling the successful photothermal therapy of cancers.[122] In addition, Au nanospheres are also widely used in the tissue engineering fields, especially in regulating the stem cell differentiation.[49] As an example, Au nanospheres with surface carboxyl motifs obvious inhibited the osteogenic differentiation of MSCs as compared to citrate, amine and hydroxyl groups.[123] By optimizing the surface chemistry, Au nanospheres can deliver the miRNA efficiently into bone mesenchymal stromal cells to enhance their osteogenic differentiation.[124] Au nanospheres can also be developed into biosensors to detect the intracellular microRNAs because of their energy conversion with fluorescent complexs.[125]

Au nanorods: Different from other nanostructures, Au nanorods have two absorption peaks: transverse mode and longitudinal mode. Their localized positions shift with the variation of aspect ratio of the nanostructures. These nanorods are typically synthesized by dropping small crystal seeds into growth solution with cetyltrimethyl ammonium bromide (CTAB) as surfactants. Au nanorods with tunable aspect ratios can be easily obtained by adjusting the reaction conditions. After the synthesis, ligand exchange, polymer absorption or silica coating is often performed for photothermal therapy and drug release. In a representative study, mesoporous silica coated Au nanorods were conjugated with arginine-glycine-aspartate (RGD) peptides and then loaded with DOX to structure multifunctional NPs, which showed great potential for chemo-photothermal therapy of cancers under NIR radiation.[126]

Au nanoshells: Au nanoshells are core/shell structured NPs with an inorganic nanocrystal as core and a layer of Au as shell. They are synthesized by assembling small Au seeds onto the surface of a core, followed by the growth of Au shell through chemical reduction. The inside core can be magnetic iron oxide NPs, Ag NPs or silica nanospheres according to different requirements.[127] The LSPR of Au nanoshells is tunable by changing the ration of core diameter and outer shell thickness. Therefore, it is high desirable to extend their absorption peaks into NIR regions for the noninvasive surface-enhanced Raman spectroscopy (SERS) imaging and photothermal therapy of cancers.[128]

Au nanostars: Branched star-shaped Au nanocrystals (Au nanostars) have recently obtained more and more attentions because of their unique structure. The sharp edges and tips enable Au nanostars exhibit LSPR in the NIR regions.[129, 130] Au nanostars also have much higher surface-to-volume ratios as compared to other Au nanostructures, which may be another advantage for their biomedical applications. For the synthesis of Au nanostars, different synthetic methods have been presented, and the seed-mediated growth route is the most commonly used one.[131] By adding different volume of Au seed solution into growth solution, Au nanostars with controlled size and branched structure can be formed.[132] Currently, Au nanostars are mainly used for molecular imaging and photothermal therapy of cancers.[133, 134] It is also possible to fabricate star-shaped structure on the outer layer of inorganic nanocrystals to enrich their functions.[28, 29]

Au nanoclusters: Au nanoclusters are nanostructures containing several to a hundred Au atoms and several template moleculars. Profited from their ultrasmall size (usually smaller than 2 nm), Au nanoclusters

have very strong x-ray absorption and photoluminescence.[135] Many different protocols have been used to synthesize thiol-protected Au nanoclusters. While some of them have fairly low quantum yields (QYs) or require very long reaction time. BSA-mediated synthesis is considered as a facile and green method to prepare Au nanoclusters with a high QYs.[136] The biomedical applications of Au nanoclusters are mainly focused on biosensing, bioimaging and radiotherapy.[135] As an example, FA-conjugated Au nanoclusters protected by ovalbumin were used for targeting fluorescent imaging of cancer cells.[137]

Au nanocages: Au nanostructures with hollow pores on the corners that look like cages are defined as Au nanocages. They are developed from silver nanocubes as templates through galvanic replacement reaction, and their size is strongly dependent on the size of silver nanocubes. To meet different applications, their LSPR can be well controlled by varying the molar ratios of templates and Au precursor. In a previous work, antibodies conjugated Au nanocages with a diameter smaller than 40 nm have been synthesized as contrast agents for specific targeting optical coherence tomography (OCT) imaging of breast cancer cells.[138] More interestingly, the hollow porous structure enables them be excellent carriers for drug delivery. A most recent study reported the preparation of cancer cell membrane coated Au nanocages with anticancer drug release capability for the combinational chemotherapy and photothermal therapy of breast cancers.[139]

1.5 Motivation and objectives

Because of their vast advantages over bulk materials, nanomaterials have attracted more and more attentions in the fields of nanomedicine. They have been widely used for the diagnosis and treatments of diseases, especially for cancers. On another hand, nanomaterials are good candidates for mimicking ECM due to their similar size and scale to proteins. Therefore, nanomaterials also have great potential for tissue engineering. Increasing evidences have showed that the physical and chemical properties of nanomaterials including size, shape and surface modification will not only change their functions, but also markedly affect the cytotoxicity, cellular uptake and mechanical property.

Among of these reported nanomaterials for biomedical applications, AuNPs have been studied and used for several decades. Various multifunctional Au nanostructures have been fabricated for molecular imaging, drug/gene delivery, biosensing and photothermal/phodynamic therapy. However, there are still some challenges in the developments of functional nanomaterials for cancer therapy and more endeavors need to be made. A larger number of researchers have investigated the influence of AuNP size, shape and surface chemistry on cellular uptake and cytotoxicity in different cell lines, except for stem cells. AuNPs have been found to have positive influence on osteogenic differentiation and negative influence on adipogenic differentiation of stem cells. But these influence is different dependent on the surface chemistry of AuNPs. So then, how about the roles of particle size and shape? It is still mysterious and should be explored. For tissue engineering, it is all known that ECM is a very important factor in regulating cell functions, while it is very difficult to fully understand their roles *in vitro*. AuNPs may be an excellent candidate to mimic the ECM and investigate their influence on differentiation of stem cells.

Therefore, the objectives of this study are to synthesize AuNPs with suitable size, shape and surface modifications for different biomedical applications. (1) Preparation of multifunctional AuNPs for enhanced

cellular uptake and targeting photothermal therapy of cancer cells. (2) Synthesis of AuNPs with different size and shape to investigate their influence on osteogenic differentiation of stem cells. (3) Exploring the potential effects of sub-10 nm AuNPs on cell viability, osteogenic differentiation and adipogenic differentiation of stem cells. (4) Development of ECM mimic AuNPs for regulating multipotent differentiation of stem cells. All of these studies will conduce to a deeper understanding of nanomaterial-cell interaction and also provide helpful information for the design and development of multifunctional nanomaterials for cancer therapy and tissue engineering.

1.6 References

1. E. C. Dreaden, A. M. Alkilany, X. Huang, C. J. Murphy and M. A. El-Sayed, *Chem. Soc. Rev.*, 2012, 41, 2740-2779.
2. K. Turcheniuk, A. V. Tarasevych, V. P. Kukhar, R. Boukherroub and S. Szunerits, *Nanoscale*, 2013, 5, 10729-10752.
3. R. Senthilkumar, D. Ş. Karaman, P. Paul, E. M. Björk, M. Odén, J. E. Eriksson and J. M. Rosenholm, *Biomater. Sci.*, 2015, 3, 103-111.
4. E. Roduner, *Chem. Soc. Rev.*, 2006, 35, 583-592.
5. G. Chen, H. Qiu, P. N. Prasad and X. Chen, *Chem. Rev.*, 2014, 114, 5161-5214.
6. Z. Yang, D. Gao, Z. Cao, C. Zhang, D. Cheng, J. Liu and X. Shuai, *Biomater. Sci.*, 2015, 3, 1035-1049.
7. J.-M. Williford, J. L. Santos, R. Shyam and H.-Q. Mao, *Biomater. Sci.*, 2015.
8. C. Giménez, C. De La Torre, M. Gorbe, E. Aznar, F. Sancenón, J. R. Murguía, R. Martínez-Máñez, M. D. Marcos and P. Amorós, *Langmuir*, 2015, 31, 3753-3762.
9. S. Shukla, C. Dickmeis, A. Nagarajan, R. Fischer, U. Commandeur and N. Steinmetz, *Biomater. Sci.*, 2014, 2, 784-797.
10. H. Wang, J. Shen, Y. Li, Z. Wei, G. Cao, Z. Gai, K. Hong, P. Banerjee and S. Zhou, *Biomater. Sci.*, 2014, 2, 915-923.
11. Q. Zhao, X. Yi, M. Li, X. Zhong, Q. Shi and K. Yang, *Nanoscale*, 2016.
12. H. Liu, Y. Yang, A. Wang, M. Han, W. Cui and J. Li, *Adv. Funct. Mater.*, 2016, 26, 2561-2570.
13. Y.-C. Li, Y.-S. Lin, P.-J. Tsai, C.-T. Chen, W.-Y. Chen and Y.-C. Chen, *Anal. Chem.*, 2007, 79, 7519-7525.
14. S. Gil and J. F. Mano, *Biomater. Sci.*, 2014, 2, 812-818.
15. J. M. Rosenholm, J. Zhang, M. Linden and C. Sahlgren, *Nanomedicine*, 2016, 11, 391-402.
16. T. D. H. Le, W. Bonani, G. Speranza, V. Sglavo, R. Ceccato, D. Maniglio, A. Motta and C. Migliaresi, *Mater. Sci. Eng., C*, 2016, 59, 471-479.
17. E. R. Gillies and J. M. Frechet, *Drug Discovery Today*, 2005, 10, 35-43.
18. I. I. Slowing, J. L. Vivero-Escoto, C.-W. Wu and V. S.-Y. Lin, *Adv. Drug Delivery Rev.*, 2008, 60, 1278-1288.
19. A. Bianco, K. Kostarelos and M. Prato, *Curr. Opin. Chem. Biol.*, 2005, 9, 674-679.

20. M. Prabaharan, J. J. Grailer, S. Pilla, D. A. Steeber and S. Gong, *Biomaterials*, 2009, 30, 6065-6075.
21. W. J. Song, J. Z. Du, T. M. Sun, P. Z. Zhang and J. Wang, *Small*, 2010, 6, 239-246.
22. J. Li, X. Shi and M. Shen, *Part. Part. Syst. Charact.*, 2014, 31, 1223-1237.
23. L. An, H. Hu, J. Du, J. Wei, L. Wang, H. Yang, D. Wu, H. Shi, F. Li and S. Yang, *Biomaterials*, 2014, 35, 5381-5392.
24. F. Pinaud, X. Michalet, L. A. Bentolila, J. M. Tsay, S. Doose, J. J. Li, G. Iyer and S. Weiss, *Biomaterials*, 2006, 27, 1679-1687.
25. J. Li, L. Zheng, H. Cai, W. Sun, M. Shen, G. Zhang and X. Shi, *ACS Appl. Mater. Interfaces*, 2013, 5, 10357-10366.
26. J. Li, Y. Hu, W. Sun, Y. Luo, X. Shi and M. Shen, *RSC Adv.*, 2016, 6, 35295-35304.
27. H. Cai, K. Li, J. Li, S. Wen, Q. Chen, M. Shen, L. Zheng, G. Zhang and X. Shi, *Small*, 2015, 11, 4584-4593.
28. J. Li, Y. Hu, J. Yang, P. Wei, W. Sun, M. Shen, G. Zhang and X. Shi, *Biomaterials*, 2015, 38, 10-21.
29. Y. Hu, R. Wang, S. Wang, L. Ding, J. Li, Y. Luo, X. Wang, M. Shen and X. Shi, *Sci. Rep.*, 2016, 6.
30. S. Jin, L. Zhou, Z. Gu, G. Tian, L. Yan, W. Ren, W. Yin, X. Liu, X. Zhang and Z. Hu, *Nanoscale*, 2013, 5, 11910-11918.
31. C. Wang, L. Cheng and Z. Liu, *Theranostics*, 2013, 3, 317-330.
32. Z. Zhu, Z. Tang, J. A. Phillips, R. Yang, H. Wang and W. Tan, *J. Am. Chem. Soc.*, 2008, 130, 10856-10857.
33. F. Li, S.-J. Park, D. Ling, W. Park, J. Y. Han, K. Na and K. Char, *J. Mater. Chem. B*, 2013, 1, 1678-1686.
34. M. K. Khaing Oo, X. Yang, H. Du and H. Wang, *Nanomedicine*, 2008, 3, 777-786.
35. B. Samanta, H. Yan, N. O. Fischer, J. Shi, D. J. Jerry and V. M. Rotello, *J. Mater. Chem.*, 2008, 18, 1204-1208.
36. I. Yildiz, *Nanotechnol. Rev.*, 2016, 5, 331-340.
37. A. Zengin, E. Yildirim, U. Tamer and T. Caykara, *Analyst*, 2013, 138, 7238-7245.
38. J. Bao, W. Chen, T. Liu, Y. Zhu, P. Jin, L. Wang, J. Liu, Y. Wei and Y. Li, *ACS Nano*, 2007, 1, 293-298.
39. D. Wang, J. He, N. Rosenzweig and Z. Rosenzweig, *Nano Lett.*, 2004, 4, 409-413.
40. W. Jiang, B. Y. Kim, J. T. Rutka and W. C. Chan, *Nat. Nanotechnol.*, 2008, 3, 145-150.
41. H. Mao, N. Kawazoe and G. Chen, *Colloids Surf., B*, 2015, 126, 63-69.
42. R. Zhang, P. Lee, V. C. Lui, Y. Chen, X. Liu, C. N. Lok, M. To, K. W. Yeung and K. K. Wong, *Nanomed-Nanotechnol.*, 2015, 11, 1949-1959.
43. J. H. Lee, Y. C. Shin, O. S. Jin, S. H. Kang, Y.-S. Hwang, J.-C. Park, S. Hong and D.-W. Han, *Nanoscale*, 2015.
44. S. Amorim, A. Martins, N. M. Neves, R. L. Reis and R. A. Pires, *J. Mater. Chem. B*, 2014, 2, 6939-6946.
45. K. Yang, W. Cao, X. Hao, X. Xue, J. Zhao, J. Liu, Y. Zhao, J. Meng, B. Sun, J. Zhang and X. Liang, *Nanoscale*, 2013, 5, 1205-1212.

46. L. Li, Z. Zhu, W. Xiao and L. Li, *Int. J. Mol. Sci.*, 2015, 16, 3188-3201.
47. A. K. Gaharwar, S. M. Mihaila, A. Swami, A. Patel, S. Sant, R. L. Reis, A. P. Marques, M. E. Gomes and A. Khademhosseini, *Adv. Mater.*, 2013, 25, 3329-3336.
48. M. Mahmood, H. Villagarcia, E. Dervishi, T. Mustafa, M. Alimohammadi, D. Casciano, M. Khodakovskaya and A. S. Biris, *J. Mater. Chem. B*, 2013, 1, 3220-3230.
49. C. Yi, D. Liu, C.-C. Fong, J. Zhang and M. Yang, *ACS Nano*, 2010, 4, 6439-6448.
50. K. Yang, W. Cao, X. Hao, X. Xue, J. Zhao, J. Liu, Y. Zhao, J. Meng, B. Sun and J. Zhang, *Nanoscale*, 2013, 5, 1205-1212.
51. X.-Q. Zhang, X. Xu, N. Bertrand, E. Pridgen, A. Swami and O. C. Farokhzad, *Adv. Drug Delivery Rev.*, 2012, 64, 1363-1384.
52. B. Sahoo, K. S. P. Devi, S. K. Sahu, S. Nayak, T. K. Maiti, D. Dhara and P. Pramanik, *Biomater. Sci.*, 2013, 1, 647-657.
53. A. Irure, M. Marradi, B. Arnáiz, N. Genicio, D. Padro and S. Penadés, *Biomater. Sci.*, 2013, 1, 658-668.
54. T. Zako, M. Yoshimoto, H. Hyodo, H. Kishimoto, M. Ito, K. Kaneko, K. Soga and M. Maeda, *Biomater. Sci.*, 2015, 3, 59-64.
55. G. Chen, I. Roy, C. Yang and P. N. Prasad, *Chem. Rev.*, 2016, 116, 2826-2885.
56. A. Espinosa, R. Di Corato, J. Kolosnjaj-Tabi, P. Flaud, T. Pellegrino and C. Wilhelm, *ACS Nano*, 2016, 10, 2436-2446.
57. Z.-Z. Yu, Q.-H. Wu, S.-L. Zhang, J.-Y. Miao, B.-X. Zhao and L. Su, *RSC Adv.*, 2016, 6, 10159-10161.
58. J. Li, J. Qiu, W. Guo, S. Wang, B. Ma, X. Mou, M. Tanes, H. Jiang and H. Liu, *Nanoscale*, 2016, 8, 7416-7422.
59. Q. Wang, B. Chen, M. Cao, J. Sun, H. Wu, P. Zhao, J. Xing, Y. Yang, X. Zhang, M. Ji and N. Gu, *Biomaterials*, 2016, 86, 11-20.
60. C. Grabinski, N. Schaeublin, A. Wijaya, H. D'Couto, S. H. Baxamusa, K. Hamad-Schifferli and S. M. Hussain, *ACS Nano*, 2011, 5, 2870-2879.
61. R. Pati, I. Das, R. K. Mehta, R. Sahu and A. Sonawane, *Toxicol. Sci.*, 2016, 150, 454-472.
62. F. Zhao, Y. Zhao, Y. Liu, X. Chang, C. Chen and Y. Zhao, *Small*, 2011, 7, 1322-1337.
63. K.-M. Kim, M.-K. Kim, H.-J. Paek, S.-J. Choi and J.-M. Oh, *Colloids Surf., B*, 2016, 145, 870-877.
64. L.-C. Cheng, X. Jiang, J. Wang, C. Chen and R.-S. Liu, *Nanoscale*, 2013, 5, 3547-3569.
65. S. Sharifi, S. Behzadi, S. Laurent, M. L. Forrest, P. Stroeve and M. Mahmoudi, *Chem. Soc. Rev.*, 2012, 41, 2323-2343.
66. Y. Tang, Y. Zhao, X. Wang and T. Lin, *J. Biomed. Mater. Res., Part A*, 2014, 102, 3803-3812.
67. G. R. Beck, S.-W. Ha, C. E. Camalier, M. Yamaguchi, Y. Li, J.-K. Lee and M. N. Weitzmann, *Nanomed-Nanotechnol.*, 2012, 8, 793-803.
68. D. Zhang, D. Liu, J. Zhang, C. Fong and M. Yang, *Mater. Sci. Eng., C*, 2014, 42, 70-77.
69. D.-M. Huang, J.-K. Hsiao, Y.-C. Chen, L.-Y. Chien, M. Yao, Y.-K. Chen, B.-S. Ko, S.-C. Hsu, L.-A. Tai, H.-Y. Cheng, S.-W. Wang, C.-S. TYang and Y.-C. Chen, *Biomaterials*, 2009, 30, 3645-3651.

70. Y. Hou, K. Cai, J. Li, X. Chen, M. Lai, Y. Hu, Z. Luo, X. Ding and D. Xu, *Int. J. Nanomed.*, 2013, 8, 3619.
71. Q. Mu, G. Du, T. Chen, B. Zhang and B. Yan, *ACS Nano*, 2009, 3, 1139-1144.
72. J.-J. Chiu, S. Usami and S. Chien, *Ann. Med.*, 2009, 41, 19-28.
73. C. Y. Tay, P. Cai, M. I. Setyawati, W. Fang, L. P. Tan, C. H. Hong, X. Chen and D. T. Leong, *Nano Lett.*, 2013, 14, 83-88.
74. Y. Li, L. Jing, Y. Yu, Y. Yu, J. Duan, M. Yang, W. Geng, L. Jiang, Q. Li and Z. Sun, *Part. Part. Syst. Charact.*, 2015, 32, 636-645.
75. H. Mao, J. Li, I. Dulińska-Molak, N. Kawazoe, Y. Takeda, H. Mamiya and G. Chen, *Biomater. sci.*, 2015, 3, 1284-1290.
76. I. V. Ogneva, S. V. Buravkov, A. N. Shubenkov and L. B. Buravkova, *Nanoscale Res. Lett.*, 2014, 9, 1-10.
77. H. Qin, C. Zhu, Z. An, Y. Jiang, Y. Zhao, J. Wang, X. Liu, B. Hui, X. Zhang and Y. Wang, *Int. J. Nanomed.*, 2014, 9, 2469.
78. B. D. Holt, P. A. Short, A. D. Rape, Y.-l. Wang, M. F. Islam and K. N. Dahl, *ACS Nano*, 2010, 4, 4872-4878.
79. I. Dulińska-Molak, H. Mao, N. Kawazoe and G. Chen, *J. Nanosci. Nanotechnol.*, 2014, 14, 2459-2465.
80. I. Dulinska-Molak, H. Mao, N. Kawazoe and G. Chen, *J. Biomed. Nanotechnol.*, 2014, 10, 651-659.
81. S. Męczyńska-Wielgosz, A. Piotrowska, A. Majkowska-Pilip, A. Bilewicz and M. Kruszewski, *Nanoscale Res. Lett.*, 2016, 11, 1.
82. B. D. Chithrani, A. A. Ghazani and W. C. Chan, *Nano Lett.*, 2006, 6, 662-668.
83. L. Florez, C. Herrmann, J. M. Cramer, C. P. Hauser, K. Koynov, K. Landfester, D. Crespy and V. Mailänder, *Small*, 2012, 8, 2222-2230.
84. J. Sun, L. Zhang, J. Wang, Q. Feng, D. Liu, Q. Yin, D. Xu, Y. Wei, B. Ding, X. Shi and X. Jiang, *Adv. Mater.*, 2015, 27, 1402-1407.
85. Y. Niu, M. Yu, S. B. Hartono, J. Yang, H. Xu, H. Zhang, J. Zhang, J. Zou, A. Dexter, W. Gu and C. Yu, *Adv. Mater.*, 2013, 25, 6233-6237.
86. V. V. Glinsky, G. V. Glinsky, O. V. Glinskii, V. H. Huxley, J. R. Turk, V. V. Mossine, S. L. Deutscher, K. J. Pienta and T. P. Quinn, *Cancer Res.*, 2003, 63, 3805-3811.
87. B. Yu, Y. Zhang, W. Zheng, C. Fan and T. Chen, *Inorg. Chem.*, 2012, 51, 8956-8963.
88. C. Ge, J. Du, L. Zhao, L. Wang, Y. Liu, D. Li, Y. Yang, R. Zhou, Y. Zhao, Z. Chai and C. Chen, *Proc. Natl. Acad. Sci. U. S. A.*, 2011, 108, 16968-16973.
89. L. Cheng, J. Liu, X. Gu, H. Gong, X. Shi, T. Liu, C. Wang, X. Wang, G. Liu, H. Xing, W. Bu, B. Sun and Z. Liu, *Adv. Mater.*, 2014, 26, 1886-1893.
90. H. Y. Nam, S. M. Kwon, H. Chung, S.-Y. Lee, S.-H. Kwon, H. Jeon, Y. Kim, J. H. Park, J. Kim, S. Her, Y.-K. Oh, I. C. Kwon, K. Kim and S. Y. Jeong, *J. Controlled Release*, 2009, 135, 259-267.
91. S. J. Tan, N. R. Jana, S. Gao, P. K. Patra and J. Y. Ying, *Chem. Mater.*, 2010, 22, 2239-2247.
92. Z. Zhang, K. Van Steendam, S. Maji, L. Balcaen, Y. Anoshkina, Q. Zhang, G. Vanluchene, R. De

Rycke, F. Van Haecke, D. Deforce, R. Hoogenboom and B. G. De Geest, *Adv. Funct. Mater.*, 2015, 25, 3433-3439.

93. D. Shao, J. Li, Y. Pan, X. Zhang, X. Zheng, Z. Wang, M. Zhang, H. Zhang and L. Chen, *Biomater. Sci.*, 2015, 3, 833-841.
94. B. Wu, P. Yu, C. Cui, M. Wu, Y. Zhang, L. Liu, C.-X. Wang, R.-X. Zhuo and S.-W. Huang, *Biomater. Sci.*, 2015, 3, 655-664.
95. A. Salvati, A. S. Pitek, M. P. Monopoli, K. Prapainop, F. B. Bombelli, D. R. Hristov, P. M. Kelly, C. Åberg, E. Mahon and K. A. Dawson, *Nat. Nanotechnol.*, 2013, 8, 137-143.
96. J. F. Stefanick, J. D. Ashley and B. Bilgicer, *ACS Nano*, 2013, 7, 8115-8127.
97. E. Fröhlich, *Int. J. Nanomed.*, 2012, 7, 5577.
98. J. Bai, T. Wang, Y. Wang and X. Jiang, *Biomater. Sci.*, 2014, 2, 493-501.
99. D. Napierska, L. C. Thomassen, V. Rabolli, D. Lison, L. Gonzalez, M. Kirsch-Volders, J. A. Martens and P. H. Hoet, *Small*, 2009, 5, 846-853.
100. X. Lu, J. Qian, H. Zhou, Q. Gan, W. Tang, J. Lu, Y. Yuan and C. Liu, *Int. J. Nanomed.*, 2011, 6, 1889.
101. P. M. Favi, M. Gao, L. Johana Sepúlveda Arango, S. P. Ospina, M. Morales, J. J. Pavon and T. J. Webster, *J. Biomed. Mater. Res., Part A*, 2015, 103, 3449-3462.
102. Y. Wang, K. C. Black, H. Luehmann, W. Li, Y. Zhang, X. Cai, D. Wan, S.-Y. Liu, M. Li, P. Kim, Z.-Y. Li, L. V. Wang, Y. Liu and Y. Xia, *ACS Nano*, 2013, 7, 2068-2077.
103. R. G. Rayavarapu, W. Petersen, L. Hartsuiker, P. Chin, H. Janssen, F. W. Van Leeuwen, C. Otto, S. Manohar and T. G. Van Leeuwen, *Nanotechnology*, 2010, 21, 145101.
104. A. M. Alkilany, P. K. Nagaria, C. R. Hexel, T. J. Shaw, C. J. Murphy and M. D. Wyatt, *Small*, 2009, 5, 701-708.
105. Y. Li, L. Feng, X. Shi, X. Wang, Y. Yang, K. Yang, T. Liu, G. Yang and Z. Liu, *Small*, 2014, 10, 1544-1554.
106. A. Asati, S. Santra, C. Kaittanis and J. M. Perez, *ACS Nano*, 2010, 4, 5321-5331.
107. M. Shen, S. H. Wang, X. Shi, X. Chen, Q. Huang, E. J. Petersen, R. A. Pinto, J. R. Baker Jr and W. J. Weber Jr, *J. Phys. Chem. C*, 2009, 113, 3150-3156.
108. H. Cai, X. An, J. Cui, J. Li, S. Wen, K. Li, M. Shen, L. Zheng, G. Zhang and X. Shi, *ACS Appl. Mater. Interfaces*, 2013, 5, 1722-1731.
109. S. Wang, Z. Teng, P. Huang, D. Liu, Y. Liu, Y. Tian, J. Sun, Y. Li, H. Ju and X. Chen, *Small*, 2015, 11, 1801-1810.
110. L. Kong, C. S. Alves, W. Hou, J. Qiu, H. Möhwald, H. Tomás and X. Shi, *ACS Appl. Mater. Interfaces*, 2015, 7, 4833-4843.
111. P. M. Tiwari, K. Vig, V. A. Dennis and S. R. Singh, *Nanomaterials*, 2011, 1, 31-63.
112. M. Hu, J. Chen, Z.-Y. Li, L. Au, G. V. Hartland, X. Li, M. Marquez and Y. Xia, *Chem. Soc. Rev.*, 2006, 35, 1084-1094.
113. X. Li, L. Jiang, Q. Zhan, J. Qian and S. He, *Colloids Surf., A*, 2009, 332, 172-179.
114. M.-C. Daniel and D. Astruc, *Chem. Rev.*, 2004, 104, 293-346.

115. X. Huang and M. A. El-Sayed, *J. Adv. Res.*, 2010, 1, 13-28.
116. X. Huang, I. H. El-Sayed, W. Qian and M. A. El-Sayed, *J. Am. Chem. Soc.*, 2006, 128, 2115-2120.
117. K. Rahme, L. Chen, R. G. Hobbs, M. A. Morris, C. O'Driscoll and J. D. Holmes, *RSC Adv.*, 2013, 3, 6085-6094.
118. B. D. Chithrani and W. C. Chan, *Nano Lett.*, 2007, 7, 1542-1550.
119. V. Biju, *Chem. Soc. Rev.*, 2014, 43, 744-764.
120. L. Dykman and N. Khlebtsov, *Chem. Soc. Rev.*, 2012, 41, 2256-2282.
121. C. Peng, J. Qin, B. Zhou, Q. Chen, M. Shen, M. Zhu, X. Lu and X. Shi, *Poly. Chem.*, 2013, 4, 4412-4424.
122. J. Nam, N. Won, H. Jin, H. Chung and S. Kim, *J. Am. Chem. Soc.*, 2009, 131, 13639-13645.
123. J. E. J. Li, N. Kawazoe and G. Chen, *Biomaterials*, 2015, 54, 226-236.
124. M. Yu, B. Lei, C. Gao, J. Yan and P. X. Ma, *Nano Res.*, 2017, 10, 49-63.
125. C. K. K. Choi, J. Li, K. Wei, Y. J. Xu, L. W. C. Ho, M. Zhu, K. K. To, C. H. J. Choi and L. Bian, *J. Am. Chem. Soc.*, 2015, 137, 7337-7346.
126. S. Shen, H. Tang, X. Zhang, J. Ren, Z. Pang, D. Wang, H. Gao, Y. Qian, X. Jiang and W. Yang, *Biomaterials*, 2013, 34, 3150-3158.
127. A. Y. Lin, J. K. Young, A. V. Nixon and R. A. Drezek, *Small*, 2014, 10, 3246-3251.
128. Y. Gao, Y. Li, Y. Wang, Y. Chen, J. Gu, W. Zhao, J. Ding and J. Shi, *Small*, 2015, 11, 77-83.
129. C. L. Nehl, H. Liao and J. H. Hafner, *Nano Lett.*, 2006, 6, 683-688.
130. E. S. Allgeyer, A. Pongan, M. Browne and M. D. Mason, *Nano Lett.*, 2009, 9, 3816-3819.
131. Y. Pei, Z. Wang, S. Zong and Y. Cui, *J. Mater. Chem. B*, 2013, 1, 3992-3998.
132. C. L. Nehl and J. H. Hafner, *J. Mater. Chem.*, 2008, 18, 2415-2419.
133. Y. Wang, L. Polavarapu and L. M. Liz-Marzán, *ACS Appl. Mater. Interfaces*, 2014, 6, 21798-21805.
134. D. Li, Y. Zhang, S. Wen, Y. Song, Y. Tang, X. Zhu, M. Shen, S. Mignani, J.-P. Majoral, Q. Zhao and X. Shi, *J. Mater. Chem. B*, 2016, 4, 4216-4226.
135. Z. Luo, K. Zheng and J. Xie, *Chem. Commun.*, 2014, 50, 5143-5155.
136. J. Xie, Y. Zheng and J. Y. Ying, *J. Am. Chem. Soc.*, 2009, 131, 888-889.
137. J. Qiao, X. Mu, L. Qi, J. Deng and L. Mao, *Chem. Commun.*, 2013, 49, 8030-8032.
138. J. Chen, F. Saeki, B. J. Wiley, H. Cang, M. J. Cobb, Z.-Y. Li, L. Au, H. Zhang, M. B. Kimmey and X. Li, *Nano Lett.*, 2005, 5, 473-477.
139. H. Sun, J. Su, Q. Meng, Q. Yin, L. Chen, W. Gu, Z. Zhang, H. Yu, P. Zhang and S. Wang, *Adv. Funct. Mater.*, 2017, 14, 1604300.

Chapter 2

Facile preparation of albumin-stabilized gold nanostars for targeted photothermal ablation of cancer cells

2.1 Summary

As the advance of nanotechnology, various functional nanoplatforms have been developed for diagnosis and treatments of early-stage cancer. Gold nanostars (AuNSs) have been extensively studied as photothermal conversion agents for cancer therapy due to their high photothermal conversion efficiency. Surface coating or modification is required to improve their colloidal stability and biocompatibility for biomedical applications. Moreover, targeting delivery of AuNSs into the tumor sites is an effective approach to improve their therapeutic efficiency. In this part, we report the use of folic acid-bovine serum albumin conjugation (BSA-FA) stabilized AuNSs (BSA-FA-AuNSs) as agents for targeted photothermal ablation of human cervical cancer cells (HeLa cells). In our approach, BSA-FA conjugation was first synthesized *via* an amidation, which was further used as a stabilizer to coat AuNSs for surface modification. The BSA-FA-AuNSs showed good dispersibility and colloidal stability in different medium. The strong absorption property in near-infrared (NIR) regions enabled the increasing temperature of AuNSs under NIR laser irradiation. The BSA-FA-AuNSs not only had a very low cytotoxicity in the studied concentrations, but also showed targeting specificity to FA receptors-overexpressed cancer cells, which was confirmed by studying the cellular uptake. In addition, the BSA-FA-AuNSs displayed a much better therapeutic efficiency to HeLa cells under the NIR laser compared with BSA-AuNSs without FA modification. The BSA-FA-AuNSs should have a great potential as photothermal conversion agents for the receptor-mediated treatment of cancer cells.

2.2 Introduction

Development of multifunctional nanoplatforms for cancer therapy still remains a great challenge.

Recently, photothermal therapy (PTT) as a non-invasive and convenient strategy for destroying cancer cells has received considerable attention.[1-3] Different from other treatments, PTT has distinct advantages of focalizing the efficient therapy on diseased region and reducing the undesirable damage to healthy tissues.[4, 5] For practical application of PTT, it generally needs photothermal conversion agents to absorb the near-infrared (NIR) light and convert it into heat.[6-8] Nowadays, a variety of nanodevices have been widely studied for PTT as the development of nanoscience and nanotechnology, for example, carbon nanotubes,[9, 10] graphene oxide,[11, 12] copper sulfide,[13, 14] molybdenum sulfide,[15] tungsten oxide[16] and gold nanostructures.[17-19] Among them, gold nanostars (AuNSs) have been considered as an ideal photothermal conversion agent due to their facile large scale preparation, tunable plasmon band, large absorption cross section and high photothermal conversion efficiency.[4, 20]

For biomedical application, photothermal conversion agents should have appropriate surface coating to provide excellent physiological stability, biocompatibility and the ability to be further functionalized. Maybe it is a good strategy to coat AuNs by using poly(ethylene glycol) (PEG) as stabilizers.[4, 21, 22] However, the non-biodegradability and difficulty for ligand incorporation of PEG should be considered in future researches.[23, 24] On the other hand, as a naturally derived polymer, bovine serum albumin (BSA) has recently been proposed as a superior alternative.[25] Benefiting from the numerous advantages such as non-toxicity, good biocompatibility, excellent biodegradability, good stability in biological environment, low immunogenicity and presence of functional groups,[26, 27] BSA has been widely used as stabilizing agents or drug carriers in the biomedical fields.[28-30] In addition, the BSA-coated nanoparticles have been found to be taken up preferentially by cancer cells as compared to normal cells,[25, 31, 32] which enables their potential application for cancer therapy and diagnosis.

For diagnosis or/and therapy of cancer, it is essential to increase the cellular uptake of agents by cancer cells while reduce their accumulation in normal tissues.[33] Various targeting ligands have been conjugated to these agents for selective binding to cancer cells.[34-36] Among the reported ligands, folic acid (FA) has been widely studied because of its high affinity to FA receptors that are overexpressed in several human carcinomas including breast, ovary, endometrium, kidney, lung, head, neck, brain and myeloid cancers.[37, 38] Up to now, many reports have demonstrated that FA-modified nanoplatforms can be successfully used for controlled drug delivery, molecular imaging and thermal therapy.[39-41]

In this part of study, a facile seed-mediated growth method was used to prepare BSA-FA conjugation stabilized AuNSs (BSA-FA-AuNSs) for targeted photothermal ablation of cancer cells. The abundant functional groups on the surface of BSA make it possible to modify with FA and adsorb onto AuNSs (Scheme 1). The prepared BSA-FA-AuNSs were dispersible in water and colloidally stable in different medium because of the surface coating of BSA. Moreover, the BSA-FA-AuNSs had obvious absorption peaks in the NIR regions, which induced the significant temperature increase under the irradiation. The cell viability assay and morphology observation revealed low cytotoxicity of BSA-FA-AuNSs in the studied concentration range. Compared with BSA-AuNSss without FA modification, the BSA-FA-AuNSs displayed a significantly enhanced uptake by cancer cells *via* the receptor-mediated pathway. Taking into consideration of the high photothermal conversion efficiency, the BSA-FA-AuNSs should have a great potential for targeted photothermal ablation of cancer cells.

2.3 Materials and methods

2.3.1 Materials

Hydrogen tetrachloroaurate tetrahydrate **(**$HAuCl_4 \cdot 4H_2O$, 99.9%), folic acid (FA), trisodium citrate dihydrate, N-hydroxysuccinimide (NHS), nitric acid and hydrochloric acid were purchased from Wako Pure Industries, Ltd. (Tokyo, Japan). Bovine serum albumin (BSA), silver nitrate ($AgNO_3$), ascorbic acid (AA), sodium borohydride ($NaBH_4$), Eagle's Minimun Essential Medium (EMEM), penicillin, streptomycin and trypsin/EDTA were purchased from Sigma-Aldrich (St. Louis, MO, USA). Fetal bovine serum (FBS) was purchased from Gibco Laboratories (Grand Island, NY, USA). 1-ethyl-3-[3-dimethylaminopropyl] carbodiimide hydrochloride (EDC) was from Peptide Institute, Inc. (Osaka, Japan). WST-1 reagent was obtained from Roche Molecular Biochemicals (Mannheim, Germany). Cellstain Live-Dead Double Staining kit was purchased from Dojindo Laboratories (Kumamoto, Japan). All the chemicals and materials were used as received without further purification. The water in all experiments was purified by Q-POD Milli-Q water purification system (Millipore Corp., Billerica, MA, USA) with resistivity of 18.2 MΩ.cm.

2.3.2 Characterization techniques

UV-vis spectra of the samples dispersed in water were recorded using a V-660 UV-Vis Spectrophotometer (Jasco Corp., Tokyo, Japan). The infrared spectra of the lyophilized samples was obtained with a Fourier transformed infrared (FTIR) spectrometer (FTIR-8400S, Shimadzu Corp., Tokyo, Japan). Thermal gravimetric analysis (TGA) was performed on a Seiko Exstar 6000 TG/DTA 6200 thermal gravimetric analyzer (SII Nanotechnology, Tokyo, Japan) under nitrogen gas from 30 °C to 1000 °C at a heating rate of 20 °C/min. Surface zeta potential and hydrodynamic size were measured by using a Delsa™ Nano C Particle Analyzer (Beckman Coulter, Fullerton, CA, USA). The morphology and size of particles were characterized by JEOL 2100F transmission electron microscopy (TEM, JEOL, Tokyo, Japan) operating at 200 kV. The samples dispersed in water were dropped onto a carbon-coated copper grid and left until dried. The particle size distributions were obtained by measuring more than 200 particles in different TEM images using ImageJ software (http://rsb.info.nih.gov/ij/download.html). The element concentration was analyzed by a Leeman Prodigy Inductively Coupled Plasma-Optical Emission Spectroscopy (ICP-OES, SPS3520UV-DD) system (SII nano technology Inc., Tokyo, Japan).

2.3.3 Synthesis of BSA-FA conjugation

The BSA-FA conjugation was synthesized by using EDC as cross-linker according to the previously reported procedure.[42] Briefly, 50 mg FA (0.11 mmol) was mixed with 30 mg EDC (0.15 mmol) and 20 mg NHS (0.17 mmol) in 10 mL DMSO under stirring at room temperature for 3 hours to activate the terminal carboxylate of FA. The activated FA solution was added dropwise into 30 mL aqueous solution of BSA (600.0 mg) under vigorous magnetic stirring (1000 rpm) at room temperature in the dark for 3 days. After that, the resultant mixture was continuously dialyzed against phosphate buffered saline (PBS) (3 times) and water (6 times) in 2 L beaker for 3 days using a dialysis membrane with molecular weight cut-off (MWCO)

of 1000 to remove the free FA and other reactants in excess. The BSA-FA powder was obtained by lyophilization and stored at -20 °C for further use.

2.3.4 Synthesis of BSA-FA-AuNSs

The BSA-FA-AuNSs were synthesized by a facile seed-mediated growth method. Prior to the synthesis, Au seed solution was firstly prepared *via* a chemical reduction route according to the previous work with some modification.[43] Briefly, 4 mL aqueous solution of trisodium citrate (35.4 mg) was rapidly added into 90 mL $HAuCl_4$ solution (0.1 mg/mL) under vigorous magnetic stirring. Subsequently, 1 mL icy cold $NaBH_4$ aqueous solution (3.3 mg) was rapidly added into the above mixture. After stirring at room temperature for 2 hours, the Au seeds solution was obtained and stored at 4 °C for further use. For the synthesis of BSA-FA-AuNSs, 0.75 mL of $HAuCl_4$ solution (30 mg/mL), 0.75 mL of Au seed solution, 0.50 mL of $AgNO_3$ solution (5 mg/mL) and 0.50 mL of AA solution (50 mg/mL) were added into 20 mL water sequentially under gently stirring. 30 seconds later, 10 mL of BSA-FA solution (10 mg/mL) was added into the growth solution and the mixture was kept stirring at room temperature for 12 hours. The products were then collected by centrifugation (10000 rpm, 5 minutes), washed with water twice, dispersed in 12 mL water and stored at 4 °C for further use. For comparison, BSA-AuNSs without FA modification were also prepared by the same method by using BSA instead of BSA-FA conjugation. Naked AuNSs were synthesized in the growth solution without BSA or BSA-FA conjugation.

2.3.5 Photothermal property of BSA-AuNSs and BSA-FA-AuNSs

To investigate the photothermal property of prepared NSs, 80 μL aqueous suspension of BSA-AuNSs or BSA-FA-AuNSs at different Au concentrations (0.5, 1.0 and 2.0 mM) in quartz cuvettes was irradiated by a 805 nm laser (Thorlabs Inc., Newton, New Jersey, USA) with a power density of 1.6 W/cm^2 for 300 seconds. During the irradiation, a digital thermometer (AS ONE Corp., Osaka, Japan) equipped with a thermocouple probe was used to measure the temperature of different samples every 10 seconds.

2.3.6 Cell culture

Human cervical carcinoma cell line (HeLa cells) was purchased from Cascade Biologics (JCRB cell bank, Tokyo, Japan). The cells were cultured in regular EMEM medium supplemented with 10% heat-inactivated FBS, penicillin (100 U/mL) and streptomycin (100 μg/mL) at 37 °C and 5% CO_2. Cells were seeded in 75 cm^2 tissue culture flasks and passaged by using 0.25% trypsin/EDTA solution.

2.3.7 Cytotoxicity assay and morphology observation

In vitro cytotoxicity of BSA-AuNSs or BSA-FA-AuNSs was evaluated by WST-1 assay of HeLa cells. The cells were seeded into 96-well plates with 100 μL fresh medium at a density of 1×10^4 cells/well and allowed to adhere for 24 hours. After 24 hours of culture, the medium was discarded carefully and 100 μL fresh medium containing pure PBS buffer (control), BSA-AuNSs or BSA-FA-AuNSs at different Au concentrations (0.1-0.6 mM) was added into each well. After incubation at 37 °C and 5% CO_2 for 24 hours, the medium was replaced with 110 μL of WST-1 solution (10 μL of WST-1 stock solution diluted with 100

μL of complete medium) and the cells were further cultured for 3 hours. The absorbance of each well was measured at 440 nm by using a plate reader (Benchmark Plus, Bio-Rad, Hercules, CA, USA) to determine the cell viability. Mean and standard deviation were reported by performing five parallel wells for each sample.

To further study the cytotoxicity of the prepared BSA-AuNSs and BSA-FA-AuNSs, the morphology of cells after being cultured with BSA-AuNSs or BSA-FA-AuNSs at the Au concentration of 0.6 mM for 24 hours was observed by an optical microscope (Olympus, Japan) with a magnification of 200× for each sample. The cells without treatments were used as control.

2.3.8 *In vitro* targeted cellular uptake assay

Quantitative assay of *in vitro* cellular uptake was performed by using ICP-OES. HeLa cells were seeded into 6-well plates at a density of 2×10^6 cells/well and cultured for 12 hours to allow the cells adhesion. The cells were then incubated with BSA-AuNSs or BSA-FA-AuNSs at different Au concentrations (0.2, 0.4 and 0.6 mM) at 37 ºC and 5% CO_2 for 6 hours. Afterwards, the cell culture medium was discarded carefully and the cells were washed 3 times with warm PBS to remove the free particles. The cells were then treated with trypsin/EDTA solution, collected by centrifugation (1000 rpm, 5 minutes) and suspended in 1.1 mL PBS. 0.1 mL cell suspension was taken out to confirm the cell concentration by a hemocytometer. The remaining cells were lysed with 1.0 mL aqua regia solution (nitric acid/hydrochloric acid, v/v = 1:3) for more than 2 days. After being diluted 5 times with water, the Au content of each sample was determined by ICP-OES.

2.3.9 Photothermal ablation of HeLa cells

HeLa cells were cultured for 24 hours to bring the cells to confluence after being seeded into 96-well plates with 100 μL fresh medium at a density of 1×10^4 cells/well. Subsequently, the cell culture medium was replaced with 100 μL fresh medium containing pure PBS buffer (control), BSA-AuNSs or BSA-FA-AuNSs at different Au concentrations (0.2, 0.4 and 0.6 mM). The cells were incubated at 37 ºC and 5% CO_2 for 18 hours and then exposed to an 805 nm laser with a power density of 1.6 W/cm^2 for 10 minutes. During the laser irradiation, the cells were maintained at room temperature. After the laser irradiation, the cells were cultured for additional 4 hours at 37 ºC and then the cell viabilities were determined by WST-1 assay. For comparison, the cells treated with BSA-AuNSs or BSA-FA-AuNSs under the same conditions without laser irradiation were used as controls.

Live/dead staining with a Cellstain Live-Dead Double Staining kit was also used to confirm the live and dead cells after the laser irradiation. HeLa cells were seeded into 24-well plates with 500 μL fresh medium at a density of 1.5×10^5 cells/well for 12 hours. The adherent cells were incubated with BSA-AuNSs or BSA-FA-AuNSs at the Au concentrations of 0.6 mM for 18 hours and then exposed under the laser for 10 minutes as described above. After further culture for 4 hours, the cells were washed twice with warm PBS, and incubated in serum-free EMEM medium containing calcein-AM and propidium iodide (PI) for 15 minutes.[44] Following that an inverted fluorescence microscope (Olympus, Japan) was used to capture the live/dead images.

2.3.10 Statistical analysis

All data were reported as mean ± standard deviation (SD). One-way ANOVA statistical analysis was performed to evaluate the significance of the experimental data. 0.05 was selected as the significance level and the data were indicated with (*) for $p < 0.05$, (**) for $p < 0.01$ and (***) for $p < 0.001$, respectively.

2.4 Results and discussion

2.4.1 Synthesis and characterization of BSA-FA-AuNSs

The schematic preparation process of BSA-FA-AuNSs is shown in Figure 2.1a. BSA was firstly modified with FA to form BSA-FA conjugation, which was used as a stabilizer to prepare BSA-FA-AuNSs in the seed-mediated growth solution. In general, cetyltrimethylammonium bromide (CTAB) was used as capping surfactant to synthesize AuNSs. To improve the biocompatibility, the AuNSs were further treated troublesomely to remove the toxic CTAB and then coated with some polymer.[6, 45] In this work, the strong adsorption capacity of BSA onto AuNSs promoted us to prepare the BSA-FA-AuNSs *via* this facile method. Through the receptor-mediated cellular binding and endocytosis, the BSA-FA-AuNSs should have a great potential for use of targeted photothermal ablation of cancer cells.

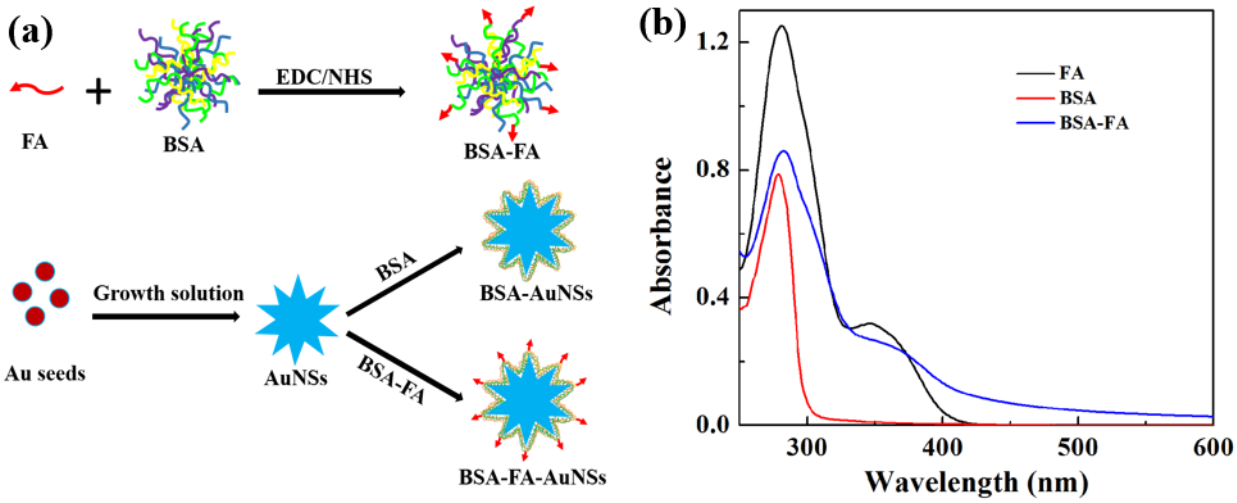

Figure 2.1 Schematic illustration of synthesis of the BSA-FA conjugation, BSA-AuNSs and BSA-FA-AuNSs (a), UV-Vis spectra of FA, BSA and BSA-FA conjugation (b).

To prepare the BSA-FA-AuNSs, BSA-FA conjugation was first synthesized and characterized. UV-Vis spectroscopy was performed to confirm the successful synthesis of BSA-FA (Figure 2.1b). It was clearly shown that the characteristic absorption peak of FA at 365 nm was observed in the absorption spectrum of BSA-FA. In contrast, no absorption feature was seen at the same wavelength for BSA without modification. An UV-Vis calibration curve of FA was drawn according to the FA concentration versus the absorption at 365 nm. The average number of FA molecules linked to each BSA was estimated to be 7.5 based on the calibration curve. It should be noted that the process of chemical modification and purification would not denatured the BSA.

The Au seed solution was prepared *via* a $NaBH_4$ reduction chemistry by using trisodium citrate as a stabilizer. Next, in the presence of BSA or BSA-FA conjugation, a seed-mediated growth method was used to generate the BSA-AuNSs and BSA-FA-AuNSs, respectively. FTIR spectroscopy was carried out to characterize the coating of BSA or BSA-FA onto the surface of NSs (Figure 2.2a). Both BSA-AuNSs and BSA-FA-AuNSs displayed two obvious peak at 1640 cm^{-1} and 1524 cm^{-1}, which should be attributed to the amide I and amide II band in the BSA, respectively.[3] In contrast, for the naked AuNSs without coating, no peak was observed at these wavenumbers, indicating the successful coating of BSA or BSA-FA onto the surface of NSs. The content of protein in the BSA-AuNSs and BSA-FA-AuNSs was quantitatively analyzed by TGA (Figure 2.2b). It was clear that the naked AuNSs only exhibited a weight loss of 1.4% because of the existence of trisodium citrate used to stabilize the Au seeds. After the coating, the weight loss of BSA-AuNSs and BSA-FA-AuNSs was measured to be 17.1% and 15.3%, respectively. Hence, the percentage of BSA and BSA-FA coated on the surface was calculated to be 15.7% and 13.9%, respectively.

Dynamic light scattering (DLS) was used to measure the average size of the NSs dispersed in water (Figure 2.2c). The hydrodynamic size of both BSA-AuNSs (152.8 ± 9.7 nm) and BSA-FA-AuNSs (169.7 ± 11.3 nm) was bigger than that of the naked AuNSs (115.6 ± 6.9 nm). This increased size should be ascribed to the formation of coating layer on the surface. Moreover, zeta potential was also measured to confirm the surface charges of prepared NSs. As shown in Figure 2.2d, the zeta potential of the naked AuNSs, BSA-AuNSs and BSA-FA-AuNSs was -30.8 ± 2.2 mV, -26.9 ± 1.7 mV and -24.2 ± 0.3 mV, respectively. Modification of naked AuNSs with BSA and BSA-FA decreased the zeta potential of NSs.

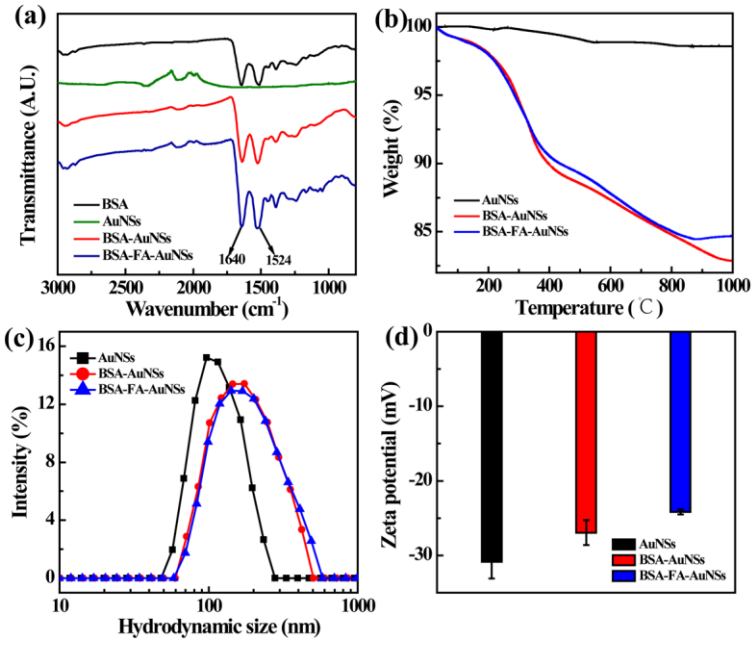

Figure 2.2 FTIR spectra of BSA, naked AuNSs, BSA-AuNSs and BSA-FA-AuNSs (a); TGA curves (b), hydrodynamic size (c) and zeta potential (d) of the naked AuNSs, BSA-AuNSs and BSA-FA-AuNSs.

The morphology and size of the BSA-AuNSs and BSA-FA-AuNSs were characterized by TEM (Figure 2.3). From the TEM images, star-like particles with a transparent polymer shell were clearly seen for both BSA-AuNSs (Figure 2.3a) and BSA-FA-AuNSs (Figure 2.3c). The mean size (tip to tip) was measured to be

96.6 ± 30.5 nm for BSA-AuNSs (Figure 2.3b) and 100.0 ± 24.4 nm for BSA-FA-AuNSs (Figure 2.3d), respectively. The sizes of BSA-AuNSs and BSA-FA-AuNSs were bigger than that of the PEGylated AuNSs (～60 nm).[4, 49]

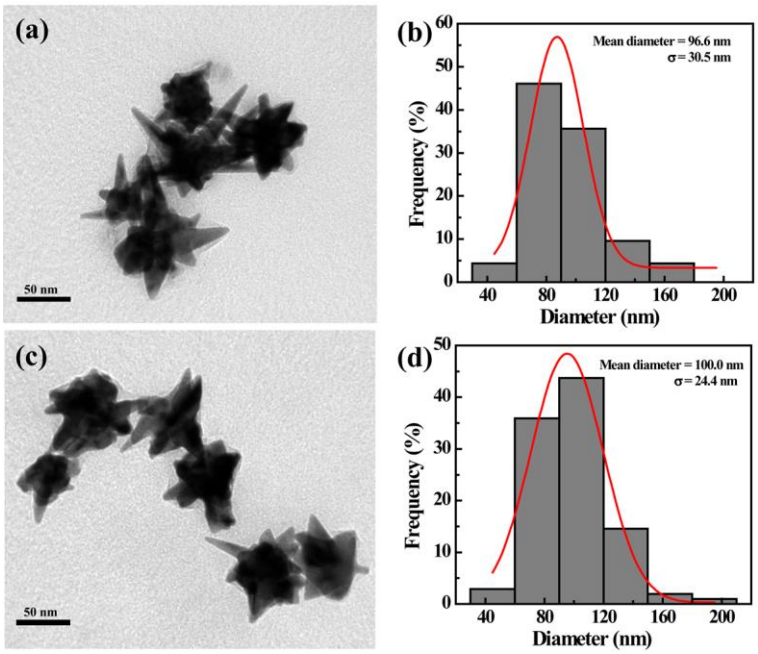

Figure 2.3 TEM images (a, c) and size distribution histograms (b, d) of BSA-AuNSs (a, b) and BSA-FA-AuNSs (c, d).

Good colloidal stability is very necessary for nanomaterials to be used as photothermal conversion agents for cancer therapy. The colloidal stability of the prepared BSA-AuNSs and BSA-FA-AuNSs was checked by DLS (Figure 2.4a). The results showed that there was no obvious increase in hydrodynamic size of both NSs dispersed in water over a period of 5 days. In addition, the BSA-AuNSs and BSA-FA-AuNSs were dispersed in water, PBS, or cell culture medium (containing 10% FBS) and the dispersion solutions were stored at 4 °C for 5 days to further check their stability in different medium. As expected, no precipitates were observed for both NSs no matter in water, PBS or cell culture medium (Figure 2.4b).

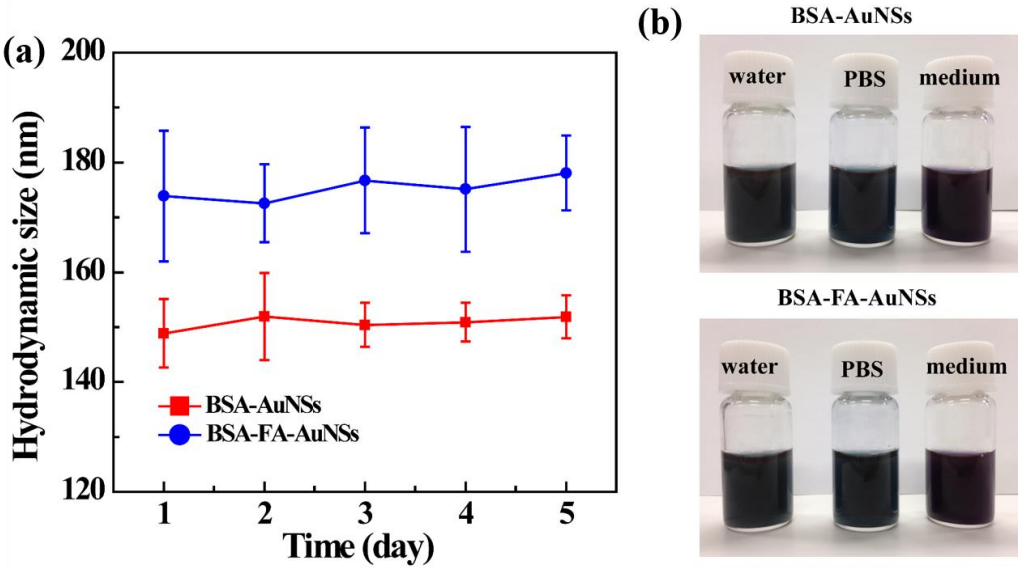

Figure 2.4 Hydrodynamic sizes of BSA-AuNSs and BSA-FA-AuNSs dispersed in water at different storage time (a). The photos of BSA-AuNSs and BSA-FA-AuNSs dispersed in water, PBS and cell culture medium (containing 10% FBS) over a period of 5 days (b).

2.4.2 Photothermal property of BSA-AuNSs and BSA-FA-AuNSs

Many nanomaterials can be used as photothermal conversion agents for hyperthermic therapy mainly due to their strong surface plasmon resonance (SPR) absorption intensity in near infrafed (NIR) region. In this study, an UV-Vis spectroscope was used to investigate the optical property of the prepared NSs (Figure 2.5a). It was clear that the BSA-AuNSs displayed an obvious SPR peak at 750 nm and a slight red-shift (from 750 nm to 763 nm) in the peak position was detected for BSA-FA-AuNSs due to the modification of FA.

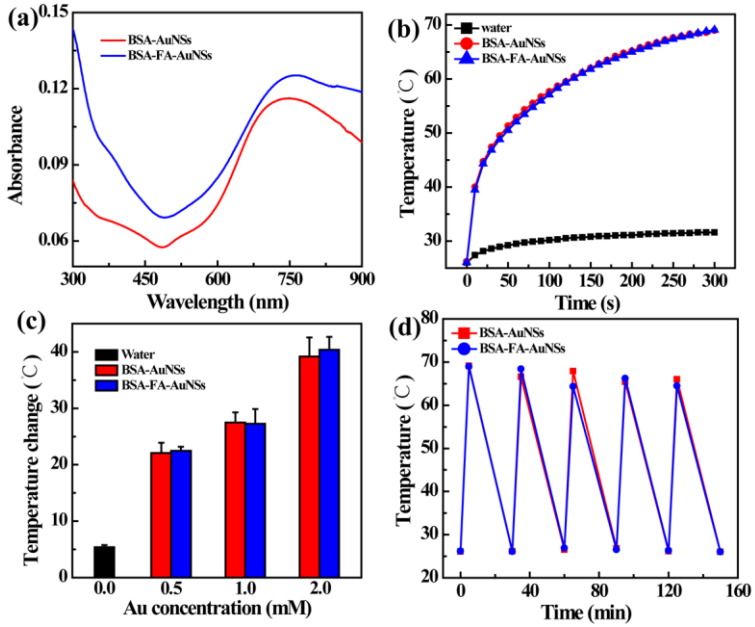

Figure 2.5 UV-Vis spectra of the BSA-AuNSs and BSA-FA-AuNSs (a); temperature increase of water, an aqueous solution of BSA-AuNSs or BSA-FA-AuNSs (b); temperature change of an aqueous solution of BSA-AuNSs or BSA-FA-AuNSs at different Au concentrations (c); temperature change of an aqueous solution of BSA-AuNSs or BSA-FA-AuNSs over five laser on/off cycles (d).

The strong absorption in the NIR region for both BSA-AuNSs and BSA-FA-AuNSs would enable their application of photothermal therapy. The temperature change of an aqueous solution containing BSA-AuNSs or BSA-FA-AuNSs at the Au concentration of 2.0 mM under laser irradiation was monitored to study their photothermal performance, the starting temperature was 26 ^{o}C for all samples (Figure 2.5b). The temperature of the BSA-AuNSs and BSA-FA-AuNSs aqueous solutions increased rapidly and reached 69 ^{o}C after 300 seconds irradiation. In contrast, the control experiment of pure water only showed a negligible temperature increase under the same irradiation condition. The temperature change of the NSs at different Au concentrations (0.5, 1.0 and 2.0 mM) was also studied. As shown in Figure 2.5c, the temperature change displayed a concentration dependent manner and higher concentration resulted in bigger temperature change. It should be noted that even at a low Au concentration of 0.5 mM, the temperature increased 22.5 °C for

BSA-FA-AuNSs and 22.0 °C for BSA-FA-AuNSs after laser irradiation for 5 minutes. In contrast, the previously reported AuNS-PEG nanoconjugates only attained a maximum temperature increase of 18 °C at a concentration of 1×10^{10} particles/mL under a laser irradiation of 3 W/cm^2 for 10 minutes.[51] In another work, human serum albumin/indocyanine green/FA complex coated AuNSs displayed a temperature increase of 19 °C after 5 minutes of irradiation (2 W/cm^2).[52] These results and comparisons suggested the high photothermal conversion efficiency of BSA-AuNSs and BSA-FA-AuNSs. Moreover, five cycles of laser on/off (the samples were irradiated by 805 nm laser for 5 minutes and then cooled down to room temperature without laser for 25 minutes) were performed to evaluate the photothermal stability of the prepared NSs. The temperature increase showed no significant change for BSA-AuNSs and BSA-FA-AuNSs after five repeating laser on/off cycles (Figure 2.5d).

2.4.3 Cytotoxicity assay, morphology observation and *in vitro* targeted cellular uptake assay

For biomedical applications, the photothermal conversion agents should exhibit low toxicity to cells. Therefore, the cytotoxicity of the prepared BSA-AuNSs and BSA-FA-AuNSs was evaluated by using WST-1 assay with HeLa cells (Figure 2.6a). It was clear that the HeLa cells treated with BSA-AuNSs and BSA-FA-AuNSs at the studied concentration range (0.1-0.6 mM) for 24 hours still kept a very high viability compared with the control cells (treated with PBS). The percentages of viable cells after treatment with BSA-AuNSs and BSA-FA-AuNSs was 91.0 ± 11.7% and 92.1 ± 4.1%, respectively, even at high Au concentration of 0.6 mM. In addition, the morphology of HeLa cells treated with BSA-AuNSs and BSA-FA-AuNSs at the Au concentration of 0.6 mM for 24 hours was observed by optical microscopy to further confirm their cytotoxicity (Figure 2.6b). Clearly, the cells treated with both BSA-AuNSs and BSA-FA-AuNSs showed a normal and healthy morphology, which was similar to that of the control cells treated with PBS. The results of both WST-1 assay and cell morphology observation suggested the prepared BSA-AuNSs and BSA-FA-AuNSs had very low cytotoxicity in the studied concentration range, which is essential for their further usage as photothermal conversion agents.

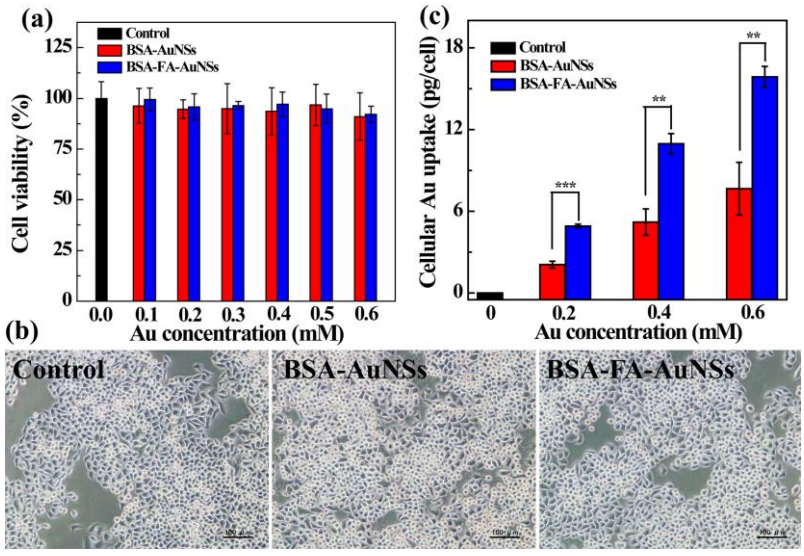

Figure 2.6 Cell viability of HeLa cells treated with PBS (control), the BSA-AuNSs and BSA-FA-AuNSs at different Au concentrations (0.1-0.6 mM) for 24 hours (a); optical microscopy of HeLa cells treated with PBS (Control),

BSA-AuNSs and BSA-FA-AuNSs at the Au concentration of 0.6 mM for 24 hours (b); Cellular uptake of NSs by HeLa cells after treatment with PBS (control), the BSA-AuNSs and BSA-FA-AuNSs at the Au concentration of 0.2, 0.4 and 0.6 mM for 6 hours (c).

FA receptors are known to be overexpressed in HeLa cells, which has be confirmed by western blot analysis in a previous work.[53] To explore the FA-mediated targeting specificity of BSA-FA-AuNSs to HeLa cells, ICP-OES was used to analyze the cellular uptake. The BSA-AuNSs without FA modification were also used for comparison. As shown in Figure 2.6c, the cellular uptake increased as a function of Au concentration for both NSs. At the same Au concentration, the HeLa cells treated with BSA-FA-AuNSs displayed much higher uptake than those treated with BSA-AuNSs. These results indicated that the BSA-FA-AuNSs could be specifically taken up by the HeLa cells overexpressing FA receptors *via* ligand-mediated endocytosis pathway, agreeing with the previously reported works.[13, 39]

2.4.4 Photothermal ablation of HeLa cells

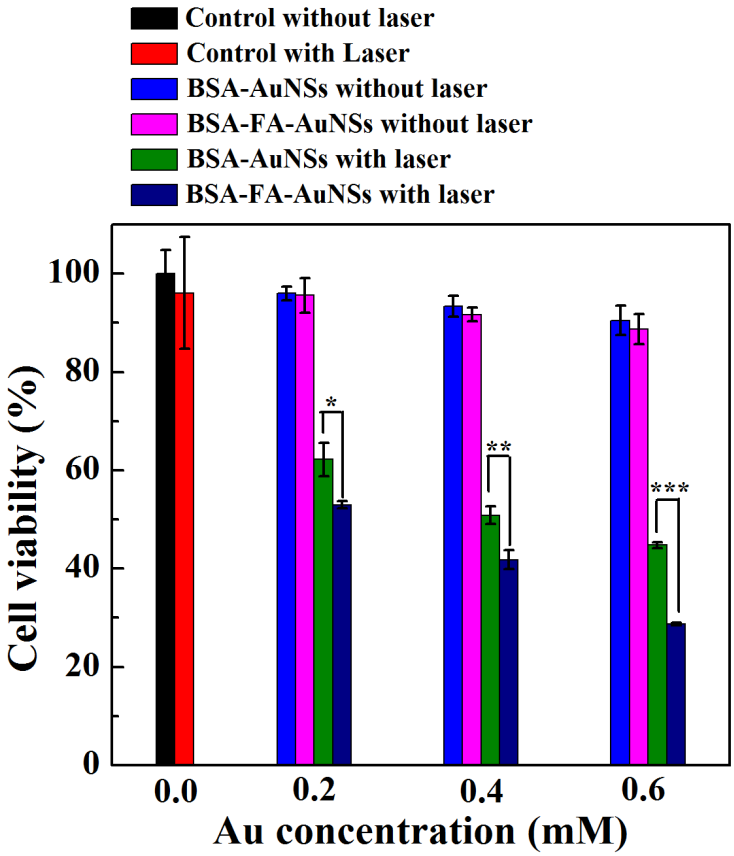

Figure 2.7 Cell viability of HeLa cells treated with PBS (control), the BSA-AuNSs and BSA-FA-AuNSs at different Au concentrations (0.2, 0.4 and 0.6 mM) and with or without laser irradiation.

The prepared BSA-FA-AuNSs had high photothermal conversion efficiency and targeting specificity to the cancer cells that overexpress FA receptors. These properties would enable application of the BSA-FA-AuNSs for targeted photothermal ablation of cancer cells. To demonstrate the effect, cell viability

of treated HeLa cells with or without laser irradiation was performed (Figure 2.7). Clearly, the control cells even irradiated with laser for 10 minutes still had a very high cell viability compared with the control cells without laser, which suggested laser irradiation itself would not have any obvious influence on the cell viability. The cells treated with BSA-AuNSs or BSA-FA-AuNSs at different Au concentrations without laser irradiation either did not display any obvious viability change. In contrast, cell viability decreased significantly when the cells treated with BSA-AuNSs or BSA-FA-AuNSs were exposed under the laser even at a very low concentration (0.2-0.6 mM), which may be due to the high photothermal conversion efficiency, extended laser irradiation time and effective cellular uptake. What's more, higher concentration resulted in lower cell viability for both BSA-AuNSs and BSA-FA-AuNSs. However, at the same Au concentration, the cell viability of the cells treated with the BSA-FA-AuNSs was significantly lower than that of the cells treated with BSA-AuNSs after the laser irradiation. For example, when the Au concentration was 0.6 mM, 71.3 ± 0.3% of the cells were killed by the BSA-FA-AuNSs under the laser irradiation. In comparison, BSA-AuNSs treated cells showed 55.2 ± 0.6% death rate after laser irradiation. The better therapeutic efficiency of BSA-FA-AuNSs should be due to the enhanced cellular uptake through receptor-mediated pathway, which was demonstrated by the ICP-OES results.

The photothermal therapeutic efficiency of the prepared NSs was further evaluated by the live/dead staining (Figure 2.8). For the control cells with or without laser irradiation, almost all the cells were live (green color). Moreover, negligible dead cells (red color) were observed for the cells incubated with BSA-AuNSs or BSA-FA-AuNSs without laser irradiation. However, when the cells were treated with the NSs and then exposed under the laser, most of the cells were killed and only a small portion of live cells were observed. Less number of live cells in the BSA-FA-AuNSs group was observed than that in the BSA-AuNSs group. The results of WST-1 assay and live/dead staining demonstrated that the BSA-FA-AuNSs had a great potential to effectively ablate cancer cells overexpressing FA receptors by combination with NIR laser irradiation.

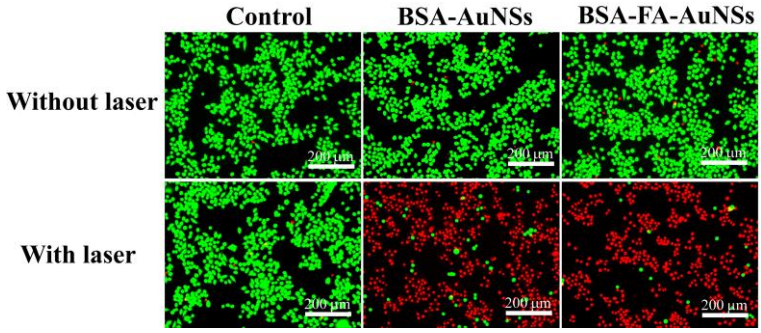

Figure 2.8 Live/dead staining of HeLa cells treated with PBS (control), the BSA-AuNSs and BSA-FA-AuNSs at the Au concentration of 0.6 mM with or without laser irradiation.

2.5 Conclusions

In summary, BSA-FA-AuNSs was successfully prepared through a facile seed-mediated growth method for targeted photothermal ablation of cancer cells. The surface coating of BSA-FA could render the nanoparticles with good water-solubility, excellent colloidal stability and low cytotoxicity in the studied

concentration, as well as targeting specificity to HeLa cells overexpressing FA receptors. The strong absorption in the NIR region would enable the BSA-FA-AuNSs to be used as photothermal conversion agents for cancer therapy. Taking into consideration of the numerous functional groups and drug loading capacity of BSA, the BSA-FA-AuNSs may be developed into multifunctional theranostic agents for diagnosis and treatment of different cancers.

2.6 References

1. H. Chen, X. Chi, B. Li, M. Zhang, Y. Ma, S. Achilefu and Y. Gu, *Biomater. Sci.*, 2014, 2, 996-1006.
2. X. Tu, Y. Ma, Y. Cao, J. Huang, M. Zhang and Z. Zhang, *J. Mater. Chem. B*, 2014, 2, 2184-2192.
3. M. Zhang, Y. Cao, L. Wang, Y. Ma, X. Tu and Z. Zhang, *ACS Appl. Mater. Interfaces*, 2015, 7, 4650-4658.
4. H. Jo, H. Youn, S. Lee and C. Ban, *J. Mater. Chem. B*, 2014, 2, 4862-4867.
5. Z. Zhou, B. Kong, C. Yu, X. Shi, M. Wang, W. Liu, Y. Sun, Y. Zhang, H. Yang and S. Yang, *Sci. Rep.*, 2014, 4, 3653.
6. J. Li, Y. Hu, J. Yang, P. Wei, W. Sun, M. Shen, G. Zhang and X. Shi, *Biomaterials*, 2015, 38, 10-21.
7. J.-G. Piao, L. Wang, F. Gao, Y.-Z. You, Y. Xiong and L. Yang, *ACS Nano*, 2014, 8, 10414-10425.
8. K. Yang, L. Hu, X. Ma, S. Ye, L. Cheng, X. Shi, C. Li, Y. Li and Z. Liu, *Adv. Mater.*, 2012, 24, 1868-1872.
9. F. Zhou, S. Wu, S. Song, W. R. Chen, D. E. Resasco and D. Xing, *Biomaterials*, 2012, 33, 3235-3242.
10. X. Liu, H. Tao, K. Yang, S. Zhang, S.-T. Lee and Z. Liu, *Biomaterials*, 2011, 32, 144-151.
11. J. T. Robinson, S. M. Tabakman, Y. Liang, H. Wang, H. Sanchez Casalongue, D. Vinh and H. Dai, *J. Am. Chem. Soc.*, 2011, 133, 6825-6831.
12. W. Zhang, Z. Guo, D. Huang, Z. Liu, X. Guo and H. Zhong, *Biomaterials*, 2011, 32, 8555-8561.
13. X. Liu, F. Fu, K. Xu, R. Zou, J. Yang, Q. Wang, Q. Liu, Z. Xiao and J. Hu, *J. Mater. Chem. B*, 2014, 2, 5358-5367.
14. L. Guo, D. D. Yan, D. Yang, Y. Li, X. Wang, O. Zalewski, B. Yan and W. Lu, *ACS Nano*, 2014, 8, 5670-5681.
15. S. Wang, K. Li, Y. Chen, H. Chen, M. Ma, J. Feng, Q. Zhao and J. Shi, *Biomaterials*, 2015, 39, 206-217.
16. Z. Chen, Q. Wang, H. Wang, L. Zhang, G. Song, L. Song, J. Hu, H. Wang, J. Liu and M. Zhu, *Adv. Mater.*, 2013, 25, 2095-2100.
17. B. Jang, J.-Y. Park, C.-H. Tung, I.-H. Kim and Y. Choi, *ACS Nano*, 2011, 5, 1086-1094.
18. Y. Ma, X. Liang, S. Tong, G. Bao, Q. Ren and Z. Dai, *Adv. Funct. Mater.*, 2013, 23, 815-822.
19. G.-S. Park, H. Kwon, D. W. Kwak, S. Y. Park, M. Kim, J.-H. Lee, H. Han, S. Heo, X. S. Li and J. H. Lee, *Nano Lett.*, 2012, 12, 1638-1642.
20. H. Chen, X. Zhang, S. Dai, Y. Ma, S. Cui, S. Achilefu and Y. Gu, *Theranostics*, 2013, 3, 633.
21. S. Wang, P. Huang, L. Nie, R. Xing, D. Liu, Z. Wang, J. Lin, S. Chen, G. Niu and G. Lu, *Adv.*

Mater., 2013, 25, 3055-3061.

22. L. Nie, S. Wang, X. Wang, P. Rong, Y. Ma, G. Liu, P. Huang, G. Lu and X. Chen, *Small*, 2014, 10, 1585-1593.
23. K. Knop, R. Hoogenboom, D. Fischer and U. S. Schubert, *Angew.Chem. Int. Ed.*, 2010, 49, 6288-6308.
24. K. P. García, K. Zarschler, L. Barbaro, J. A. Barreto, W. O'Malley, L. Spiccia, H. Stephan and B. Graham, *Small*, 2014, 10, 2516-2529.
25. P. Murawala, A. Tirmale, A. Shiras and B. Prasad, *Mater. Sci. Eng., C*, 2014, 34, 158-167.
26. L. Qi, Y. Guo, J. Luan, D. Zhang, Z. Zhao and Y. Luan, *J. Mater. Chem. B*, 2014, 2, 8361-8371.
27. G. J. Quinlan, G. S. Martin and T. W. Evans, *Hepatology*, 2005, 41, 1211-1219.
28. F.-P. Gao, Y.-X. Lin, L.-L. Li, Y. Liu, U. Mayerhöffer, P. Spenst, J.-G. Su, J.-Y. Li, F. Würthner and H. Wang, *Biomaterials*, 2014, 35, 1004-1014.
29. A. Mewada, S. Pandey, M. Thakur, D. Jadhav and M. Sharon, *J. Mater. Chem. B*, 2014, 2, 698-705.
30. Y. Li, L. Feng, X. Shi, X. Wang, Y. Yang, K. Yang, T. Liu, G. Yang and Z. Liu, *Small*, 2014, 10, 1544-1554.
31. A. M. Alkilany, P. K. Nagaria, C. R. Hexel, T. J. Shaw, C. J. Murphy and M. D. Wyatt, *Small*, 2009, 5, 701-708.
32. R. Khandelia, A. Jaiswal, S. S. Ghosh and A. Chattopadhyay, *Small*, 2013, 9, 3494-3505.
33. I. K. Kwon, S. C. Lee, B. Han and K. Park, *J. Control. Release*, 2012, 164, 108-114.
34. D. Shan, P. Cai, P. Prasad, A. M. Rauth and X. Y. Wu, *Cancer Res.*, 2013, 73, 4339-4339.
35. Y. Wang, J. Xu, X. Xia, M. Yang, S. Vangveravong, J. Chen, R. H. Mach and Y. Xia, *Nanoscale*, 2012, 4, 421-424.
36. G. Tian, W. Yin, J. Jin, X. Zhang, G. Xing, S. Li, Z. Gu and Y. Zhao, *J. Mater. Chem. B*, 2014, 2, 1379-1389.
37. I. G. Campbell, T. A. Jones, W. D. Foulkes and J. Trowsdale, *Cancer Res.*, 1991, 51, 5329-5338.
38. J. Li, L. Zheng, H. Cai, W. Sun, M. Shen, G. Zhang and X. Shi, *Biomaterials*, 2013, 34, 8382-8392.
39. Y. Wu, R. Guo, S. Wen, M. Shen, M. Zhu, J. Wang and X. Shi, *J. Mater. Chem. B*, 2014, 2, 7410-7418.
40. L. Sun, Z. Wei, H. Chen, J. Liu, J. Guo, M. Cao, T. Wen and L. Shi, *Nanoscale*, 2014, 6, 8878-8883.
41. X. Shi, H. Gong, Y. Li, C. Wang, L. Cheng and Z. Liu, *Biomaterials*, 2013, 34, 4786-4793.
42. C. Du, D. Deng, L. Shan, S. Wan, J. Cao, J. Tian, S. Achilefu and Y. Gu, *Biomaterials*, 2013, 34, 3087-3097.
43. J. Li, L. Zheng, H. Cai, W. Sun, M. Shen, G. Zhang and X. Shi, *ACS Appl. Mater. Interfaces*, 2013, 5, 10357-10366.
44. H. Mao, N. Kawazoe and G. Chen, *Biomaterials*, 2013, 34, 2472-2479.
45. I. Baginskiy, T.-C. Lai, L.-C. Cheng, Y.-C. Chan, K.-Y. Yang, R.-S. Liu, M. Hsiao, C.-H. Chen, S.-F. Hu and L.-J. Her, *J. Phys. Chem. C*, 2013, 117, 2396-2410.
46. C. Zhang, L. Zhao, Y. Dong, X. Zhang, J. Lin and Z. Chen, *Eur. J. Pharm. Biopharm.*, 2010, 76, 10-16.

47. J. J. Pillai, A. K. T. Thulasidasan, R. J. Anto, D. N. Chithralekha, A. Narayanan and G. S. V. Kumar, *J. Nanobiotechnology*, 2014, 12, 25.
48. A. Retnakumari, S. Setua, D. Menon, P. Ravindran, H. Muhammed, T. Pradeep, S. Nair and M. Koyakutty, *Nanotechnology*, 2010, 21, 055103.
49. Y. Tian, S. Luo, H. Yan, Z. Teng, Y. Pan, L. Zeng, J. Wu, Y. Li, Y. Liu and S. Wang, *J. Mater. Chem. B*, 2015, 3, 4330-4337.
50. Y. Li, J. Ma and Z. Ma, *Electrochim. Acta*, 2013, 108, 435-440.
51. S. Barbosa, A. Topete, M. Alatorre-Meda, E. M. Villar-Alvarez, A. Pardo, C. Alvarez-Lorenzo, A. Concheiro, P. Taboada and V. c. Mosquera, *J. Phys. Chem. C*, 2014, 118, 26313-26323.
52. A. Topete, M. Alatorre-Meda, P. Iglesias, E. M. Villar-Alvarez, S. Barbosa, J. A. Costoya, P. Taboada and V. Mosquera, *ACS Nano*, 2014, 8, 2725-2738.
53. W.-H. Chen, X.-D. Xu, G.-F. Luo, H.-Z. Jia, Q. Lei, S.-X. Cheng, R.-X. Zhuo and X.-Z. Zhang, *Sci. Rep.*, 2013, 3, 3468.

Chapter 3

Gold nanoparticle size and shape influence on osteogenesis of mesenchymal stem cells

3.1 Summary

Gold nanoparticles (AuNPs) have been extensively explored for biomedical applications due to their advantages of facile synthesis and surface functionalization. Previous studies have suggested that AuNPs can induce differentiation of stem cells into osteoblasts. However, how the size and shape of AuNPs affect the differentiation response of stem cells has not been elucidated. In this part, a series of bovine serum albumin (BSA)-coated Au nanospheres, Au nanostars and Au nanorods with different diameter of 40, 70 and 110 nm were synthesized and their effects on osteogenic differentiation of human mesenchymal stem cells (hMSCs) were investigated. All the AuNPs showed good cytocompatibility and did not influence proliferation of hMSCs at the studied concentration. Osteogenic differentiation of hMSCs was dependent on the size and shape of AuNPs. The sphere-40, sphere-70 and rod-70 significantly increased the alkaline phosphatase (ALP) activity and calcium deposition of cells while rod-40 reduced the ALP activity and calcium deposition. Gene profiling revealed that the expression of osteogenic marker genes was down-regulated after incubation with rod-40. However, up-regulation of these genes was found in the sphere-40, sphere-70 and rod-70 treatment. Moreover, it was found that the size and shape of AuNPs affected the osteogenic differentiation of hMSCs through regulating the activation of Yes-associated protein (YAP). These results indicate the size and shape of AuNPs had an influence on the osteogenic differentiation of hMSCs, which should provide useful guidance for preparation of AuNPs with defined size and shape for their biomedical applications.

3.2 Introduction

Nanoscaled materials have attracted extensive attention in biomedicine and tissue engineering with the progress of nanoscience and nanotechnology.[1-5] Among these previously reported nanomaterials, gold nanoparticles (AuNPs) have naturally become one of the most outstanding candidates in different

fundamental researches and practical applications.[6-10] AuNPs have many prominent advantages such as distinct physicochemical properties, excellent biocompatibility, facile synthesis method and surface functionalization.[11-13] To date, various nanoplatforms based on AuNPs have been constructed for molecular imaging,[14-18] drug/gene delivery,[19-21] photothermal/photodynamics therapy,[22-24] immunological assay,[25, 26] stem cell tracking[27, 28] and tissue engineering.[8]

One remarkable feature of AuNPs is the easy control of their size, shape and surface chemistry during synthesis.[29-31] These features render the AuNPs with different properties and functions, as well as influence their behaviors in biological systems.[32] Many efforts have been made to study cellular uptake of AuNPs by varying their size, shape or surface chemistry.[33-36] For example, Au nanospheres with a diameter of 50 nm exhibit the maximum cellular uptake and the uptake of Au nanospheres is much higher than Au nanorods when their size is approximate.[34] Another similar study reports that cellular uptake of Au nanorods is highly dependent on their aspect ratio and a higher aspect ratio results in lower uptake.[33] In addition, the size, shape and surface chemistry of AuNPs also display different influences on their cytotoxicity.[37-39] A recent study indicates that at a similar size, Au nanospheres have higher cytotoxicity than Au nanostars.[40] Furthermore, the influences of size, shape or surface chemistry of AuNPs on immunological responses,[41] gene transfection efficiency[42] and photothermal therapeutic efficiency[43, 44] have also been studied.

In recent years, AuNPs have been extensively explored for tissue engineering applications, especially for their potential use in modulating the differentiation of stem cells. It has been reported that AuNPs can promote osteogenic differentiation and inhibit adipogenic differentiation of mouse mesenchymal stem cells (mMSCs) through the p38 mitogen-activated protein kinase (MAPK) pathway.[45] In another study, osteogenic differentiation of human adipose-derived stem cells (ADSCs) shows dependence on the size of AuNPs.[12] AuNPs with the size of 30 nm and 50 nm are effective in enhancing osteogenic differentiation. In addition, AuNPs functionalized with cyclodextrin curcumin complexes can inhibit the osteoclast differentiation of bone marrow-derived macrophages (BMMs).[46] However, AuNPs did not affect the osteogenesis of MG63 osteoblast-like cells.[47]

Human mesenchymal stem cells (hMSCs) play a crucial role in tissue engineering because of their inherent ability to differentiate into multiple lineages, such as adipocytes, chondrocytes, myocytes and osteoblasts.[48, 49] As the differentiation activity of stem cells may be affected by AuNPs, understanding the response of hMSCs to AuNPs with diverse size, shape and surface chemistry is necessary. In our recent work, amine and hydroxyl group functionalized AuNPs do not inhibit osteogenic differentiation, but carboxyl group functionalized AuNPs treatment reduces the alkaline phosphatase (ALP) activity and matrix mineralization of hMSCs.[50] However, the response of hMSCs to varying size and shape of AuNPs is still unknown and detailed study should be performed to optimize the features of AuNPs for their different tissue engineering applications.

In this part, different kinds of AuNPs with well-defined sizes and shapes were prepared and were used to study the effects of particle size and shape on osteogenic differentiation of hMSCs. Before cell culture experiments, the AuNPs were coated with bovine serum albumin (BSA) and then characterized by different techniques. The cell viability, cell proliferation and cellular uptake of hMSCs after treatment with these AuNPs were analyzed. Moreover, osteogenic differentiation activity of the treated stem cells was evaluated

to investigate if the size and shape of AuNPs have some effects on hMSCs osteogenesis.

3.3 Materials and methods

3.3.1 Materials

Hydrogen tetrachloroaurate tetrahydrate **(**$HAuCl_4 \cdot 4H_2O$, 99.9%), hydrochloric acid, nitric acid, trisodium citrate dehydrate, paraformaldehyde and hydroquinone were purchased from Wako Pure Chemical Industries, Ltd. (Tokyo, Japan). Hexadecyltrimethylammonium bromide (CTAB), bovine serum albumin (BSA), ascorbic acid (AA), sodium borohydride ($NaBH_4$), silver nitrate ($AgNO_3$), Dulbecco's modified Eagle's Medium (DMEM), penicillin, streptomycin, dexamethasone, β-glycerophosphate, 2-amino-2-methyl-1,3-propanediol, naphthol AS-MX phosphate, fast blue RR salt and trypsin/EDTA were purchased from Sigma-Aldrich (St. Louis, MO, USA). Fetal bovine serum (FBS) was purchased from Gibco Laboratories (Grand Island, NY, USA). WST-1 reagent were obtained from Roche Molecular Biochemicals (Mannheim, Germany). Cellstain Live-Dead Double Staining kit and 4'-6-diamidino-2-phenylindole (DAPI) solution were purchased from Dojindo Laboratories (Kumamoto, Japan). Monoclonal mouse anti-Yes-associated protein (YAP) primary antibody was purchased from Santa Cruz Biotechnology, Inc. (Santa Cruz, CA). Alexa Fluor 488 goat anti-mouse IgG antibody was purchased from Invitrogen™ (Grand Island, NY). All the chemical reagents were used as received without further purification. The water used in all the experiments was ultrapure water with resistivity of 18.2 MΩ.cm purified by a Q-POD Milli-Q water purification system (Millipore Corp., Billerica, MA, USA).

3.3.2 Characterization techniques

UV-Vis spectra were recorded on a V-660 UV-Vis Spectrophotometer (Jasco Corp., Tokyo, Japan). The samples were dispersed in water before measurements. The morphology and size of the NPs were observed with a JEOL 2100F transmission electron microscopy (TEM, JEOL, Tokyo, Japan) with operating voltage of 200 kV. The samples were prepared by dropping 8 μL particle solution onto a carbon-covered copper grid, following by drying in air. The ImageJ software (National Institutes of Health, Bethesda, Maryland, USA) was used to measure their sizes. Zeta potential and hydrodynamic size measurements were performed on a zeta-potential & particle size analyzer (ELSZ-2000, Otsuka Electronics Co., Ltd, Japan). The concentration of gold element was determined by a Leeman Prodigy Inductively Coupled Plasma-Optical Emission Spectroscopy (ICP-OES, SPS3520UV-DD) system (SII nano technology Inc., Tokyo, Japan).

3.3.3 Synthesis of AuNPs with different sizes and shapes

Au nanospheres with different sizes were synthesized by citrate reduction of $HAuCl_4$ according to the previous report.[12] Briefly, 100 mL of $HAuCl_4$ solution (0.1 mg/mL) was heated to 110 °C and refluxed. Then certain volume of trisodium citrate solution (10.0 mg/mL) was added to the above-mentioned solution quickly and the reaction was continued under vigorous magnetic stirring. The size of the Au nanospheres was controlled by adjusting the amounts of trisodium citrate. After that, the solution was refluxed until it cooled

down to room temperature. The solution was then centrifuged to remove excess citrate in the Au nanospheres solution. The precipitation was dispersed into BSA aqueous solution (10 mg/mL) and the mixture was kept stirring at room temperature for 24 hours. The resultant BSA-coated Au nanospheres (sphere-40, sphere-70 and sphere-110) were washed twice by centrifugation to remove unbounded BSA and redispersed in water.

Au nanostars with a diameter of 40, 70 and 110 nm were synthesized according to our previous report.[51] The growth solution was prepared by adding $HAuCl_4$ solution (30.0 mg/mL, 0.75 mL), Au seed solution, $AgNO_3$ solution (5.0 mg/mL, 0.3 mL) and AA solution (38.0 mg/mL, 0.5 mL) into 25 mL water under gently stirring. Usage of different volume of Au seed solution resulted in the Au nanostars having different diameters. Then BSA aqueous solution (10 mg/mL) was also added into the growth solution and the resultant solution was stirred at room temperature for 24 hours. The BSA-coated Au nanostars (star-40, star-70 and star-110) were then collected by centrifugation, washed with water and redispersed in water for further use.

Au nanorods with a longitudinal length of 40 nm and 70 nm were synthesized using the seed-mediated growth method according to a previous work with some modification.[52] CTAB-capped Au seeds were at first obtained by chemical reduction of $HAuCl_4$ with $NaBH_4$ and used within 2 hours. Under gently stirring, 0.48 mL of Au seed solution was then added to the growth solution containing 200 mL of 0.1 M CTAB, 10 mL of 0.01 M $HAuCl_4$, 4 mL of 1.0 M HCl, 0.44 mL or 2.20 mL of 10 mM $AgNO_3$ and 1.6 mL of 0.1 M AA. After incubating for 12 hours, the reaction was finally stopped by centrifugation and the Au nanorods were washed with water to remove free CTAB. By adjusting the added amount of $AgNO_3$, Au nanorods with different longitudinal were formed. For the synthesis of Au nanorods with a longitudinal length of 110 nm, an efficient and facile one-pot method was adopted.[53] In brief, 7.6 mL of $HAuCl_4$ (0.01 M), 2.0 mL of $AgNO_3$ (0.02 M) and 1.6 mL of hydroquinone (0.62 M) were sequentially added into 178.0 mL of CTAB solution (0.11 M) to yield a colorless solution. Subsequently, 126.0 μL of $NaBH_4$ solution (0.5 M) was added and the resultant mixture was kept standing at 30 °C for 24 hours. Finally, the mixture was centrifuged and washed with water to remove the free CTAB. To coat BSA on the three types of Au nanorods, BSA aqueous solution (10 mg/mL) was poured into the Au nanorods solution and the mixture was kept stirring at room temperature for 24 hours. The final BSA-coated Au nanorods (rod-40, rod-70 and rod-110) were washed twice with water and redispersed in water.

3.3.4 Cell culture

Human bone marrow-derived mesenchymal stem cells (hMSCs) were purchased from Lonza (Walkersville MD, USA). The hMSCs were cultured in 75 cm^2 tissue culture flasks with normal cell culture medium at 37 °C and 5% CO_2. The cell culture growth medium was DMEM supplemented with 10% heat-inactivated FBS, 4500 mg/L glucose, 4 mM glutamine, 100 U/mL penicillin, 100 μg/mL streptomycin, 0.1 mM nonessential amino acids, 0.4 mM proline, 1 mM sodium pyruvate and 50 μg/mL ascorbic acid. The cell osteogenic induction medium was DMEM supplemented with 10% heat-inactivated FBS, 1000 mg/L glucose, 584 mg/L glutamine, 100 U/mL penicillin, 100 μg/mL streptomycin, 0.1 mM nonessential amino acids, 50 μg/mL ascorbic acid, 100 nM dexamethasone and 10 mM β-glycerophosphate. For the cytotoxicity assay, cells were cultured for a short-term (3 days) and a high cell density of 2.5×10^4 cells/cm^2 was used. For evaluation of cellular uptake, proliferation and osteogenic differentiation, the cells were cultured for 21

days and a low cell density (0.5×10^4 cells/cm^2) was used.

3.3.5 Cytotoxicity assay

The cytotoxicity of AuNPs with different sizes and shapes was evaluated by WST-1 assay of hMSCs. The cells were seeded into 96-well plates with 200 μL fresh cell culture growth medium at a density of 2.5×10^4 cells/cm^2. The cells were cultured for 24 hours to allow adherence and then the medium was replaced by 200 μL fresh cell culture growth medium containing pure PBS (control), sphere-40, sphere-70, sphere-110, star-40, star-70, star-110, rod-40, rod-70 or rod-110 at the Au concentrations of 0.1, 0.3 and 0.5 mM. After incubation with the AuNPs for 3 days, the cells were washed with PBS and 110 μL fresh medium containing 10 μL WST-1 reagent was added into each well. The cells were cultured for another 3 hours, following by measuring the absorbance of each well at 440 nm using a plate reader (Benchmark Plus, Bio-Rad, Hercules, CA, USA) to evaluate the cell viability. In addition, live/dead staining with a Cellstain live/dead double staining kit was also performed to visualize live and dead cells. The cells treated with the AuNPs at an Au concentration of 0.5 mM for 3 days were washed with PBS and then incubated in serum-free medium containing calcein-AM and propidium iodide (PI) at 37 °C for 15 minutes, following by observation under an inverted fluorescence microscope (Olympus, Japan).

3.3.6 Cell proliferation assay

The proliferation of hMSCs in osteogenic induction medium containing the AuNPs for 7, 14 and 21 days was determined using the WST-1 assay and live and dead cells were visualized by live/dead staining as described above. The cells were seeded into 96-well plates with 100 μL fresh growth medium at a density of 0.5×10^4 cells/cm^2. Next day, 100 μL fresh osteogenic induction medium with PBS or various AuNPs at an Au concentration of 50.0 μM was added into each well to replace the old medium. The medium was changed every 2-3 days with fresh medium containing AuNPs. After culture for 7, 14 and 21 days, the cells were used for WST-1 assay and live/dead staining.

3.3.7 Cellular uptake assay

The hMSCs were seeded in 6-well plates at a density of 0.5×10^4 cells/cm^2 and then incubated with various AuNPs at an Au concentration of 50.0 μM for 21 days in 2.0 mL osteogenic induction medium. Subsequently, the medium was removed and the cells were washed twice with PBS carefully. The cells were then trypsinized, collected and washed with PBS through two cycles of centrifugation and re-suspension. Finally, the collected cells were re-suspended in PBS, counted with a hemocytometer and lysed with aqua regia solution. After being diluted with water and filtered through a 0.22 μm membrane, the Au content in the cells of different treatments was measured by ICP-OES.

3.3.8 Alkaline phosphatase (ALP) staining and ALP activity assay

The hMSCs were seeded in 24-well plates at a density of 0.5×10^4 cells/cm^2 in 0.5 mL of fresh cell growth medium and were cultured at 37 °C and 5% CO_2 for 1 day. The medium in each well was replaced by 0.5 mL osteogenic induction medium supplemented with PBS (control) or various AuNPs at an Au

concentration of 50.0 μM. After 14 days of culture, the cells were washed twice with PBS and subsequently fixed with 4% paraformaldehyde at room temperature for 10 minutes. The fixed cells were further washed twice with PBS and incubated with 0.1% naphthol AS-MX phosphate and 0.1% fast blue RR salt in 56 mM 2-amino-2-methyl-1,3-propanediol working solution (pH = 9.9) at room temperature for 10 minutes. After discarding the working solution and washing the plates with PBS, the cells were observed using an optical microscope.

ALP activity assay was carried out by using the Sensolyte® *p*NPP alkaline phosphatase assay kit (Anaspec, USA) according to the manufacturer's instructions. The cells were incubated with the AuNPs in the osteogenic induction medium for 14 days as described above. The cells in each well were washed twice with PBS, scraped off the plates and collected into a microcentrifuge tube. After incubation at 4 °C for 10 minutes under agitation, the cell suspensions were centrifuged at 2500× *g* for 10 minutes to collect the supernatant. The supernatant was incubated with *p*-nitrophenyl phosphate (*p*NPP) substrate solution and color change was measured with a plate reader at a wavelength of 405 nm. A calibration curve was drawn by using ALP standard solution to determine the concentration of ALP in each well. Cell number in each well was counted with a hemocytometer to normalize the relative ALP amount.

3.3.9 Alizarin Red S (ARS) staining and calcium deposition assay

For calcium phosphate ARS staining, hMSCs were incubated with each type of AuNPs in 0.5 mL osteogenic induction medium at an Au concentration of 50.0 μM for 21 days. After culture, the cells were washed twice with PBS, fixed with 4% paraformaldehyde at room temperature for 10 minutes and incubated with 0.1% Alizarin Red S solution at room temperature for 30 minutes. The cells were further washed twice with PBS and observed using an optical microscopy.

For a quantitative calcium deposition assay, the stained cells were dried in the air and then eluted with 5% perchloric acid at room temperature for 20 minutes. The solution in each well was transferred into a 96-well plate and the absorbance was recorded with a plate reader at 405 nm. The results were normalized by cell number in each well.

3.3.10 Quantitative real-time polymerase chain reaction (PCR)

The hMSCs were seeded in 6-well plates at a density of 0.5×10^4 cells/cm^2 and incubated with various AuNPs at an Au concentration of 50.0 μM in osteogenic induction medium. After 21 days of culture, the cells were washed twice with PBS and collected for RNA extraction with the RNAeasy Minikit (Qiagen, Netherlands) according to the manufacturer's instructions. A first stand cDNA synthesis kit was used to convert the obtained RNA to cDNA. Real-time PCR was performed on a 7500 Real-Time PCR system (Applied Biosystems, USA) according to our previously reported protocol.[50] The gene expression normalized to glyceraldehyde 3-phosphate dehydrogenase (GAPDH) was expressed as fold change. The primers and probes used for real-time PCR are listed in Table 3.1.

Table 3.1 The primers and probes for real-time PCR.

mRNA	Oligonucleotide

18 S rRNA	Hs99999901_s1
GAPDH	Hs99999905_m1
ALP	Forward 5'-GACCCTTGACCCCCACAAT-3' Reverse 5'-GCTCGTACTGCATGTCCCCT-3' Probe 5'-TGGACTACCTATTGGGTCTCTTCGAGCCA-3'
IBSP	Forward 5'-TGCCTTGAGCCTGCTTCC-3' Reverse 5'-GCAAAATTAAAGCAGTCTTCATTTTG-3' Probe 5'-CTCCAGGACTGCCAGAGGAAGCAATCA-3'
SPPI	Forward 5'-CTCAGGCCAGTTGCAGCC-3' Reverse 5'-CAAAAGCAAATCACTGCAATTCTC-3' Probe 5'-AAACGCCGACCAAGGAAAACTCACTACC-3'
Runx2	Hs00231692_m1

3.3.11 YAP immunofluorescence

The hMSCs were seeded in 24-well plates at a density of 0.5×10^4 cells/cm^2 and incubated with various AuNPs at an Au concentration of 50.0 μM in osteogenic induction medium for 3 days. After 3 days culture, the cells were washed twice with PBS and fixed with 4% paraformaldehyde at room temperature for 10 minutes. Subsequently, the cells were washed twice with PBS, incubated with 1% Triton X-100 at room temperature for 10 minutes, washed another twice with PBS and incubated with 2% BSA solution at room temperature for 30 minutes. After being further washed thrice with PBS, the cells were incubated with monoclonal mouse anti-YAP primary antibody (1:100) overnight at 4 °C. The cells were washed thrice with PBS (5 minutes/time) and then incubated with Alexa Fluor 488 goat anti-mouse IgG antibody (1:800) at room temperature for 1 hour. Finally, the cells were washed twice with PBS and incubated with DAPI solution (1:800) at room temperature for 10 minutes. Following two additional washing with PBS, the cells were observed under an inverted fluorescence microscope. To quantify the number of hMSCs with or without nuclear localized YAP, an ImageJ software was used to analyze the captured images (n = 9 fields per group). The signal intensity of cell nucleus and cytoplasm in each cell was measured by an ImageJ software. The cells were denoted as hMSCs with nuclear localized YAP if the signal intensity of nucleus was twice higher than that of cytoplasm. Otherwise, the cells were denoted as hMSCs without nuclear localized YAP. The number of hMSCs with nuclear localized YAP in each sample was counted according to above mentioned standard. DAPI staining was used to count the total number of cells in each sample. The percentage of hMSCs with nuclear localization of YAP was obtained by dividing the number of hMSCs with

nuclear localized YAP by the total number of cells.

3.3.12 Statistical analysis

All data are presented as mean ± standard deviation (SD) with experiments repeated in triplicate (n = 3). Statistical analysis was performed using One-way ANOVA to evaluate the significance of the experimental data. The data are indicated with (*) for $p < 0.05$, (**) for $p < 0.01$ and (***) for $p < 0.001$.

3.4 Results

3.4.1 Synthesis and characterization of AuNPs with different sizes and shapes

The AuNPs with controlled size and shape (sphere-40, -70, -110; star-40, -70, -110; rod-40, -70, -110) were synthesized according to the previously reported methods, following by coating with BSA to afford them good colloidal stability and excellent biocompatibility. The prepared AuNPs were used as a model system to investigate the effects of nanoparticle size and shape on the osteogenic differentiation of hMSCs.

The visible colors and optical properties of AuNPs are known to be strongly sensitive to their size and shape.[54] As shown in the photos of the aqueous solutions of the AuNPs (Figure 3.1a), the AuNPs exhibited distinct colour variation depending on their size and shape. The optical properties of the AuNPs were characterized by UV-Vis spectroscopy (Figure 3.1b-d). For Au nanospheres and Au nanostars, the NPs displayed obvious surface plasmon resonance (SPR) peaks from 500 to 800 nm range and their SPR peaks red-shifted as the nanoparticle size increased. The maximum absorption peaks of sphere-40, sphere-70, sphere-110, star-40, star-70 and star-110 were observed at 532, 544, 558, 637, 711 and 790 nm, respectively. In contrast to Au nanospheres and Au nanostars, Au nanorods had two SPR peaks in the UV-Vis spectra, which corresponded to their transverse and longitudinal modes. The rod-40, rod-70 and rod-110 exhibited a strong longitudinal SPR peak at the wavelength of 606, 864 and 882 nm, respectively. As the aspect ratio of rod-40 was much lower than that of rod-70 and rod-110 (see below), the spectrum of rod-40 was obviously different from that of rod-70 and rod-110.

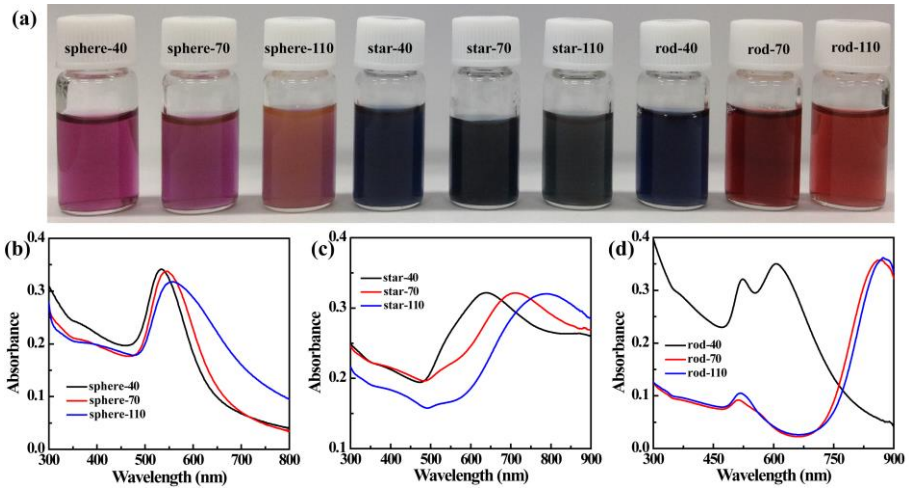

Figure 3.1 Photographs (a) and UV-Vis spectra (b-d) of various AuNPs.

TEM was used to characterize the morphology of the AuNPs (Figure 3.2) and their size distribution was calculated based on the obtained TEM images. From the TEM images, the Au nanospheres, Au nanostars and Au rods had spherical, star-like and rod-like structures as designed, respectively. Most of the AuNPs were found to be monodisperse. The diameters of sphere-40, sphere-70 and sphere-110 were determined to be 36.0 ± 8.0, 68.3 ± 10.4 and 107.0 ± 18.8 nm, respectively. The star-40, star-70 and star-110 had a mean size (tip to tip) of 36.8 ± 7.8, 67.9 ± 16.5 and 112.6 ± 23.8 nm, respectively. The mean size of rod-40, rod-70 and rod-110 was 35.2 ± 6.5 × 20.1 ± 3.3, 66.3 ± 7.3 × 13.7 ± 1.8 and 117.3 ± 13.6 nm × 27.0 ± 6.1 nm in length × width, respectively. The aspect ratio was calculated to be 1.8, 4.8 and 4.3 for rod-40, rod-70 and rod-110, respectively.

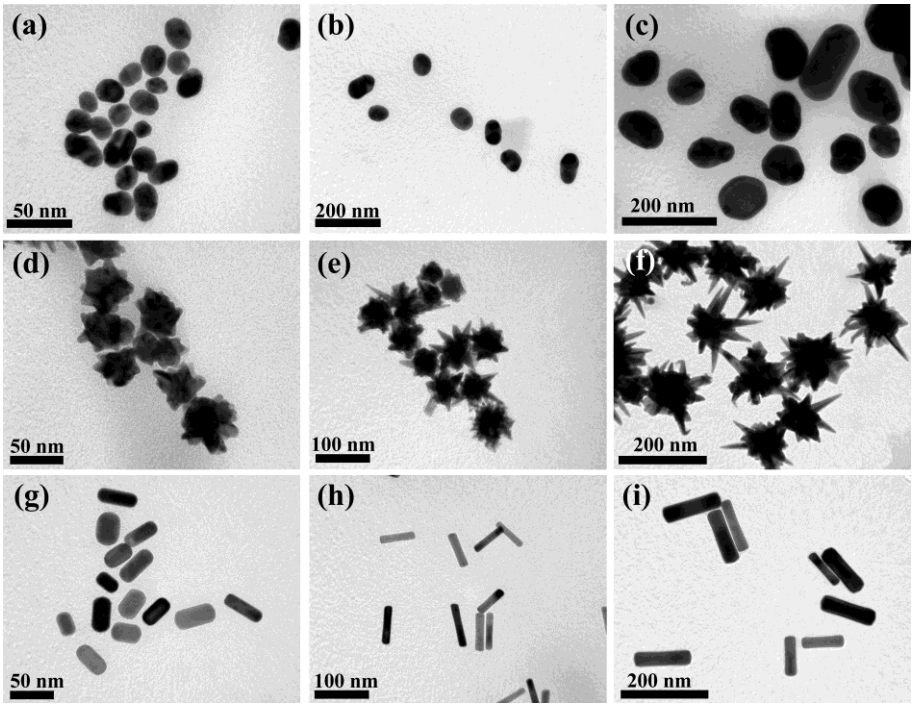

Figure 3.2 TEM images of various AuNPs: sphere-40 (a), sphere-70 (b), sphere-110 (c), star-40 (d), star-70 (e), star-110 (f), rod-40 (g), rod-70 (h) and rod-110 (i).

Dynamic light scattering (DLS) and zeta potential measurements were used to measure the hydrodynamic size and surface potential of the AuNPs dispersed in water (Table 3.2). Polydispersity index (PDI), a parameter calculated from cumulant analysis of the DLS-measured intensity autocorrelation function, is generally used to describe the width of the particle size distribution of NPs. The low PDI suggested that all the AuNPs had a narrow size distribution. The hydrodynamic size of Au nanospheres and Au nanostars was a little larger than that measured from their TEM images. The hydrodynamic size of Au nanorods was in a range between the longitudinal length and transverse length measured from TEM images except rod-40. After the BSA coating, the AuNPs displayed negative charged surfaces, as shown in Table 3.2.

Table 3.2 Zeta potential, hydrodynamic size and polydispersity index (PDI) of various AuNPs. Data are provided as mean ± S.D. (n= 3)

Sample	Zeta potential (mV)	Hydrodynamic size (nm)	PDI

sphere-40	-23.15 ± 0.65	50.50 ± 2.00	0.30 ± 0.01
sphere-70	-24.18 ± 2.32	76.63 ± 1.71	0.32 ± 0.01
sphere-110	-25.98 ± 0.80	119.57 ± 3.50	0.16 ± 0.01
star-40	-21.93 ± 1.93	69.80 ± 0.78	0.24 ± 0.01
star-70	-21.34 ± 2.85	96.70 ± 1.51	0.25 ± 0.01
star-110	-25.94 ± 1.49	133.30 ± 1.97	0.12 ± 0.01
rod-40	-31.67 ± 0.44	65.50 ± 2.36	0.32 ± 0.01
rod-70	-32.06 ± 0.32	54.10 ± 5.33	0.21 ± 0.04
rod-110	-30.95 ± 0.34	98.87 ± 7.17	0.26 ± 0.02

3.4.2 Cytotoxicity assay of AuNPs with different sizes and shapes

The cytotoxicity of the AuNPs with different sizes and shapes was assessed by using WST-1 assay and live/dead staining. It was clear that all the AuNPs showed negligible cytotoxicity to hMSCs at the studied Au concentration of 0.1, 0.3 and 0.5 mM for 1 and 2 days of culture. Further extension of the incubation time to 3 days, the AuNPs still displayed very low cytotoxicity even at the high concentration of 0.5 mM, with exception for rod-40 (Figure 3.3a-c). For the rod-40 group, the viability of hMSCs after treatments at Au concentration of 0.1, 0.3 and 0.5 mM was 84.8 ± 10.0, 67.1 ± 4.3 and 58.7 ± 3.0%, respectively (Figure 3.3c). The live and dead cells after incubation with various AuNPs at an Au concentration of 0.5 mM for 3 days were visualized by live/dead staining. As shown in Figure 3.3d, nearly no dead cells (red color) were observed for cells incubated with sphere-40, sphere-70, sphere-110, star-40, star-70, star-110, rod-70 and rod-110. However, when hMSCs were cultured with rod-40 at an Au concentration of 0.5 mM for 3 days, the number of live cells (green color) decreased and many dead cells (red color) appeared. This was in agreement with the results of WST-1 assay. These results indicate that all the AuNPs showed very low cytotoxicity to hMSCs when the Au concentration was not higher than 0.1 mM. Therefore, in the following proliferation and osteogenic differentiation experiments, an Au concentration of 50.0 μM was used.

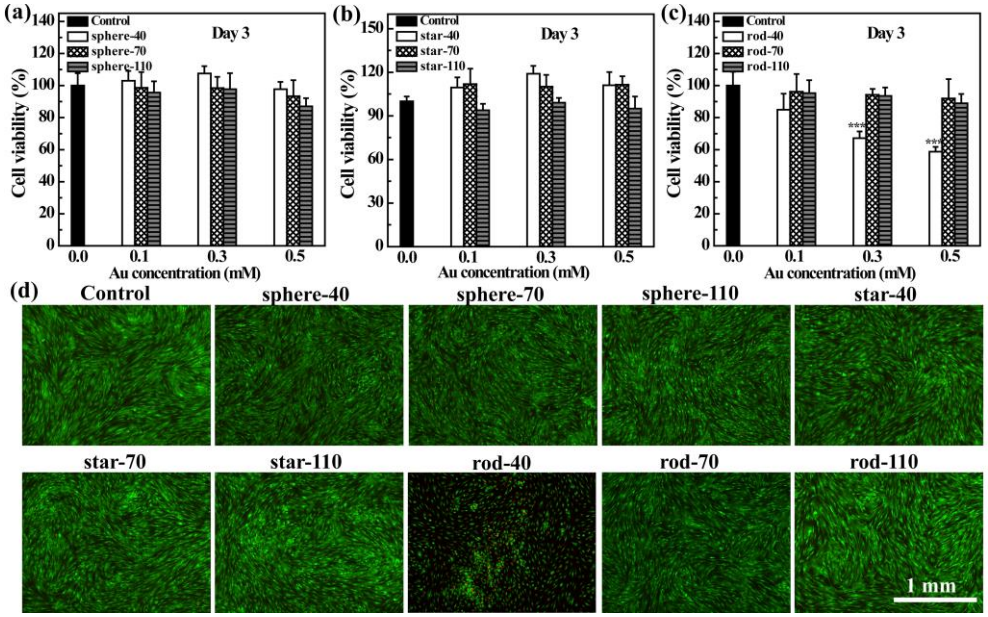

Figure 3.3 Cell viability of hMSCs incubated with PBS (control) or various AuNPs in growth medium at the Au concentration of 0.1, 0.3 and 0.5 mM for 3 days (a-c); Live/dead staining of hMSCs incubated with PBS (control) or various AuNPs in growth medium at an Au concentration of 0.5 mM for 3 days (d).

3.4.3 Cell proliferation assay

The effect of prepared AuNPs on the proliferation of hMSCs in osteogenic induction medium was assessed to further confirm their biocompatibility. From the results of live/dead staining (Figure 3.4a), almost no dead cells were observed and the number of live cell increased for all groups with prolonged culture time. The cells changed their morphology from fibroblast-like to polygonal after 14 days of culture in osteogenic induction medium. The morphological change indicated that hMSCs underwent an osteogenic differentiation process in osteogenic induction medium, agreeing with previous report.[45] WST-1 assay revealed that the cell number increased with a time-dependent manner for all the experimental groups (Figure 3.4b). Moreover, proliferation of hMSCs cultured with AuNPs was similar to or slightly higher than that of the control cells. The results suggest that all of the prepared AuNPs did not have any influence on the proliferation of hMSCs at an Au concentration of 50.0 μM.

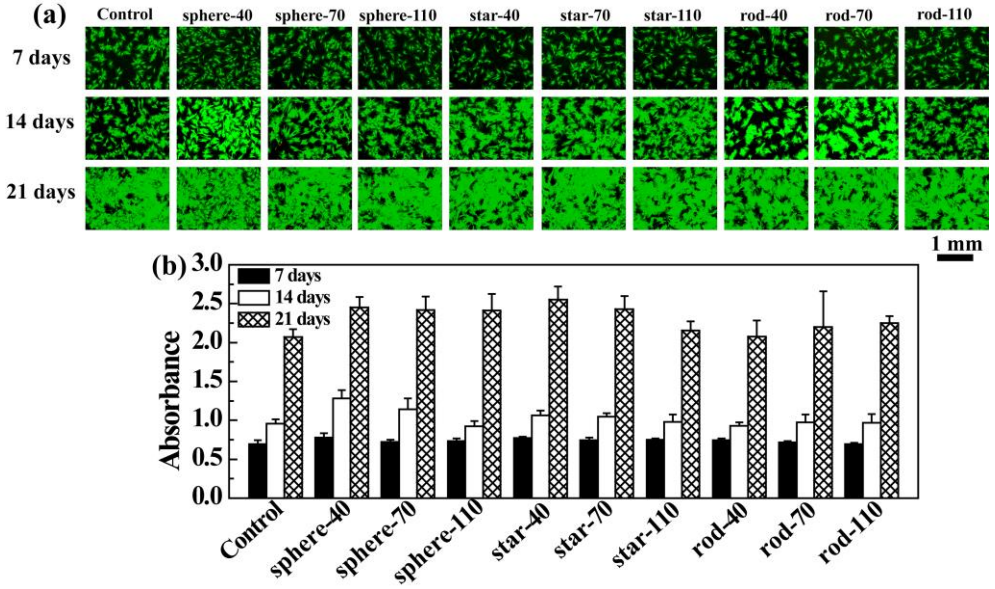

Figure 3.4 Live/dead staining (a) and WST-1 assay (b) to evaluate the cell proliferation of hMSCs after incubation with PBS (control) or various AuNPs in osteogenic induction medium at an Au concentration of 50.0 μM for 7, 14 and 21 days.

3.4.4 Cellular uptake assay

It has reported that cellular uptake of NPs is dependent on not only cell types, but also on the features of NPs including size, shape and surface chemistry.[32] The uptake of AuNPs by hMSCs was evaluated after the cells were cultured in osteogenic induction medium containing each type of AuNPs for 21 days (Figure 3.5). Some AuNPs clusters (indicated by arrows in Figure 3.5a) were observed inside the cells and on their extracellular matrices (ECM) when AuNPs were supplemented in culture medium. However, no AuNPs clusters were observed in the cells cultured in control medium. The amount of AuNPs clusters was obviously

different. Cellular uptake of sphere-40, sphere-70, sphere-110 and rod-110 was intuitively higher than that of star-40, star-70, star-110, rod-40 and rod-70. ICP-OES analysis was further performed to quantify the cellular uptake (Figure 3.5b). It was clear that the shape affected the Au uptakes, which increased in the order of Au nanostars, Au nanorods and Au nanospheres. Cellular uptake of AuNPs was also strongly dependent on the size of AuNPs. A larger size resulted in higher uptake for all the Au nanostars, Au nanorods and Au nanospheres. These results suggest that the AuNPs were uptaken by hMSCs in a size and shape-dependent manner.

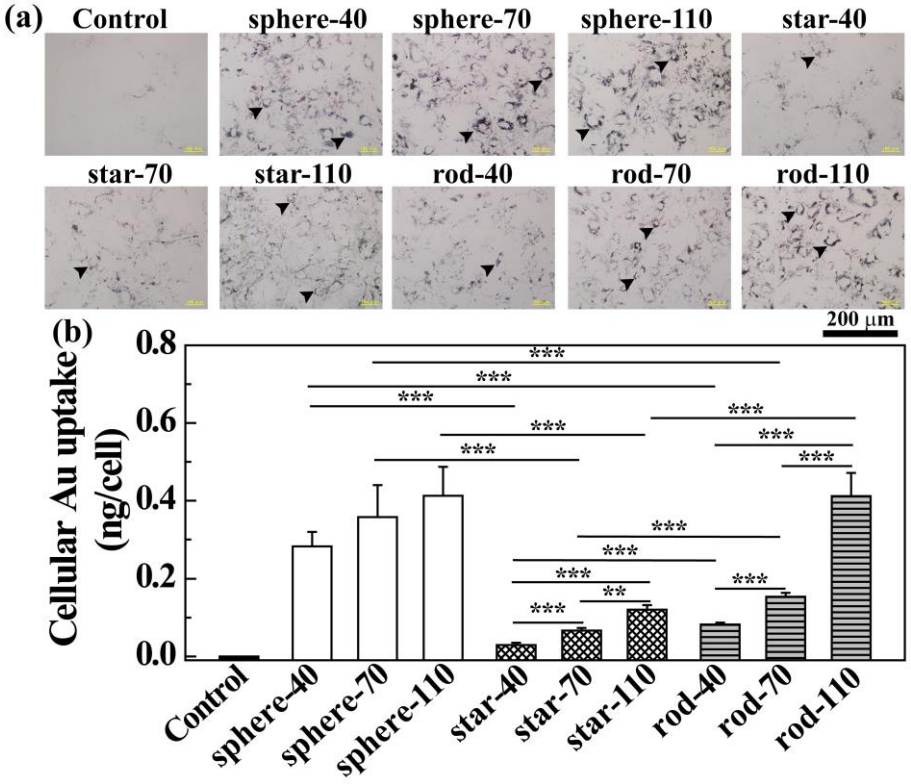

Figure 3.5 Optical micrographs (a) and cellular uptake assay (b) of hMSCs after incubation with PBS (control) or various AuNPs in osteogenic induction medium at an Au concentration of 50.0 μM for 21 days.

3.4.5 ALP staining and ALP activity assay

ALP activity is generally used as an early stage marker of osteogenic differentiation.[55-57] ALP staining and ALP activity assay were performed to investigate the osteogenic differentiation activity of hMSCs after 14 days of culture. The ALP staining (Figure 3.6a) demonstrated that slightly more intense staining was observed in the cells cultured with sphere-40, sphere-70, sphere-110 and rod-70 than that of the control groups. The cells cultured with rod-40 displayed the least degree of staining, which was much less than the control group. The results of ALP activity assay corresponded well with that of the ALP staining, as shown in Figure 3.6b. The cells cultured with sphere-40, sphere-70, sphere-110 and rod-70 had significantly higher ALP amount than the control cells. The ALP amount in the cells cultured with star-40, star-70, star-110 and rod-110 showed no significant difference with control group. However, the ALP amount in the cells cultured with rod-40 was significantly lower than that of control group. The cells cultured with rod-40 had the lowest ALP amount. The results indicate that ALP expression in hMSCs was strongly affected by the size and shape

of AuNPs.

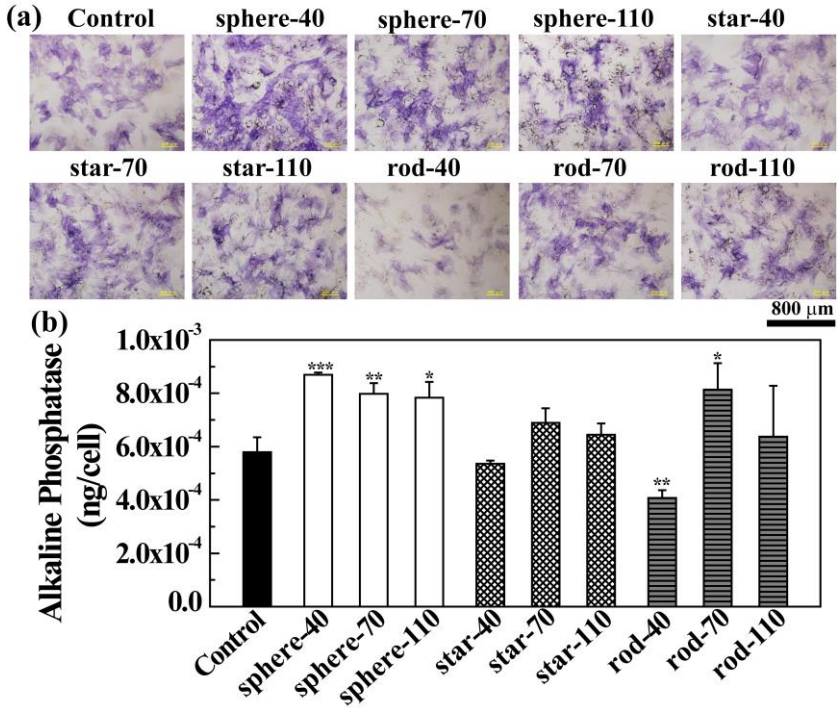

Figure 3.6 ALP staining (a) and ALP activity assay (b) of hMSCs after incubation with PBS (control) or various AuNPs in osteogenic induction medium at an Au concentration of 50.0 μM for 14 days.

3.4.6 ARS staining and calcium deposition assay

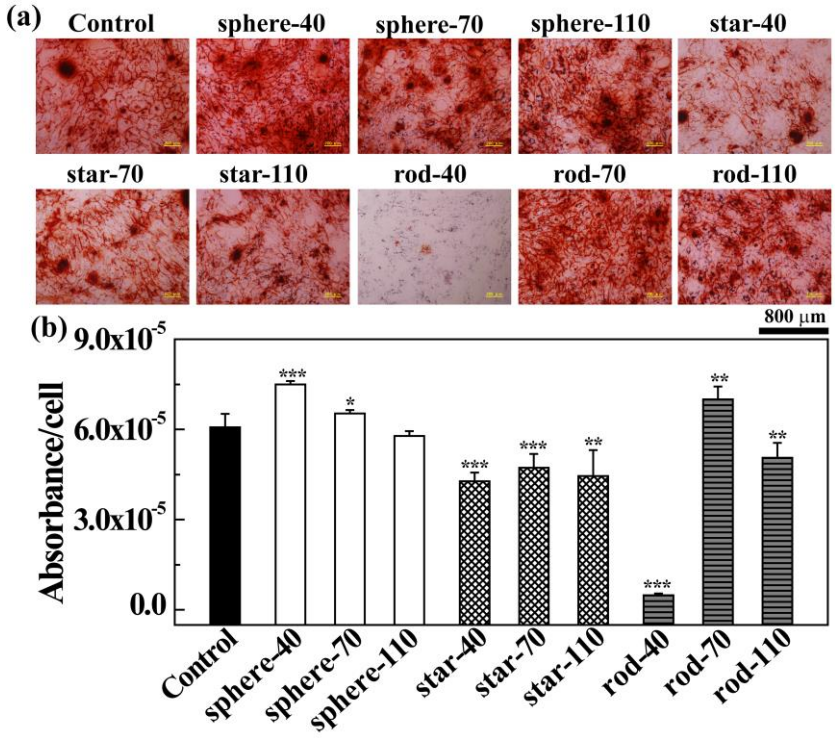

Figure 3.7 ARS staining (a) and calcium deposition assay (b) of hMSCs after incubation with PBS (control) or various AuNPs in osteogenic induction medium at an Au concentration of 50.0 μM for 21 days.

To confirm bone matrix maturation and mineralization, calcium deposition was evaluated for cells cultured with each type of AuNPs in osteogenic induction medium for 21 days. Deposition of calcium phosphate was indicated by the red web-like staining, as shown in Figure 3.7a. All of the experimental groups except treatment with rod-40 were positively stained. The hMSCs cultured with star-40, star-70 and star-110 showed less staining than cells in other positive groups. A quantitative analysis of mineralization was performed by eluting ARS from the stained cells (Figure 3.7b). Compared to control group, cells cultured with sphere-40, sphere-70 and sphere-70 displayed a significant increase in the amount of calcium deposition. There was no significant difference between sphere-110 and control groups. However, calcium deposition of the cells cultured with star-40, star-70, star-110, rod-40 and rod-110 was significantly lower than that of the control group, particularly in rod-40 treatment. The cells cultured with rod-40 had the lowest amount of calcium deposition.

3.4.7 Gene expression analysis

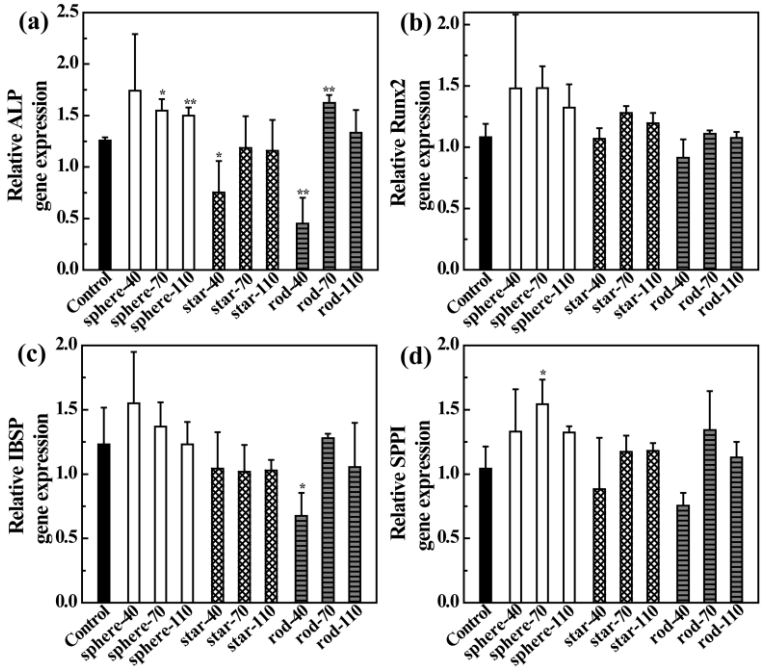

Figure 3.8 The expression of osteogenic differentiation specific genes in hMSCs after incubation with PBS (control) or various AuNPs in osteogenic induction medium at an Au concentration of 50.0 μM for 21 days: ALP (a), Runx2 (b), IBSP (c) and SPPI (d).

The expression of osteogenic marker genes such as ALP, runt-related transcription factor 2 (Runx2), bone sialoprotein 2 (IBSP) and secreted phosphoprotein I (SPPI) in hMSCs were assayed by quantitative real-time PCR after 21 days of culture (Figure 3.8). The results showed that star-40 and rod-40 induced down-regulation of ALP significantly, while the ALP gene was up-regulated by sphere-40, sphere-70, sphere-110 and rod-70 as compared with control group (Figure 3.8a). Runx2 gene expression was slightly up-regulated in cells cultured with sphere-40, sphere-70, sphere-110, star-70, star-110 and rod-70 and down-regulated in cells cultured with rod-40, although the difference was not significant (Figure 3.8b). Rod-40 induced down-regulation of IBSP gene significantly (Figure 3.8c) while the expression of IBSP gene

in the cells cultured with sphere-40, sphere-70 and rod-70 was higher than that of the control cells. For the SPPI gene expression, star-40 and rod-40 showed down-regulation effect while other AuNPs showed up-regulation effect, especially for sphere-40, sphere-70, sphere-110 and rod-70 (Figure 3.8d). These results suggest that the gene expression profile of osteogenic marker in hMSCs was different after treatments with each type of AuNPs. The sphere-40, sphere-70 and rod-70 induced up-regulation of ALP, Runx2, IBSP and SPPI, while rod-40 resulted down-regulation of these genes. Also, the expression of ALP, IBSP and SPPI in star-40 treated group was down-regulated as compared with control. The gene expression results corresponded well with the ALP activity and calcium deposition assay results.

3.4.8 YAP immunofluorescence

The expression of activated Yes-associated protein (YAP) in hMSCs after treatment with various AuNPs was assessed by immunofluorescence staining (Figure 3.9a). It has been reported that YAP localization in either nucleus (activated YAP) or/and cytoplasm (deactivated YAP) is dependent on cell mechanical state.[58] Nuclear localized YAP can be observed when mechanical signals are translated into nucleus. Compared to control, the treatments of sphere-40, sphere-70 and rod-70 increased the percentages of hMSCs with nuclear localization of YAP. However, the treatment of rod-40 reduced the YAP activity in nucleus as most of the YAP was located in the cytoplasm. For the other treated groups, the cells showed similar level of activated YAP to control cells. The percentage of hMSCs with nuclear localization of YAP after various treatments was quantified to show the YAP activity in the cell nucleus (Figure 3.9b). Obviously, the treatments of sphere-40, sphere-70 and rod-70 promoted the YAP activity when compared with control. No significant difference was observed among sphere-110, star-40, star-70, star-110 and rod-110 treated groups and control group. However, the cells cultured with rod-40 had the lowest level of YAP activity, which was significantly lower than the control cells.

3.5 Discussion

The biological functions and applications of AuNPs are generally associated with their size and shape.[44] In this study, nine types of AuNPs with different sizes and shapes were used for culture of hMSCs to investigate the effects of AuNPs size and shape on osteogenic differentiation of hMSCs. The AuNPs with different sizes and shapes were synthesized through different methods, followed by coating with BSA. BSA was chosen because of its advantages of non-toxicity, good biodegradability, good stability in biological environment and low immunogenicity.[59] Thus it was an effective strategy to afford the AuNPs with good colloidal stability, excellent biocompatibility and identical surface chemistry by BSA coating.[60] The obtained AuNPs showed different colors and optical SPR peaks in water depending on their size and shape. The size and shape of AuNPs were successfully controlled according to our design, which was confirmed by TEM. All the AuNPs had a negative zeta potential because of the successful BSA coating. The Au nanorods displayed a lower zeta potential than other counterparts, which may be due to more BSA coating on their surfaces. The hydrodynamic size of the AuNPs was analyzed by DLS and the low PDIs indicated their narrow size distributions in water.

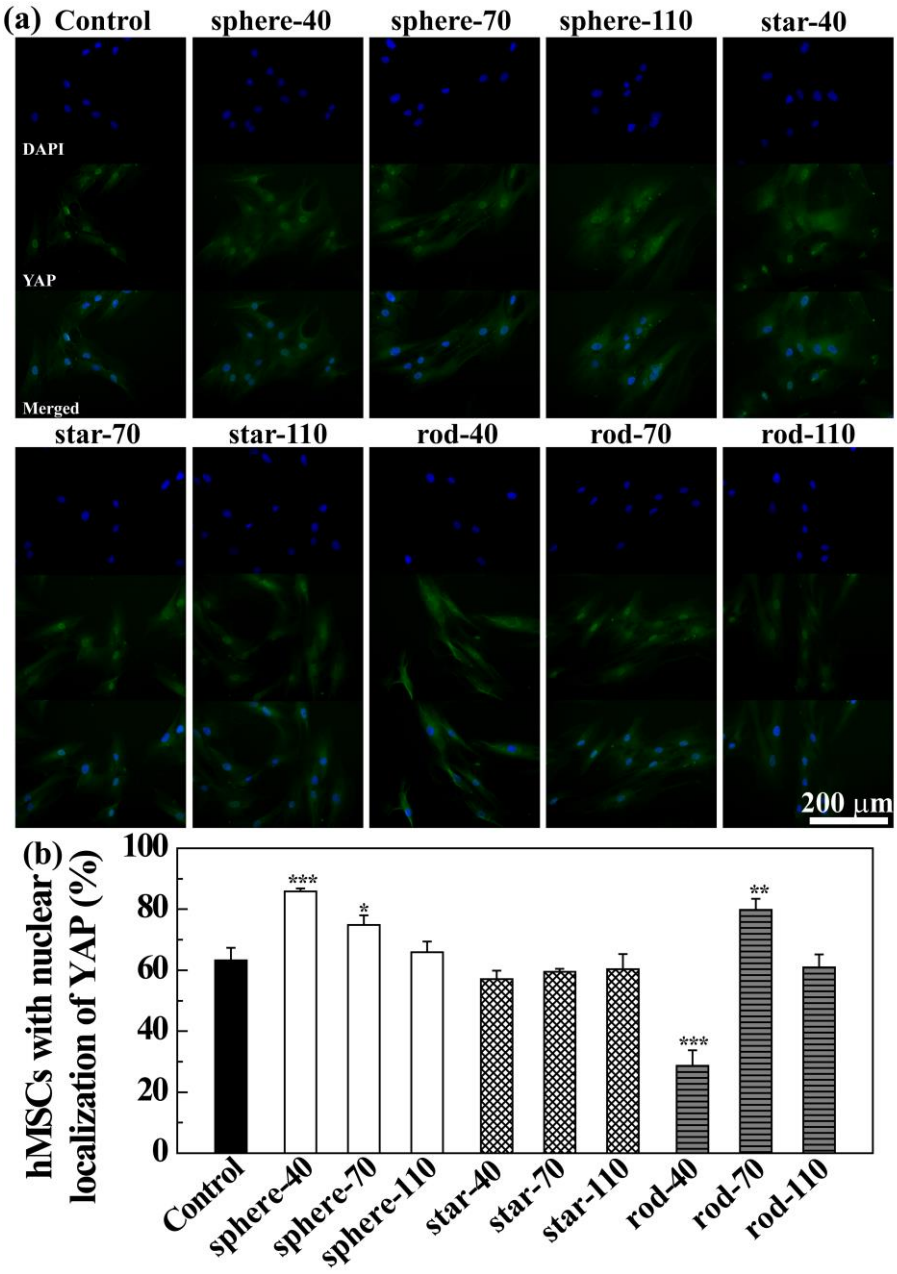

Figure 3.9 YAP staining of hMSCs (a) and percentage of hMSCs with nuclear localization of YAP (b) after incubation with PBS or various AuNPs in osteogenic induction medium at an Au concentration of 50.0 μM for 3 days (n = 9 fields per group).

The influence of the AuNPs on hMSCs behavior was evaluated by using different methods. Firstly, the AuNPs did not show any obvious cytotoxicity to hMSCs at the Au concentration of 0.1-0.5 mM after 1 and 2 days of incubation. However, the cell viability reduced significantly when the cells were cultured with rod-40 at an Au concentration of 0.3 and 0.5 mM for 3 days, while other particles did not. Rod-40 showed higher cytotoxicity than rod-70 and rod-110, which was in agreement with previous report.[61] It should be noted that the cytotoxic CTAB was used for the synthesis of Au nanorods, which could not be washed off completely during washing. Though the BSA was electrostatically absorbed onto the positively charged CTAB-coated Au nanorods, the reminding CTAB would cause some adverse effects during cell culture. It has been

reported that Au nanorods with a higher aspect ratio had a higher surface area than their counterparts with a lower aspect ratio and the loading amount of CTAB was thus proportionally higher for the low aspect ratio Au nanorods.[61] This may be one of the reasons why rod-40 showed some cytotoxicity at a high concentration while rod-70 and rod-110 did not. Based on the results of AuNPs concentration influence on cell viability, 50.0 μM of Au concentration was used for further experiments. Secondly, all the AuNPs at an Au concentration of 50.0 μM did not affect the cell proliferation of hMSCs in osteogenic induction medium after 21 days of culture. Thirdly, the size and shape of AuNPs had some effect on their cellular uptake. There are many pathways involved in mediating the intracellular uptake of NPs: phagocytosis, pinocytosis, caveolae-dependent endocytosis and clathrin-mediated endocytosis.[39] Although we did not confirm the specific pathway, we presumed the AuNPs should be uptaken by MSCs through these pathways, especially for caveolae-dependent endocytosis. To date, this is the first report to compare cellular uptake of Au nanostars, Au rods and Au nanospheres. The cellular uptake in cells increased in the order of Au nanostars < Au nanorods < Au nanospheres. It is speculated that the interaction between AuNPs and cell membrane receptors should be somewhat different dependent on the shape of AuNPs.[34] For the size effect, it was found that AuNPs with a larger size showed a higher uptake. It has been reported that 50 nm spherical NPs generally have a higher cellular uptake than other sizes after a short-term culture.[34] The increased uptake for larger particles in the present study is because the amount of uptaken Au other than the number of AuNPs was measured. The ALP and calcium deposition assay were performed to evaluate if the hMSCs displayed different osteogenic differentiation activity after incubation with AuNPs. ALP is an early stage marker of osteogenic differentiation, which generally has the maximum level expression at 2 weeks during osteogenesis.[62] Hence, ALP staining and ALP activity assay were carried out after the cells were cultured for 14 days in this study. The results showed that ALP content in sphere-40, sphere-70, sphere-110 and rod-70 treated groups was significantly higher than that in the control groups while rod-40 treatment obviously reduced ALP content as compared with control. Calcium deposition is a late-stage marker for the osteogenic differentiation of MSCs.[63] It was interesting to find that the calcium deposition was almost inhibited completely by rod-40 after 21 days of culture. However, sphere-40, sphere-70 and rod-70 showed more matrix deposition as compared with the control. It has been reported that the features of AuNPs have different influences on ALP activity and calcium deposition formation.[12, 50, 64] 20-nm AuNPs have been reported to be more potent than 40-nm AuNPs in increasing the ALP activity and bone nodules of primary osteoblasts.[64] In another work, it has been reported that the osteogenic differentiation of ADSCs is dependent on the size of AuNPs, where 30-nm and 50-nm AuNPs promote the ALP activity and calcium deposition more effectively than other counterparts.[12] Similar results in another study, 30 nm AuNPs at a concentration of 10^{-11} ppm was the best combination of size and concentration to increase the ALP activity in osteoblasts.[65] The results in this work indicate that the size and shape of AuNPs would affect the ALP activity and calcium deposition of hMSCs. It is well described that many osteogenic marker genes are regulated during osteogenesis.[45, 66] ALP as an early stage osteogenic specific gene, plays an important role in bone formation and mineralization.[45] The reduced ALP activity in the rod-40 treated group should be due to the down-regulation of ALP gene, while the up-regulation in sphere-40, sphere-70, sphere-110 and rod-70 treated groups resulted in an increased ALP activity. Runx2 is another crucial early marker gene, which

determines the osteoblast lineage from the pluripotent MSCs.[45, 67] The slight difference in Runx2 gene expression among all groups suggest that the cells developed into osteoblast after 21 days of culture with or without treatment with various AuNPs. The IBSP gene expression is directly related to calcium deposition in the ECM during mineralization stage.[12] Therefore, the expression of IBSP in rod-40 treated groups was significantly lower than that in the control group. This was in accordance with the results of ARS staining and calcium deposition assay. The SPPI gene performs some important functions in bone and its expression is an indicator of osteogenesis.[55] The expression of SPPI gene was up-regulated in sphere-40, sphere-70, sphere-110 and rod-70 treated groups, while down-regulated in star-40 and rod-40 treated groups, indicating the different osteogenic differentiation activity of hMSCs after various treatments. Overall, some osteogenic marker genes were found to be up-regulated or down-regulated after treatments with AuNPs depending on their size and shape as compared to the control. It has been reported that NPs may serve as mechanical stimuli to activate some signaling pathways in stem cells and thus induce their osteogenic differentiation.[45, 63] Recent studies have revealed that the mechanical signals can regulate the YAP activity and subcellular localization that are associated with the differentiation of stem cells.[68, 69] Therefore, in this study, we speculated that the AuNPs with different sizes and shapes might affect the osteogenic differentiation of hMSCs through regulation of the nuclear YAP activity. To confirm the hypothesis, the localization of activated YAP in hMSCs after treatments with various AuNPs was examined. The results showed that sphere-40, sphere-70 and rod-70 promoted while rod-40 inhibited the nuclear YAP activity significantly. No obvious influence was observed for the other AuNPs when compared with control. The higher percentages of hMSCs with nuclear localized YAP in sphere-40, sphere-70 and rod-70 treated groups might facilitate early osteogenic differentiation of hMSCs by increasing the expression of some early osteogenic marker genes.[69] However, rod-40 inhibited the osteogenic differentiation of hMSCs through reducing the nuclear YAP activity. Based on the results, a possible schematic diagram was proposed to describe the effects of AuNPs with different sizes and shapes on the osteogenic differentiation of hMSCs (Figure 3.10). The AuNPs were taken up by cells in a size and shape-dependent manner. The AuNPs would cause different mechanical signals on the cells because of their varying size and shape. It is possible that some integrin signaling pathway was activated in response to the changing of mechanical stress. The specific signaling pathway is unclear and need to be further studied. However, our results suggested that the mechanical signals would be transduced through YAP activation and therefore regulated the osteogenic gene expression. The up-regulation of ALP, Runx2, IBSP and SPPI in the groups after sphere-40, sphere-70 and rod-70 treatment resulted in the increased ALP activity and calcium deposition in hMSCs. However, the down-regulation of these genes led to a reduction in ALP activity and calcium deposition in the rod-40 treated groups. The effect of sphere-110, star-40, star-70, star-110 and rod-110 on the expression of these gens and ALP activity and calcium deposition was not evident. In summary, Au nanostars (star-40, star-70 and star-110) and bigger AuNPs (sphere-110, star-110 and rod-110) showed negligible effects on osteogenic differentiation of hMSCs. Smaller Au nanospheres (sphere-40 and sphere-70) and smaller Au nanorods (rod-40 and rod-70) affected the cell osteogenesis significantly. The cellular uptake, surface protein adsorption and potential cytotoxicity of AuNPs may play some roles in affecting the cell functions. Future studies should be performed to fully understand the biological mechanism about the influence of particle size and shape.

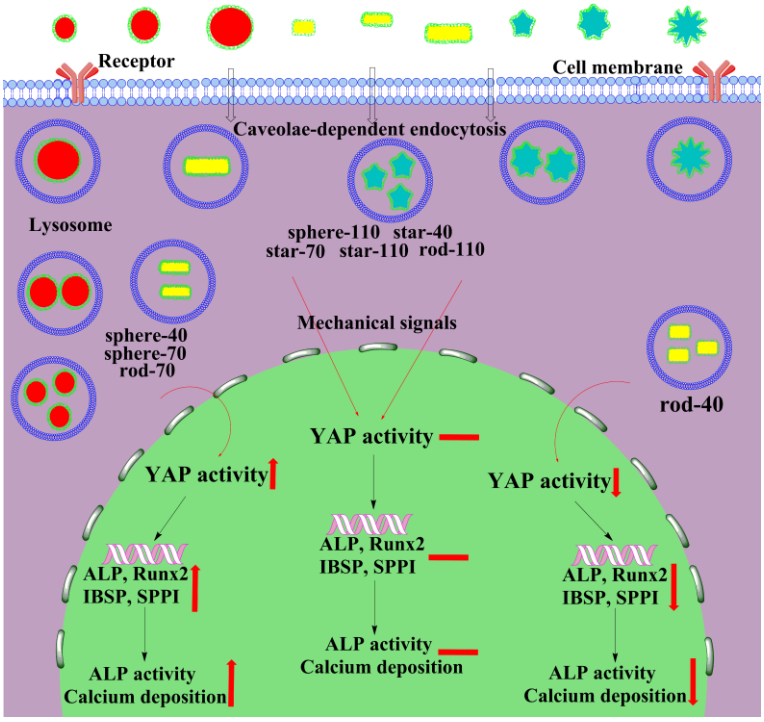

Figure 3.10 Schematic diagram of the influence of various AuNPs on osteogenic differentiation of hMSCs.

Many works have reported that Au nanospheres promote the osteogenic differentiation of various stem cells.[12, 45, 64, 70] This study is the first report to compare the effect of Au nanospheres, Au nanostars and Au nanorods on the osteogenic differentiation of hMSCs. Interestingly, rod-70 increased but rod-40 inhibited the osteogenesis ability of hMSCs. Considering that rod-70 could generate heating under laser irradiation,[71-73] the combination of photothermal therapy and stem cell therapy may provide an effective strategy to treatment various diseases. On the other hand, further study should be performed to investigate if rod-40 can be used as a therapeutic agent in treating osteoporosis and other bone diseases.[46] For star-40, star-70 and star-110, they have the potential to be developed as probes for long-term stem cell labeling without affecting the proliferation and differentiation of cells.[74] In summary, the results of this work will provide some useful information for the design of various NPs for different tissue engineering and biomedical applications.

3.6 Conclusions

In summary, the effect of AuNPs size and shape on the osteogenic differentiation of hMSCs was investigated. At a low Au concentration, the AuNPs with different sizes and shapes showed no any obvious influence on cell viability and cell proliferation of hMSCs. The AuNPs were taken up by the cells in a size and shape-dependent manner. Increased ALP activity and calcium deposition were found in cells incubated with sphere-40, sphere-70 and rod-70, while incubation with rod-40 reduced ALP activity and calcium deposition. Expression of osteogenic marker genes was up-regulated by sphere-40, sphere-70 and rod-70 treatment and down-regulated by rod-40 treatment. The mechanism study indicate that the size and shape of AuNPs could affect the osteogenic differentiation of hMSCs through regulating the nuclear YAP activity. The present study will offer beneficial information for the design and development of gold nanomaterial-based

platform for different biomedical applications such as therapeutic nanocarriers and tissue engineering scaffolds.

3.7 References

1. J. Li, X. Shi and M. Shen, *Part. Part. Syst. Char.*, 2014, 31, 1223-1237.
2. D.-E. Lee, H. Koo, I.-C. Sun, J. H. Ryu, K. Kim and I. C. Kwon, Chem. *Soc. Rev.*, 2012, 41, 2656-2672.
3. L. Dykman and N. Khlebtsov, *Chem. Soc. Rev.*, 2012, 41, 2256-2282.
4. V. Sokolova, A. M. Westendorf, J. Buer, K. Überla and M. Epple, *J. Mater. Chem. B*, 2015, 3, 4767-4779.
5. X. Zhang, X. Zhang, S. Wang, M. Liu, L. Tao and Y. Wei, *Nanoscale*, 2013, 5, 147-150.
6. Z. Zhang, C. Shao, P. Zou, P. Zhang, M. Zhang, J. Mu, Z. Guo, X. Li, C. Wang and Y. Liu, *Chem. Commun*., 2011, 47, 3906-3908.
7. M. Prabaharan, J. J. Grailer, S. Pilla, D. A. Steeber and S. Gong, *Biomaterials*, 2009, 30, 6065-6075.
8. A. Orza, O. Soritau, L. Olenic, M. Diudea, A. Florea, D. Rus Ciuca, C. Mihu, D. Casciano and A. S. Biris, *ACS Nano*, 2011, 5, 4490-4503.
9. J. Li, L. Zheng, H. Cai, W. Sun, M. Shen, G. Zhang and X. Shi, *ACS Appl. Mater. Interfaces*, 2013, 5, 10357-10366.
10. D. Bartczak, S. Nitti, T. M. Millar and A. G. Kanaras, *Nanoscale*, 2012, 4, 4470-4472.
11. E. Hutter, S. Boridy, S. Labrecque, M. Lalancette-Hébert, J. Kriz, F. M. Winnik and D. Maysinger, *ACS Nano*, 2010, 4, 2595-2606.
12. W.-K. Ko, D. N. Heo, H.-J. Moon, S. J. Lee, M. S. Bae, J. B. Lee, I.-C. Sun, H. B. Jeon, H. K. Park and I. K. Kwon, *J. Colloid Interface Sci.*, 2015, 438, 68-76.
13. X. Liu, H. Huang, G. Liu, W. Zhou, Y. Chen, Q. Jin and J. Ji, *Nanoscale*, 2013, 5, 3982-3991.
14. J. Zhang, C. Li, X. Zhang, S. Huo, S. Jin, F.-F. An, X. Wang, X. Xue, C. Okeke and G. Duan, *Biomaterials*, 2015, 42, 103-111.
15. J. Chen, F. Saeki, B. J. Wiley, H. Cang, M. J. Cobb, Z.-Y. Li, L. Au, H. Zhang, M. B. Kimmey and X. Li, *Nano Lett.*, 2005, 5, 473-477.
16. D. Kim, S. Park, J. H. Lee, Y. Y. Jeong and S. Jon, *J. Am. Chem. Soc.*, 2007, 129, 7661-7665.
17. Y. Cao, Y. He, H. Liu, Y. Luo, M. Shen, J. Xia and X. Shi, *J. Mater. Chem. B*, 2015, 3, 286-295.
18. H. Liu, H. Wang, Y. Xu, M. Shen, J. Zhao, G. Zhang and X. Shi, *Nanoscale*, 2014, 6, 4521-4526.
19. D. Pissuwan, T. Niidome and M. B. Cortie, *J. Controlled Release*, 2011, 149, 65-71.
20. J. Zhu, L. Zheng, S. Wen, Y. Tang, M. Shen, G. Zhang and X. Shi, *Biomaterials*, 2014, 35, 7635-7646.
21. L. Kong, C. S. Alves, W. Hou, J. Qiu, H. Möhwald, H. Tomás and X. Shi, *ACS Appl. Mater. Interfaces*, 2015, 7, 4833-4843.
22. J. Li, Y. Hu, J. Yang, P. Wei, W. Sun, M. Shen, G. Zhang and X. Shi, *Biomaterials*, 2015, 38, 10-21.
23. G. Terentyuk, E. Panfilova, V. Khanadeev, D. Chumakov, E. Genina, A. Bashkatov, V. Tuchin, A.

Bucharskaya, G. Maslyakova and N. Khlebtsov, *Nano Res.*, 2014, 7, 325-337.

24. S. Wang, P. Huang, L. Nie, R. Xing, D. Liu, Z. Wang, J. Lin, S. Chen, G. Niu and G. Lu, *Adv. Mater.*, 2013, 25, 3055-3061.
25. N. T. K. Thanh and Z. Rosenzweig, *Anal. Chem.*, 2002, 74, 1624-1628.
26. Y.-T. Wang, X.-M. Lu, F. Zhu, P. Huang, Y. Yu, L. Zeng, Z.-Y. Long and Y.-M. Wu, *Biomaterials*, 2011, 32, 7988-7998.
27. L. Ricles, S. Y. Nam, E. A. Trevino, S. Emelianov and L. J. Suggs, *J. Mater. Chem. B*, 2014, 2, 8220-8230.
28. Y. S. Zhang, Y. Wang, L. Wang, Y. Wang, X. Cai, C. Zhang, L. V. Wang and Y. Xia, *Theranostics*, 2013, 3, 532.
29. E. C. Dreaden, A. M. Alkilany, X. Huang, C. J. Murphy and M. A. El-Sayed, *Chem. Soc. Rev.*, 2012, 41, 2740-2779.
30. G. Maiorano, L. Rizzello, M. A. Malvindi, S. S. Shankar, L. Martiradonna, A. Falqui, R. Cingolani and P. P. Pompa, *Nanoscale*, 2011, 3, 2227-2232.
31. N. M. Schaeublin, L. K. Braydich-Stolle, A. M. Schrand, J. M. Miller, J. Hutchison, J. J. Schlager and S. M. Hussain, *Nanoscale*, 2011, 3, 410-420.
32. A. Albanese, P. S. Tang and W. C. Chan, Annu. Rev. *Biomed. Eng.*, 2012, 14, 1-16.
33. Y. Qiu, Y. Liu, L. Wang, L. Xu, R. Bai, Y. Ji, X. Wu, Y. Zhao, Y. Li and C. Chen, *Biomaterials*, 2010, 31, 7606-7619.
34. B. D. Chithrani, A. A. Ghazani and W. C. Chan, *Nano Lett.*, 2006, 6, 662-668.
35. B. D. Chithrani and W. C. Chan, *Nano Lett.*, 2007, 7, 1542-1550.
36. E. C. Cho, Q. Zhang and Y. Xia, *Nat. Nanotechnol.*, 2011, 6, 385-391.
37. A. M. Alkilany, P. K. Nagaria, C. R. Hexel, T. J. Shaw, C. J. Murphy and M. D. Wyatt, *Small*, 2009, 5, 701-708.
38. T. S. Hauck, A. A. Ghazani and W. C. Chan, *Small*, 2008, 4, 153-159.
39. F. Zhao, Y. Zhao, Y. Liu, X. Chang, C. Chen and Y. Zhao, *Small*, 2011, 7, 1322-1337.
40. P. M. Favi, M. Gao, L. Johana Sepúlveda Arango, S. P. Ospina, M. Morales, J. J. Pavon and T. J. Webster, *J. Biomed. Mater. Res., Part A*, 2015, 103, 3449-3462.
41. K. Niikura, T. Matsunaga, T. Suzuki, S. Kobayashi, H. Yamaguchi, Y. Orba, A. Kawaguchi, H. Hasegawa, K. Kajino and T. Ninomiya, *ACS Nano*, 2013, 7, 3926-3938.
42. P. Yan, R. Wang, N. Zhao, H. Zhao, D.-F. Chen and F.-J. Xu, *Nanoscale*, 2015, 7, 5281-5291.
43. S. Wang, Z. Teng, P. Huang, D. Liu, Y. Liu, Y. Tian, J. Sun, Y. Li, H. Ju and X. Chen, *Small*, 2015, 11, 1801-1810.
44. Y. Wang, K. C. Black, H. Luehmann, W. Li, Y. Zhang, X. Cai, D. Wan, S.-Y. Liu, M. Li and P. Kim, *ACS Nano*, 2013, 7, 2068-2077.
45. C. Yi, D. Liu, C.-C. Fong, J. Zhang and M. Yang, *ACS Nano*, 2010, 4, 6439-6448.
46. D. N. Heo, W.-K. Ko, H.-J. Moon, H.-J. Kim, S. J. Lee, J. B. Lee, M. S. Bae, J.-K. Yi, Y.-S. Hwang and J. B. Bang, *ACS Nano*, 2014, 8, 12049-12062.
47. S.-W. Tsai, J.-W. Liaw, Y.-C. Kao, M.-Y. Huang, C.-Y. Lee, L.-R. Rau, C.-Y. Huang, K.-C. Wei and

T.-C. Ye, *PloS One*, 2013, 8, e76545.

48. M. F. Pittenger, A. M. Mackay, S. C. Beck, R. K. Jaiswal, R. Douglas, J. D. Mosca, M. A. Moorman, D. W. Simonetti, S. Craig and D. R. Marshak, *Science*, 1999, 284, 143-147.
49. S. Wang, R. Castro, X. An, C. Song, Y. Luo, M. Shen, H. Tomás, M. Zhu and X. Shi, *J. Mater. Chem.*, 2012, 22, 23357-23367.
50. J. E. J. Li, N. Kawazoe and G. Chen, *Biomaterials*, 2015, 54, 226-236.
51. J. Li, R. Cai, N. Kawazoe and G. Chen, *J. Mater. Chem. B*, 2015, 3, 5806-5814.
52. Y. Xiang, X. Wu, D. Liu, L. Feng, K. Zhang, W. Chu, W. Zhou and S. Xie, *J. Phys. Chem. C*, 2008, 112, 3203-3208.
53. L. Zhang, K. Xia, Z. Lu, G. Li, J. Chen, Y. Deng, S. Li, F. Zhou and N. He, *Chem. Mater.*, 2014, 26, 1794-1798.
54. P. K. Jain, K. S. Lee, I. H. El-Sayed and M. A. El-Sayed, *J. Phys. Chem. B*, 2006, 110, 7238-7248.
55. S. Amorim, A. Martins, N. M. Neves, R. L. Reis and R. A. Pires, *J. Mater. Chem. B*, 2014, 2, 6939-6946.
56. J. Shao, S. Chen and C. Du, *J. Mater. Chem. B*, 2015, 3, 5291-5299.
57. Q. Gan, J. Zhu, Y. Yuan, H. Liu, J. Qian, Y. Li and C. Liu, *J. Mater. Chem. B*, 2015, 3, 2056-2066.
58. C. Yang, M. W. Tibbitt, L. Basta and K. S. Anseth, *Nat. Mater.*, 2014, 13, 645-652.
59. L. Qi, Y. Guo, J. Luan, D. Zhang, Z. Zhao and Y. Luan, *J. Mater. Chem. B*, 2014, 2, 8361-8371.
60. Y. Li, L. Feng, X. Shi, X. Wang, Y. Yang, K. Yang, T. Liu, G. Yang and Z. Liu, *Small*, 2014, 10, 1544-1554.
61. R. G. Rayavarapu, W. Petersen, L. Hartsuiker, P. Chin, H. Janssen, F. W. Van Leeuwen, C. Otto, S. Manohar and T. G. Van Leeuwen, *Nanotechnology*, 2010, 21, 145101.
62. D. Liu, C. Yi, D. Zhang, J. Zhang and M. Yang, *ACS Nano*, 2010, 4, 2185-2195.
63. K. Yang, W. Cao, X. Hao, X. Xue, J. Zhao, J. Liu, Y. Zhao, J. Meng, B. Sun and J. Zhang, *Nanoscale*, 2013, 5, 1205-1212.
64. D. Zhang, D. Liu, J. Zhang, C. Fong and M. Yang, *Mater. Sci. Eng., C*, 2014, 42, 70-77.
65. Y. Yao, X. Shi and F. Chen, *J. Nanosci. Nanotechnol.*, 2014, 14, 4851-4857.
66. W. Zhang, J. Liu, H. Shi, N. Liu, K. Yang, L. Shi, B. Gu, H. Wang, J. Ji and P. K. Chu, *J. Mater. Chem. B*, 2015, 3, 1856-1863.
67. X. Zhou, W. Feng, K. Qiu, L. Chen, W. Wang, W. Nie, X. Mo and C. He, *ACS Appl. Mater. Interfaces*, 2015, 7, 15777-15789.
68. S. Dupont, L. Morsut, M. Aragona, E. Enzo, S. Giulitti, M. Cordenonsi, F. Zanconato, J. Le Digabel, M. Forcato and S. Bicciato, *Nature*, 2011, 474, 179-183.
69. J.-H. Hong and M. B. Yaffe, *Cell cycle*, 2006, 5, 176-179.
70. S. Y. Choi, M. S. Song, P. D. Ryu, A. T. N. Lam, S.-W. Joo and S. Y. Lee, *Int. J. Nanomed.*, 2015, 10, 4383.
71. X. Liu, N. Huang, H. Li, H. Wang, Q. Jin and J. Ji, *ACS Appl. Mater. Interfaces*, 2014, 6, 5657-5668.
72. J. Qin, Z. Peng, B. Li, K. Ye, Y. Zhang, F. Yuan, X. Yang, L. Huang, J. Hu and X. Lu, *Nanoscale*, 2015, 7, 13991-14001.

73. H. Hou, L. Chen, H. He, L. Chen, Z. Zhao and Y. Jin, *J. Mater. Chem. B*, 2015, 3, 5189-5196.

74. H. Mao, R. Cai, N. Kawazoe and G. Chen, *Nanoscale*, 2014, 6, 1552-1559.

Chapter 4

Sub-10 nm gold nanoparticles promote adipogenesis and inhibit osteogenesis of mesenchymal stem cells

4.1 Summary

Sub-10 nm gold nanoparticles (AuNPs) have attracted extensive attention for different biomedical applications because of their small size. However, the influence of small NPs on differentiation of human bone marrow-derived mesenchymal stem cells (hMSCs) is unclear. In this study, 4-nm small AuNPs (Au4-*m*PEG NPs) were synthesized to investigate their influence on osteogenic and adipogenic differentiation of hMSCs with 40-nm counterparts (Au40-*m*PEG NPs) as a comparison. Different from Au40-*m*PEG NPs, Au4-*m*PEG NPs reduced the ALP activity, calcium deposition and osteogenic marker gene expression while increased the oil droplets formation and adipogenic marker gene expression in hMSCs. The mechanism study indicated that Au4-*m*PEG NPs treatment did not affect cellular mechanical property significantly but induced a high level of reactive oxygen species (ROS). The results provide some insights on the influence of sub-10 nm AuNPs on stem cell functions and applications of these small particles for tissue engineering.

4.2 Introduction

With the rapid advance of nanotechnology, a large number of nanoscale materials have been successfully developed for various biomedical applications including molecular imaging, cancer therapy, gene/drug delivery and tissue engineering.[1-3] Amongst these reported nanomaterials, gold nanoparticles (AuNPs) have received increasing attentions because of their simple synthesis, relatively good biocompatibility and excellent optical properties.[4-6] In addition, the size, shape and surface chemistry of AuNPs can be facilely controlled according to different demands.[7-9] Their physicochemical properties have obvious influence on cellular interactions, such as cytotoxicity, cellular uptake and cell functions.[10-12]

Nevertheless, most of the previous studies and applications have been focused on AuNPs larger than 10 nm.

Recently, sub-10 nm AuNPs have emerged as attractive candidates for biomedical applications because of their high payload-to-carrier ratio and rapid renal clearance.[13] Therefore, these NPs have been widely used for molecular imaging and gene/drug delivery.[14, 15] More importantly, as the size scale is commensurate with proteins, sub-10 nm AuNPs can well mimic extracellular matrix (ECM).[16] However, sub-10 nm AuNPs have been reported to have higher cytotoxicity than their counterparts larger than 10 nm.[11] In another study, 2- and 6-nm AuNPs have been reported to be more effective than larger ones (10- and 16-nm) in acting as carriers for gene therapy of cancer cells.[6] Therefore, the cellular influence and biomedical applications of AuNPs is generally dependent on their size.

Stem cells are considered as an attractive cell source for tissue engineering due to their self-renewal capacity and inherent ability to differentiate into multiple lineages.[17] AuNPs with a diameter of 20 nm have been reported to have a positive influence on osteogenic differentiation and negative effect on adipogenic differentiation of stem cells.[18] More importantly, the size of AuNPs plays a very important role in affecting the stem cell differentiation.[19] However, it is still unknown how sub-10 nm AuNPs affect differentiation of stem cells.

In this study, small AuNPs with an average size of 4 nm was synthesized to investigate their influence on osteogenic and adipogenic differentiation of human bone marrow-derived mesenchymal stem cells (hMSCs).

4.3 Materials and methods

4.3.1 Materials

Methoxy-poly(ethylene glycol)-thiol (*m*PEG-SH, Mw = 2000) was purchased from Yuka Sangyo Co., Ltd. (Tokyo, Japan). Hydrogen tetrachloroaurate tetrahydrate **(**$HAuCl_4 \cdot 4H_2O$, 99.9%), methanol, acetic acid, trisodium citrate, 4% paraformaldehyde and 2-propanol were purchased from Wako Pure Chemical Industries, Ltd. (Tokyo, Japan). Fetal bovine serum (FBS) was purchased from Gibco Lab. (Grand Island, NY, USA). Sensolyte pNPP alkaline phosphatase assay kit was purchased from AnaSpec (Fremont, CA, USA). Cellstain live/dead double staining kit and 4'-6-diamidino-2-phenylindole (DAPI) solution was obtained from Dojindo Lab. (Kumamoto, Japan). 2',7'-dichlorodihydrofluorescein diacetate (DCFH-DA) assay kit was purchased from Abcam Inc. (Cambridge, MA, USA). Alexa Fluor 488 phalloidin were purchased from Invitrogen (Grand Island, NY, USA). WST-1 reagent was purchased from Roche Molecular Biochemicals (Mannheim, Germany). Ascorbic acid (AA), sodium borohydride ($NaBH_4$), tiopronin, penicillin, streptomycin, proline, sodium pyruvate, glutamine, nonessential amino acids, Oil Red O, insulin, dexamethasone, β-glycerophosphate, 2-amino-2-methyl-1,3-propanediol, methyl-isobutylxanthine, indomethacin, naphthol AS-MX phosphate, fast blue RR salt, Alizarin Red S, Dulbecco's modified Eagle's Medium (DMEM), trypsin/EDTA and perchloric acid were purchased from Sigma-Aldrich (St. Louis, MO, USA). All the chemical reagents were used as received without further purification. Water used in all the experiments was purified by a Q-POD Milli-Q water purification system (Millipore Corp., Billerica, MA,

USA) to have a resistivity of 18.2 MΩ.cm.

4.3.2 Synthesis of Au4-*m*PEG and Au40-*m*PEG NPs

A seed-mediated method was applied to synthesize Au4-*m*PEG NPs. At first, Au seed solution was prepared according to a previous work.[20] $HAuCl_4$ (0.40 mmol) and tiopronin (1.2 mmol) were co-dissolved in 21 mL of methanol/acetic acid solution (6:1, v/v). After continuous stirring, 7.5 mL of $NaBH_4$ solution (8 mmol) was added slowly and the solution was kept stirring for 2 hours. The resultant product was dialyzed against water for 3 days using a dialysis membrane with molecular weight cut-off (MWCO) of 1000. Subsequently, the Au seed solution was used to prepare Au4-*m*PEG NPs. 0.6 mL of $HAuCl_4$ solution (30.0 mg/mL), 12.0 mL of Au seed solution, 0.2 mL of ascorbic acid solution (80.0 mg/mL) and 1.0 mL of *m*PEG-SH aqueous solution (2.0 mg/mL) were successively dropped into 20 mL water under gently stirring. The resultant solution was kept stirring at room temperature for 24 hours. After that, the product was dialyzed against water for 3 days using a dialysis membrane (12-14 kD MWCO, Spectrum Laboratories Inc., Rancho Dominguez, CA, USA).

Au40-*m*PEG NPs were prepared in a similar manner, but the used Au seed solution was prepared by citrate reduction method from $HAuCl_4$ solution according to a previous study.[21] Growth solution was prepared by successively adding $HAuCl_4$ solution (30.0 mg/mL, 0.6 mL), Au seed solution (24.0 mL), ascorbic acid solution (80.0 mg/mL, 0.2 mL) and 1.0 mL of *m*PEG-SH aqueous solution (2.0 mg/mL) into 20 mL water under gently stirring. After stirring at room temperature for 24 hours, the product was collected by centrifugation and washed with water for 3 times.

4.3.3 Characterization techniques

Transmission electron microscopy (TEM) images were obtained from a JEOL 2100F analytical electron microscope (JEOL, Tokyo, Japan) with an operating voltage of 200 kV. For each sample, 300 NPs in different TEM images were randomly selected and measured using an ImageJ software to assess the size and size distribution of the particles. Zeta potential and hydrodynamic size measurements were performed on a zeta-potential & particle size analyzer (ELSZ-2000, Otsuka Electronics Co., Ltd, Tokyo, Japan). Element concentration was assessed by a Leeman Prodigy Inductively Coupled Plasma-Optical Emission Spectroscopy (ICP-OES, SPS3520UV-DD) system (SII nano technology Inc., Tokyo, Japan).

4.3.4 Cell culture

Human bone marrow-derived mesenchymal stem cells (hMSCs) purchased from LONZA (Walkersville MD, USA) were cultured in MSCGM™ medium in a humidified atmosphere of 5% CO_2 at 37 °C. The hMSCs at passage 4 (P4) were used for the entire experiments. Cell growth medium was DMEM supplemented with 10% heat-inactivated FBS, 4500 mg/L glucose, 4 mM glutamine, 100 U/mL penicillin, 100 μg/mL streptomycin, 0.1 mM nonessential amino acids, 0.4 mM proline, 1 mM sodium pyruvate and 50 μg/mL ascorbic acid. Osteogenic induction medium was DMEM supplemented with 10% heat-inactivated FBS, 1000 mg/L glucose, 584 mg/L glutamine, 100 U/mL penicillin, 100 μg/mL streptomycin, 0.1 mM nonessential amino acids, 50 μg/mL ascorbic acid, 100 nM dexamethasone and 10 mM β-glycerophosphate.

Adipogenic induction medium was DMEM supplemented with 10% heat-inactivated FBS, 4500 mg/L glucose, 4 mM glutamine, 100 U/mL penicillin, 100 μg/mL streptomycin, 0.1 mM nonessential amino acids, 0.4 mM proline, 1 mM sodium pyruvate, 50 μg/mL ascorbic acid, 1 μM dexamethasone, 0.5 mM methyl-isobutylxanthine, 10 μg/mL insulin and 200 μM indomethacin.

4.3.5 Cytotoxicity assay of AuNPs

The hMSCs were seeded into 24-well plates at a density of 0.5×10^4 cells/cm^2 and cultured overnight for cell attachment. And then, the medium in each well was replaced by 0.5 mL fresh cell growth medium containing Au4-*m*PEG or Au40-*m*PEG NPs at an Au concentration of 0.1 mM. The cells were incubated with NPs for 7 days and the culture medium was changed every 3 days. At each time point, the cells were washed with PBS and then used for WST-1 assay and live/dead staining (n = 3).

4.3.6 Cellular uptake of AuNPs

The hMSCs were seeded into 6-well plates at a density of 1×10^4 cells/cm^2 in 2 mL growth medium. After 24 hours of culture for cell attachment, the medium was discarded and fresh cell growth medium containing Au4-*m*PEG or Au40-*m*PEG NPs at an Au concentration of 0.05 or 0.1 mM was added into each well and the medium was changed every 3 days. After 7 days of incubation, the cells were washed with PBS carefully to remove the free NPs, harvested by tyrpsinization, counted by hemocytometer and then dissolved in aqua regia solution. Finally, the samples were diluted with water and Au content was measured by ICP-OES (n = 3).

4.3.7 Alkaline phosphatase (ALP) staining and ALP activity assay

The hMSCs were seeded in 24-well plates at a density of 0.5×10^4 cells/cm^2 and cultured overnight for cell attachment. Then the cells were incubated with Au4-*m*PEG or Au40-*m*PEG NPs at an Au concentration of 0.05 mM in osteogenic induction medium for 14 days. The medium was changed every 2 or 3 days. And then, the cells were washed with PBS, fixed with 4% paraformaldehyde and incubated with 0.1% naphthol AS-MX phosphate and 0.1% fast blue RR salt in 56 mM 2-amino-2-methyl-1,3-propanediol working solution (pH = 9.9). The stained cells were observed with an optical microscope. Sensolyte® pNPP alkaline phosphatase assay kit was used to quantify the ALP activity according to our previously reported protocols.[17] The ALP amount was normalized to the cell number in each well (n = 3).

4.3.8 Alizarin Red S (ARS) staining and calcium deposition assay

After being incubated with Au4-*m*PEG or Au40-*m*PEG NPs at an Au concentration of 0.05 mM in osteogenic induction medium for 21 days, the cells were washed with PBS, fixed with 4% paraformaldehyde and incubated with 0.1% ARS solution. And then, the cells were washed with PBS again and observed under an optical microscopy. For calcium deposition assay, the stained cells were dried in the air and then the dye in each well was dissolved by 5% perchloric acid. The dissolved dye solution (n = 3) was transferred into a 96-well plate and their absorbance at 405 nm was read by a microplate reader (Benchmark Plus, Bio-Rad, Hercules, CA, USA).

4.3.9 Oil Red O staining

The hMSCs were seeded into 24-well plates in cell growth medium at a density of 2×10^4 cells/cm^2 and cultured overnight for cell attachment. And then, the cells were incubated with Au4-*m*PEG or Au40-*m*PEG NPs at an Au concentration of 0.05 mM in adipogenic induction medium with a regular change of fresh medium every 3 days. After 14 days of culture, the cells were successively washed with PBS, fixed with 4% paraformaldehyde, soaked in 60% 2-propanol and incubated with Oil Red O working solution. An optical microscope was used to observe the stained cells after washing with water. Finally, the stained cells were dried in the air and 2-propanol was used to extract the Oil Red O dye. The solution in each well was transferred into a 96-well plate and their absorbance at 540 nm was read by a microplate reader (n = 3).

4.3.10 Quantitative real-time polymerase chain reaction (PCR)

After being incubated with Au4-*m*PEG or Au40-*m*PEG NPs at an Au concentration of 0.05 mM in osteogenic induction medium or adipogenic induction medium for 14 days, the cells were washed with PBS and collected for RNA extraction with a RNAeasy Mini kit (Qiagen, Netherlands) according to the manufacturer's instructions. After the obtained RNA was quantified and converted to cDNA, quantitative real-time PCR was performed to assay the expression of osteogenic and adipogenic related marker genes (n = 3). The primers and probes used for real-time PCR are listed in Table 3.1 and Table 4.1.

Table 4.1. The primers and probes for real-time PCR.

mRNA	Oligonucleotide
FABP4	Hs00609791_m1
FASN	Hs00188012_m1
CEBPA	Hs00269972_s1

4.3.11 Intracellular reactive oxygen species (ROS) measurement

The hMSCs were incubated with Au4-*m*PEG or Au40-*m*PEG NPs at an Au concentration of 0.05 mM in osteogenic induction medium or adipogenic induction medium for 7, 14 and 21 days. And then, the cells were washed with PBS and incubated in 2',7'-dichlorofluorescin diacetate (DCFH-DA) working solution (2 μM) at 37 °C for 45 minutes. Triton X-100 solution was used to lyse the cells and the cell debris in each well were collected into a microtube and centrifuged at 2500× g for 10 minutes. After that, the supernatant was transferred into a 96-well plate and the fluorescence intensity was measured with a microplate reader at an excitation wavelength of 485 nm and an emission wavelength of 525 nm.[22] The ROS level was normalized to total cell number in each well and presented as a relative value to control group (n = 3).

4.3.12 F-actin immunostaining and mechanical property measurements

The hMSCs were incubated with Au4-*m*PEG or Au40-*m*PEG NPs at an Au concentration of 0.05 mM in growth medium for 7 days. After that, the cells were performed for F-actin immunostaining and atomic force

microscopy (AFM) measurements. For F-actin immunostaining, the cells were washed twice with PBS, fixed with 4% paraformaldehyde at room temperature for 10 minutes, permeabilized with 1% Triton X-100 for 5 minutes and then blocked with 2% bovine serum albumin (BSA) solution for 30 minutes. And then, the cells were successively incubated at room temperature with Alexa Fluor 488 phalloidin (1:40) for 30 minutes and DAPI solution (1:800) for 10 minutes. The fluorescence images were captured by using an inverted fluorescence microscope after the cells were further washed with PBS. For the AFM measurements, the cells were washed with PBS and the mechanical property of living cells was measured with a commercially available MFP-3D-Bio AFM microscope according to our previously reported method.[23, 24]

4.3.13 Statistical analysis

All data were reported as mean ± standard deviation (SD) with experiments repeated in triplicate (n = 3). One-way ANOVA statistical analysis was performed to evaluate the significance of the experimental data. 0.05 was selected as the significance level and the data were indicated with (*) for $p < 0.05$, (**) for $p < 0.01$ and (***) for $p < 0.001$, respectively.

4.4 Results and discussion

4.4.1 Characterization of Au4-*m*PEG and Au40-*m*PEG NPs

In order to investigate the influence of sub-10 nm AuNPs on osteogenic and adipogenic differentiation of hMSCs, Au4-*m*PEG NPs were synthesized and Au40-*m*PEG NPs were used for a comparison. TEM images showed that the as-prepared Au4-*m*PEG NPs were spherical and homogeneously distributed with an average diameter of 4.1 ± 1.0 nm (Figure 4.1a and b). The size of Au40-*m*PEG NPs was measured to be 39.4 ± 7.7 nm (Figure 4.1c and d).

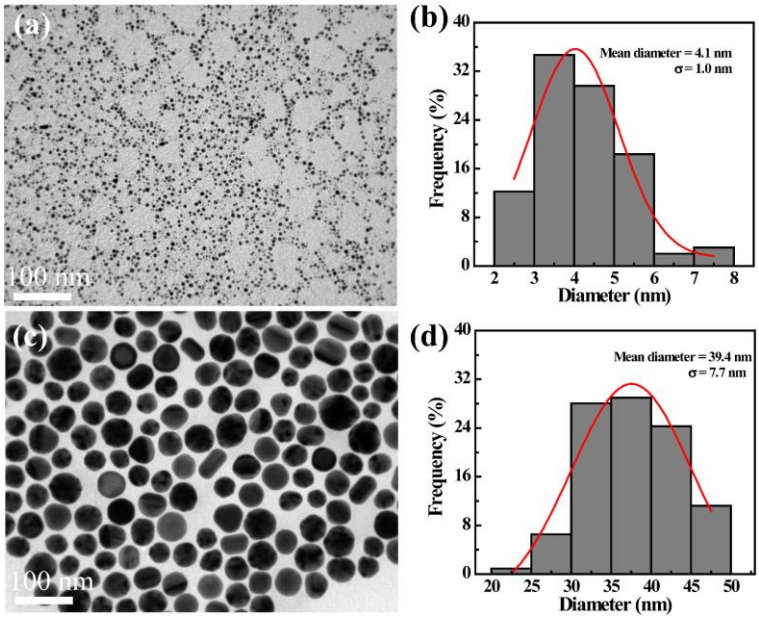

Figure 4.1 TEM images and size distribution histograms of Au4-*m*PEG NPs (a, b) and Au40-*m*PEG NPs (c, d).

The surface potential of Au4-*m*PEG and Au40-*m*PEG NPs in water was -23.4 ± 1.8 mV and -26.8 ± 3.2 mV, respectively. The two types of AuNPs showed similar surface potential because of the same surface coating of PEG. The hydrodynamic size of Au4-*m*PEG NPs and Au40-*m*PEG NPs was measured to be 65.9 ± 2.8 and 59.3 ± 0.8 nm by dynamic light scattering (DLS). The hydrodynamic size of Au4-*m*PEG NPs was much bigger than the size measured from the TEM images. This might be because the DLS measured the clusters of ultra-small NPs in aqueous solution, which was in agreement with previous work.[25] After 7 days of storage, their hydrodynamic sizes did not have any obvious change, suggesting the good colloidal stability of Au4-*m*PEG NPs and Au40-*m*PEG NPs.

4.4.2 Cytotoxicity assay of Au4-*m*PEG and Au40-*m*PEG NPs

Live/dead staining was performed to visualize cell viability after incubation with NPs for different time. The number of live cells (green color) in Au4-*m*PEG NPs group was almost the same as those in control and Au40-*m*PEG NPs groups after 1 day of incubation (Figure 4.2a). However, after culture for 3 and 7 days, the number of live cells in Au4-*m*PEG NPs group decreased compared with the control and Au40-*m*PEG NPs groups. The results of WST-1 assay showed that the cells treated with Au40-*m*PEG NPs for 1, 3 and 7 days had a similar cell viability as the control cells, suggesting the good biocompatibility of Au40-*m*PEG NPs (Figure 4.2b). However, Au4-*m*PEG NPs treatment group had a significantly lower cell viability than did the control and Au40-*m*PEG NPs groups after 3 and 7 days of incubation. The results suggested that Au4-*m*PEG NPs had a higher cytotoxicity than the Au40-*m*PEG NPs at an Au concentration of 0.1 mM. High cytotoxicity of sub-10 nm AuNPs has also been reported in previous works.[12, 26] AuNPs with an average size of 2.81 and 5.52 nm have been reported to have a higher cytotoxicity than AuNPs with an average size of 38.05 nm.[26] The results indicated that the cytotoxicity of NPs was dependent on their size and sub-10 nm NPs generally displayed a high cytotoxicity. Based on these results, a low Au concentration (0.05 mM) was used in the following osteogenic and adipogenic differentiation experiments to ensure high cell viability.

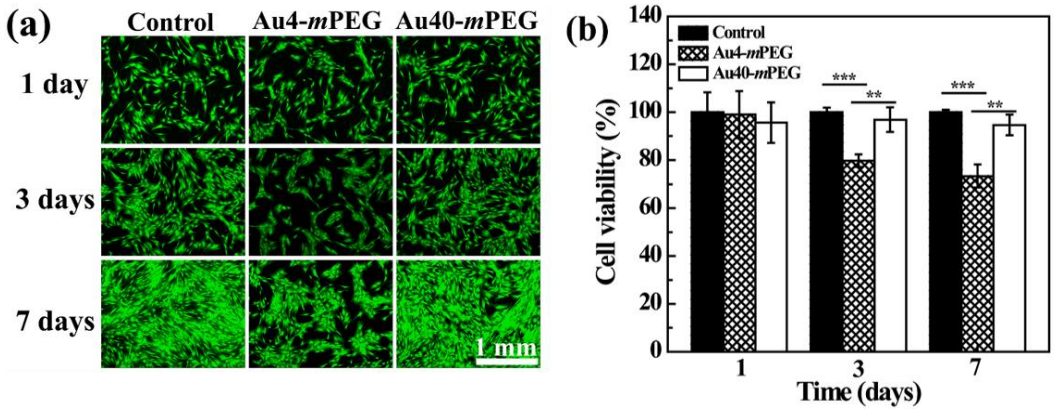

Figure 4.2 Live/dead staining (a) and WST-1 assay (b) of hMSCs after incubation without AuNPs (control) or with Au4-*m*PEG or Au40-*m*PEG NPs at an Au concentration of 0.1 mM for 1, 3 and 7 days.

4.4.3 Cellular uptake assay of Au4-*m*PEG and Au40-*m*PEG NPs

For biomedical applications, cellular uptake of NPs is very important. Cellular uptake of Au4-*m*PEG

and Au40-*m*PEG NPs was investigated by ICP-OES. The cells cultured with AuNPs displayed obvious cellular uptake of AuNPs and the cellular uptake increased as Au concentration increased for both Au4-*m*PEG and Au40-*m*PEG NPs (Figure 4.3). At the same Au concentration, Au4-*m*PEG NPs showed significantly higher cellular uptake than did the Au40-*m*PEG NPs. It has been previously reported that AuNPs with a size around 50 nm had the maximal uptake, which was presented by "particle numbers of AuNPs".[27] However, the "weight of Au element" was used in this work, which should be the reason why the cellular uptake was inconsistent with the previous results. In addition, the surface stabilizers of NPs, cell types and culture time may also affect the differences in cellular uptake between previous reports and the present work.

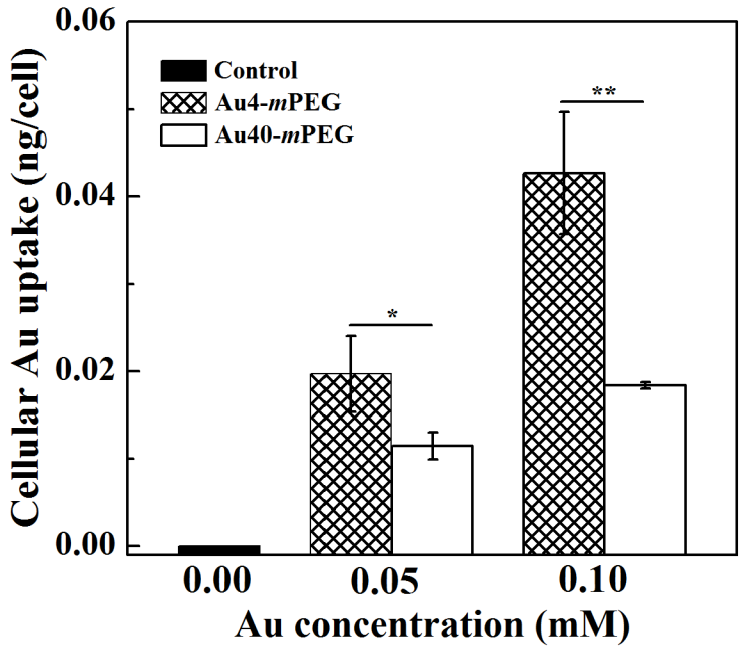

Figure 4.3 Cellular uptake assay of AuNPs after hMSCs were cultured with Au4-*m*PEG or Au40-*m*PEG NPs at an Au concentration of 0.05 and 0.1 mM for 7 days.

4.4.4 ALP staining, ALP activity assay, ARS staining and calcium deposition assay

After 14 days of incubation in osteogenic induction medium, hMSCs were stained to check ALP expression. The staining intensity of the cells treated with Au4-*m*PEG NPs was obviously less than that of the control cells and the cells treated with Au40-*m*PEG NPs (Figure 4.4a). The quantitative ALP activity suggested that treatment with Au4-*m*PEG NPs significantly reduced ALP activity, while treatment of Au40-*m*PEG NPs increased ALP activity as compared with the control group (Figure 4.4c). ALP is considered as an early stage marker during osteogenesis.[28] Therefore, the reduced ALP activity indicated that Au4-*m*PEG NPs might inhibit the osteogenic differentiation of hMSCs.

Bone matrix maturation and mineralization are vital processes for osteogenic differentiation of stem cells.[29] ARS staining was performed to evaluate the mineralization level after 21 days of culture in osteogenic induction medium. Dense red web-like staining was observed in the control and Au40-*m*PEG NPs treated groups. However, the ARS staining intensity was much less in the Au4-*m*PEG NPs treated cells

(Figure 4.4b). Furthermore, the ARS staining was eluted and quantified. Au4-*m*PEG NPs treated cells showed significantly lower calcium deposition while Au40-*m*PEG NPs treated cells showed significantly higher calcium deposition than did the control (Figure 4.4d). The results suggested that Au4-*m*PEG NPs had an inhibitive effect on the matrix mineralization of hMSCs.

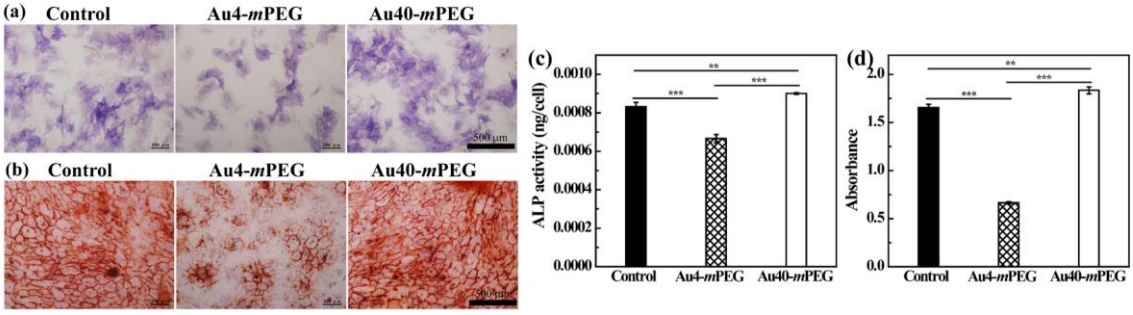

Figure 4.4 ALP staining (a) and ALP activity assay (c) of hMSCs after incubation without AuNPs (control) or with Au4-*m*PEG and Au40-*m*PEG NPs in osteogenic induction medium for 14 days. ARS staining (b) and calcium deposition assay (d) of hMSCs after incubation in osteogenic induction medium for 21 days.

4.4.5 Oil Red O staining and oil droplets formation

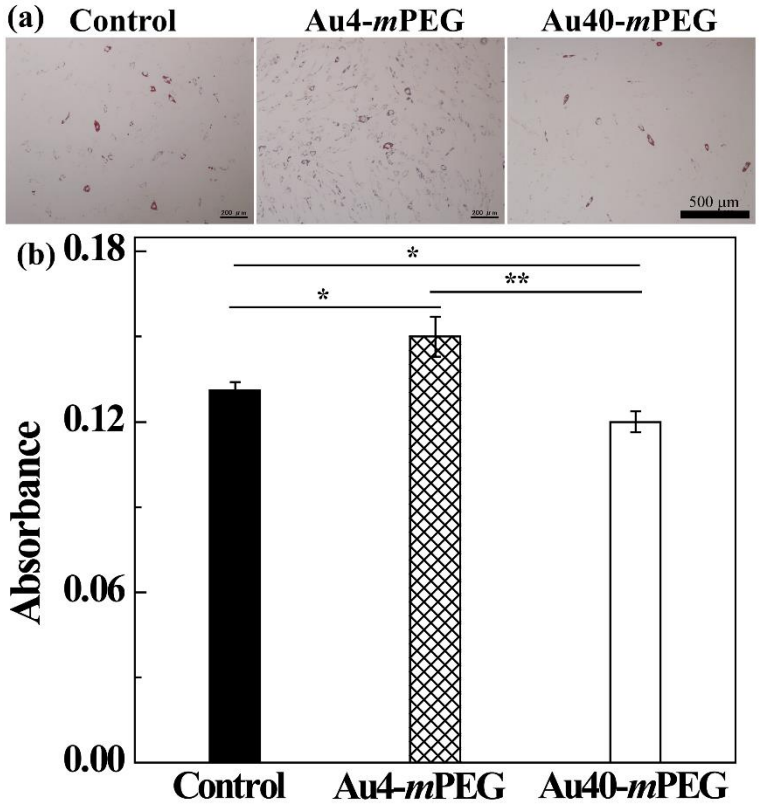

Figure 4.5 Oil Red O staining (a) and oil droplets formation (b) of hMSCs after incubation without AuNPs (control) or with Au4-*m*PEG or Au40-*m*PEG NPs in adipogenic induction medium at an Au concentration of 0.05 mM for 14 days.

The influence of Au4-*m*PEG NPs on adipogenic differentiation of hMSCs was checked by analyzing oil droplets formation. The cells cultured with Au4-*m*PEG NPs showed much higher staining intensity while the

cells cultured with Au40-*m*PEG NPs showed much lower staining intensity than did the control (Figure 4.5a). Oil droplets formation was further quantified by measuring the absorbance of dissolved Oil red O staining. Au4-*m*PEG NPs treated cells showed the highest level of oil droplets formation, which was significantly higher than that of control and Au40-*m*PEG NPs treated cells (Figure 4.5b). The results suggested that Au4-*m*PEG NPs had a promotive effect while Au40-*m*PEG NPs showed inhibitive effect on adipogenic differentiation of hMSCs.

4.4.6 Gene expression analysis

To further elucidate the influence of Au4-*m*PEG NPs and Au40-*m*PEG NPs on the osteogenic and adipogenic differentiation of hMSCs at gene level, expression of some marker genes related to osteogenesis and adipogenesis was analyzed. Expression of osteogenic marker genes is shown in Figure 4.6a. ALP is an early stage gene during osteogenesis that regulates the bone formation and mineralization.[30] Au4-*m*PEG NPs slightly down-regulated while Au40-*m*PEG NPs up-regulated ALP gene expression. Bone sialoprotein 2 (IBSP) is calcium deposition production related gene.[31] IBSP expression was decreased in the Au4-*m*PEG NPs treated cells and increased in the Au40-*m*PEG NPs treated cells as compared to the control. Secreted phosphoprotein I (SPPI) performs important functions in bone cells and its expression indicates the success of osteogenesis from stem cells.[32] Expression of SPPI gene showed a similar trend as ALP and IBSP genes. These results suggested that Au4-*m*PEG NPs down-regulated while Au40-*m*PEG NPs up-regulated the osteogenic marker genes in hMSCs.

Expression of adipogenic marker genes is shown in Figure 4.6b. Fatty acid binding protein 4 (FABP4) and fatty acid synthase (FASN) are late adipogenic marker genes.[33] The expression of genes encoding FABP4 and FASN was up-regulated by Au4-*m*PEG NPs and down-regulated by Au40-*m*PEG NPs. CCAAT/enhancer binding protein (CEBPA) is a key adipogenic transcription factor.[34] Au4-*m*PEG NPs treated cells had a slightly higher expression of CEBPA gene while Au40-*m*PEG NPs treated cells had a lower expression than the control. The results suggested that Au4-*m*PEG NPs could promote the expression of adipogenic marker gene in hMSCs.

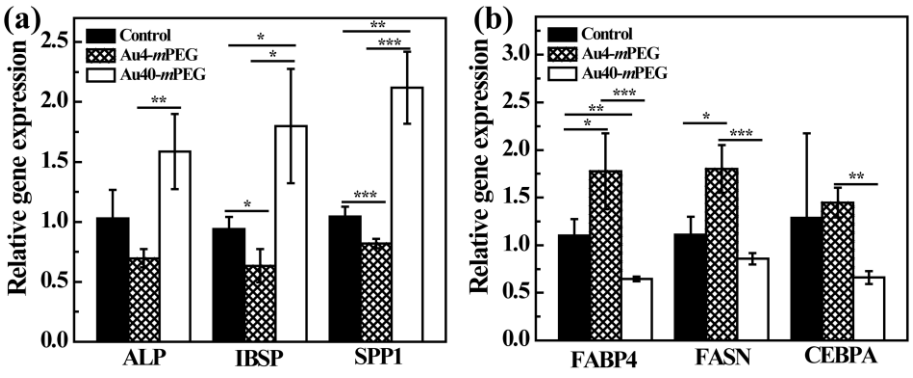

Figure 4.6 Gene expression of ALP, IBSP and SPPI in hMSCs after incubation without AuNPs (control) or with Au4-*m*PEG or Au40-*m*PEG NPs in osteogenic induction medium for 14 days (a), and gene expression of FABP4, FASN and CEBPA in hMSCs after incubation without AuNPs (control) or with Au4-*m*PEG or Au40-*m*PEG NPs in adipogenic induction medium for 14 days (b).

4.4.7 Intracellular ROS measurement

ROS has been reported to play an important role in mediating stem cell differentiation.[35, 36] Intracellular ROS level in hMSCs during osteogenic and adipogenic induction culture was measured. The results showed that Au40-*m*PEG NPs had a minimal impact on intracellular ROS level while Au4-*m*PEG NPs induced a very high level of ROS during both osteogenic and adipogenic induction culture of hMSCs (Figure 4.7a and b). ROS level in the Au4-*m*PEG NPs treated cells was significantly higher than that in the control and Au40-*m*PEG NPs treated cells, especially after 14 and 21 days of culture. Some previous studies have also shown that sub-10 nm AuNPs could induce elevated ROS level in cells.[37, 38] 1.5-nm AuNPs have been reported to generate significant amount of ROS in a human keratinocyte cell line (HaCaT), regardless of their surface charge.[37] 2-nm AuNPs have been reported to generate a high level of ROS and ROS production was dependent on the particle functionalization.[38] Increased hydrophobicity of NPs resulted in high ROS level. With good agreement with previous reports, our results also indicated that Au4-*m*PEG NPs induced significant ROS generation during cell culture.

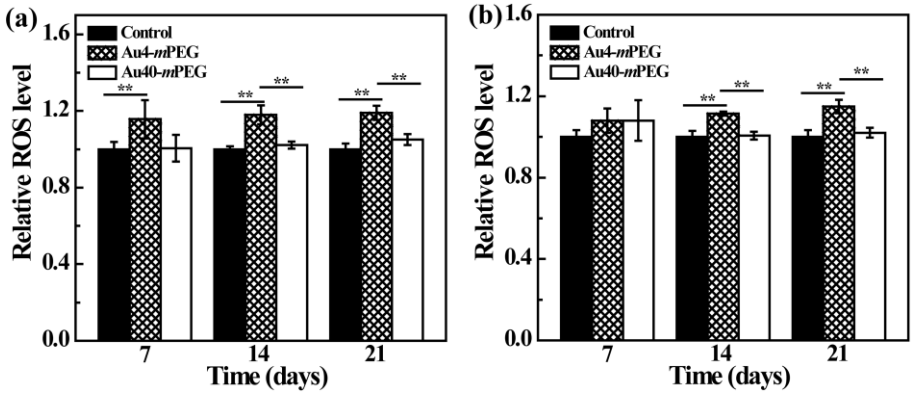

Figure 4.7 ROS level in hMSCs after incubation without AuNPs (control) or with Au4-*m*PEG or Au40-*m*PEG NPs in osteogenic induction medium (a) or adipogenic induction medium (b) for 7, 14 and 21 days.

4.4.8 F-actin cytoskeleton and cell mechanical property

Immunofluorescent staining was performed to study the F-actin cytoskeleton of hMSCs after culture with NPs. There was no obvious difference in F-actin filaments between the control and Au4-*m*PEG NPs treated cells (Figure 4.8a). However, Au40-*m*PEG NPs treated cells showed slightly increased F-actin stress fibers, suggesting that AuNPs of this size could enhance the actin assembly of hMSCs. In this study, AuNPs with different sizes resulted in different influence on F-actin cytoskeleton, which may be because of the different NP-cell interaction affected by NP size.

By using AFM, the influence of Au4-*m*PEG NPs and Au40-*m*PEG NPs on mechanical property of hMSCs was investigated. Although the Young's modulus distribution histograms were similar, the histogram of cells treated with Au40-*m*PEG NPs became wider compared with those of the control and Au4-*m*PEG NPs treated cells (Figure 4.8b-d). The Young's modulus of the control, Au4-*m*PEG NPs and Au40-*m*PEG NPs treated cells was 2.39 ± 0.28, 2.34 ± 0.30 and 2.61 ± 0.36 kPa, respectively. The results indicated that cellular mechanical property of hMSCs was increased after culture with Au40-*m*PEG NPs.

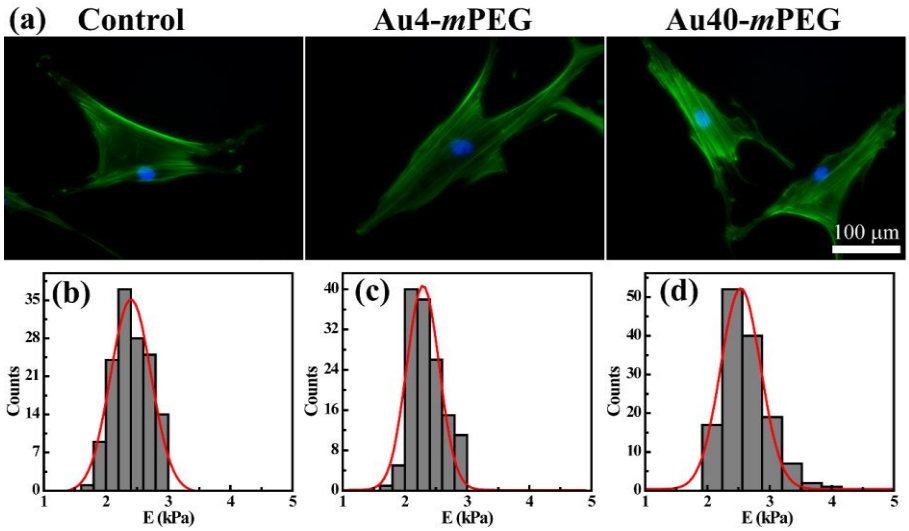

Figure 4.8 Immunofluorescence staining of F-actin in hMSCs (a) and representative Young's modulus distributions of hMSCs after incubation without AuNPs (b) or with Au4-*m*PEG NPs (c) or Au40-*m*PEG NPs (d) for 7 days.

Influence of AuNPs on multiple differentiation of stem cells has been widely studied. A previous study reported that 20-nm AuNPs could promote osteogenic differentiation but inhibit adipogenic differentiation of mouse MSCs through the p38 mitogen-activated protein kinase (MAPK) pathway.[18] In another study, AuNPs accelerated osteogenic differentiation in human adipose-derived stem cells (ADSCs) through the Wnt/β-catenin signaling pathway.[39] The physical and chemical properties of AuNPs including size, shape and surface chemistry also show obvious effects on cell differentiation, especially for osteogenic differentiation. Ko et al. have demonstrated that 30- and 50-nm AuNPs were more effective in enhancing osteogenic differentiation of ADSCs than did their counterparts of other size (15, 75 and 100 nm).[31] In addition, Au nanospheres with a size of 40 and 70 nm and Au nanorods with a size of 70 nm increased while Au nanorods with a size of 40 nm reduced the osteogenic differentiation levels of hMSCs.[17] Au nanostars with a size of 40, 70 and 110 nm, Au nanospheres and Au nanorods with a size of 110 nm showed negligible influences on this process. For the influence of NP surface chemistry, AuNPs functionalized with amine, hydroxyl and citrate groups did not inhibit the osteogenic differentiation, while AuNPs functionalized with carboxyl group markedly reduced the ALP activity and matrix mineralization in hMSCs.[21] However, most of these studies have been focused on the AuNPs with a size larger than 10 nm.

Sub-10 nm AuNPs have recently shown great potential in biomedical fields. Currently, various payloads conjugated sub-10 nm AuNPs have attracted extensive attentions for delivery purpose because of their very small size.[20] To understand the roles of sub-10 nm AuNPs in nanomedicine, it is necessary to elucidate their influences on stem cell differentiation. In this study, the effect of Au4-*m*PEG NPs on differentiation, cytoskeleton disturbance and stiffness variation of hMSCs was compared with that of Au40-*m*PEG NPs. Au4-*m*PEG NPs inhibited osteogenic differentiation but promoted the adipogenic differentiation of hMSCs, which was completely opposite to Au40-*m*PEG NPs. Increasing evidences implicate that excessive amount of ROS prevents osteogenic differentiation but promotes adipogenic differentiation of MSC.[40] After incubation with Au4-*m*PEG NPs, the hMSCs showed significantly higher ROS level than the control and Au40-*m*PEG NPs treated cells, no matter in osteogenic induction medium or adipogenic induction medium.

This should be the reason why Au4-*m*PEG NPs inhibited the osteogenesis but promoted the adipogenesis of hMSCs. In a recent work, Ag NPs coated surfaces were found to enhance adipogenesis compared to osteogenesis in hMSCs through the Ag NPs induced ROS generation.[41] On another hand, the accumulation of NPs inside cells can cause cell cytoskeleton and mechanical property change.[42] Au4-*m*PEG NPs and Au40-*m*PEG NPs showed different effect on cytoskeleton assembly and cellular mechanical property. Au40-*m*PEG NPs increased the Young's modulus of hMSCs, while Au4-*m*PEG NPs did not have obvious influence compared with the control. This may be due to the different interaction between cells and AuNPs that was affected by the size of AuNPs. Our previous study suggested that high mechanical property contributed to osteogenic differentiation but impaired adipogenic differentiation of hMSCs.[43] Therefore, the promotive effect of Au40-*m*PEG NPs on osteogenic differentiation of hMSCs should be mainly through the enhanced cytoskeleton tension and cellular Young's modulus.

Treatment of NPs may induce ROS generation or change cellular mechanical property. The results in the present study suggested that ROS and mechanical property might function as weights of the balance to regulate cell differentiation. Increased mechanical property was beneficial to osteogenesis while high ROS level promoted adipogenesis of stem cells. Actually, cell differentiation is a very complicated process that involves many possible mechanisms and signaling pathways. The different influence of Au4-*m*PEG NPs and Au40-*m*PEG NPs on osteogenic and adipogenic differentiation should attributed to the high ROS level and enhanced mechanical property, respectively. The results in this study should provide a meaningful guidance to use different size NPs for tissue engineering.

4.5 Conclusions

In summary, the influence of sub-10 nm AuNPs on osteogenic and adipogenic differentiation of hMSCs was studied with 40-nm counterparts as a comparison. Surface coating of PEG afforded AuNPs good colloidal stability and similar surface charge. Au4-*m*PEG NPs had a higher cytotoxicity and cellular uptake than did the Au40-*m*PEG NPs at the studied concentrations. The influence of Au4-*m*PEG NPs and Au40-*m*PEG NPs on hMSCs differentiation was opposite. The inhibitive effect of Au4-*m*PEG NPs on osteogenic differentiation and their promotive effect on adipogenic differentiation should be due to highly induced ROS level. The results should be useful for the design and development of novel NPs for different biomedical applications.

4.6 References

1. D. Pissuwan, T. Niidome and M. B. Cortie, *J. Controlled Release*, 2011, 149, 65-71.
2. D. N. Heo, W.-K. Ko, M. S. Bae, J. B. Lee, D.-W. Lee, W. Byun, C. H. Lee, E.-C. Kim, B.-Y. Jung and I. K. Kwon, *J. Mater. Chem. B*, 2014, 2, 1584-1593.
3. S. Wang, J. Zhao, F. Hu, X. Li, X. An, S. Zhou, Y. Chen and M. Huang, *J. Mater. Chem. B*, 2016, 4, 7368-7378.
4. L. Dykman and N. Khlebtsov, *Chem. Soc. Rev.*, 2012, 41, 2256-2282.

5. J. Li, X. Shi and M. Shen, *Part. Part. Syst. Charact.*, 2014, 31, 1223-1237.
6. S. Huo, S. Jin, X. Ma, X. Xue, K. Yang, A. Kumar, P. C. Wang, J. Zhang, Z. Hu and X.-J. Liang, *ACS Nano*, 2014, 8, 5852-5862.
7. J. Li, L. Zheng, H. Cai, W. Sun, M. Shen, G. Zhang and X. Shi, *ACS Appl. Mater. Interfaces*, 2013, 5, 10357-10366.
8. J. Li, R. Cai, N. Kawazoe and G. Chen, *J. Mater. Chem. B*, 2015, 3, 5806-5814.
9. S. Wang, Z. Teng, P. Huang, D. Liu, Y. Liu, Y. Tian, J. Sun, Y. Li, H. Ju and X. Chen, *Small*, 2015, 11, 1801-1810.
10. A. Albanese, P. S. Tang and W. C. Chan, *Annu. Rev. Biomed. Eng.*, 2012, 14, 1-16.
11. Y. Pan, S. Neuss, A. Leifert, M. Fischler, F. Wen, U. Simon, G. Schmid, W. Brandau and W. Jahnen‐Dechent, *Small*, 2007, 3, 1941-1949.
12. A. Verma and F. Stellacci, *Small*, 2010, 6, 12-21.
13. Y. Jiang, S. Huo, T. Mizuhara, R. Das, Y.-W. Lee, S. Hou, D. F. Moyano, B. Duncan, X.-J. Liang and V. M. Rotello, *ACS Nano*, 2015, 9, 9986-9993.
14. Y. Cao, Y. He, H. Liu, Y. Luo, M. Shen, J. Xia and X. Shi, *J. Mater. Chem. B*, 2015, 3, 286-295.
15. W. Hou, P. Wei, L. Kong, R. Guo, S. Wang and X. Shi, *J. Mater. Chem. B*, 2016, 4, 2933-2943.
16. M. De, C.-C. You, S. Srivastava and V. M. Rotello, *J. Am. Chem. Soc.*, 2007, 129, 10747-10753.
17. J. Li, J. E. J. Li, J. Zhang, X. Wang, N. Kawazoe and G. Chen, *Nanoscale*, 2016, 8, 7992-8007.
18. C. Yi, D. Liu, C.-C. Fong, J. Zhang and M. Yang, *ACS Nano*, 2010, 4, 6439-6448.
19. D. Zhang, D. Liu, J. Zhang, C. Fong and M. Yang, *Mater. Sci. Eng., C*, 2014, 42, 70-77.
20. A. Kumar, H. Ma, X. Zhang, K. Huang, S. Jin, J. Liu, T. Wei, W. Cao, G. Zou and X.-J. Liang, *Biomaterials*, 2012, 33, 1180-1189.
21. J. E. J. Li, N. Kawazoe and G. Chen, *Biomaterials*, 2015, 54, 226-236.
22. M. J. Akhtar, M. Ahamed, S. Kumar, M. Khan, J. Ahmad and S. A. Alrokayan, *Int. J. Nanomedicine*, 2012, 7, 845-857.
23. H. Mao, J. Li, I. Dulińska-Molak, N. Kawazoe, Y. Takeda, H. Mamiya and G. Chen, *Biomater. Sci.*, 2015, 3, 1284-1290.
24. X. Wang, T. Nakamoto, I. Dulińska-Molak, N. Kawazoe and G. Chen, *J. Mater. Chem. B*, 2016, 4, 37-45.
25. B. Zhou, L. Zheng, C. Peng, D. Li, J. Li, S. Wen, M. Shen, G. Zhang and X. Shi, *ACS Appl. Mater. Interfaces*, 2014, 6, 17190-17199.
26. H. J. Yen, S. h. Hsu and C. L. Tsai, *Small*, 2009, 5, 1553-1561.
27. B. D. Chithrani, A. A. Ghazani and W. C. Chan, *Nano Lett.*, 2006, 6, 662-668.
28. F. H. Glorieux, F. Rauch, H. Plotkin, L. Ward, R. Travers, P. Roughley, L. Lalic, D. F. Glorieux, F. Fassier and N. J. Bishop, *J. Bone Miner. Res.*, 2000, 15, 1650-1658.
29. S. Shrestha, P. Jiang, M. H. Sousa, P. C. Morais, Z. Mao and C. Gao, *J. Mater. Chem. B*, 2016, 4, 245-256.
30. J. Deng, H. Zheng, X. Zheng, M. Yao, Z. Li and C. Gao, *Nano Res.*, 2016, 9, 3683-3694.
31. W.-K. Ko, D. N. Heo, H.-J. Moon, S. J. Lee, M. S. Bae, J. B. Lee, I.-C. Sun, H. B. Jeon, H. K. Park and I. K. Kwon, *J. Colloid Interface Sci.*, 2015, 438, 68-76.

32. S. Amorim, A. Martins, N. M. Neves, R. L. Reis and R. A. Pires, *J. Mater. Chem. B*, 2014, 2, 6939-6946.
33. T. Hoshiba, N. Kawazoe, T. Tateishi and G. Chen, *Adv. Mater.*, 2010, 22, 3042-3047.
34. H. S. Camp, D. Ren and T. Leff, *Trends Mol. Med.*, 2002, 8, 442-447.
35. W. Wang, Y. Zhang, W. Lu and K. Liu, *PloS One*, 2015, 10, e0120629.
36. C. T. Chen, Y. R. V. Shih, T. K. Kuo, O. K. Lee and Y. H. Wei, *Stem Cells*, 2008, 26, 960-968.
37. N. M. Schaeublin, L. K. Braydich-Stolle, A. M. Schrand, J. M. Miller, J. Hutchison, J. J. Schlager and S. M. Hussain, *Nanoscale*, 2011, 3, 410-420.
38. A. Chompoosor, K. Saha, P. S. Ghosh, D. J. Macarthy, O. R. Miranda, Z. J. Zhu, K. F. Arcaro and V. M. Rotello, *Small*, 2010, 6, 2246-2249.
39. S. Y. Choi, M. S. Song, P. D. Ryu, A. T. N. Lam, S.-W. Joo and S. Y. Lee, *Int. J. Nanomed.*, 2015, 10, 4383.
40. F. Atashi, A. Modarressi and M. S. Pepper, *Stem Cells Dev.*, 2015, 24, 1150-1163.
41. W. He, T. A. Elkhooly, X. Liu, A. Cavallaro, S. Taheri, K. Vasilev and Q. Feng, *J. Mater. Chem. B*, 2016, 4, 1466-1479.
42. G. Ciofani, L. Ricotti, C. Canale, D. D'Alessandro, S. Berrettini, B. Mazzolai and V. Mattoli, *Colloids Surf., B*, 2013, 102, 312-320.
43. X. Wang, X. Hu, I. Dulińska-Molak, N. Kawazoe, Y. Yang and G. Chen, *Sci. Rep.*, 2016, 6, 28708.

Chapter 5

Biomimetic AuNPs with tunable RGD density regulate multipotent differentiation of human mesenchymal stem cells

5.1 Summary

Nanostructured materials have drawn a broad attention for their applications in biomedical fields. Ligand-modified nanomaterials can well mimic the dynamic extracellular matrix (ECM) microenvironments to regulate cell functions and fates. In this part, ECM mimetic AuNPs with tunable surface RGD density were designed and synthesized to induce the chondrogenic, osteogenic and adipogenic differentiation of human mesenchymal stem cells (hMSCs). The biomimetic AuNPs showed good biocompatibility without affecting the cell proliferation in the studied concentration range. The RGD motifs on AuNPs surface facilitated cellular uptake of NPs through integrin-mediated endocytosis. The biomimetic NPs had a promotive effect on chondrogenic differentiation of hMSCs in 3D cell pellet culture while an inhibitive effect on osteogenic differentiation of hMSCs. Their effect on adipogenic differentiation was negative when RGD density was low and changed to positive when RGD density was high. The overall effect of biomimetic NPs on MSC differentiation was dependent on RGD density. This study provides a strategy for fabricating biomimetic NPs to regulate cell differentiation, which holds great potentials in tissue engineering and biomedical applications.

5.2 Introduction

The extracellular matrix (ECM) has a complicated composition and structure that contains many ligand-enriched proteins in various types of tissues and organs.[1] ECM interacts with cells through various pathways, in particular through receptor-ligand bindings.[2, 3] The interaction between cells and ECM provides indispensable signals to manipulate cell functions.[4] It has been reported that ECM plays a very important role in regulating the multiple differentiation of stem cells.[5] However, the function of ECM is still mysterious because of its complexity and dynamicity. An increasing number of ECM mimetic biomaterials and scaffolds

have been developed to elucidate the role of ECM in stem cell differentiation.[6-8] However, it has been difficult to mimic the nanoclustering of ECM molecules and to modulate their density, which are very important for receptor-ligand interaction and signal transduction.

In recent years, nanoparticles (NPs) have shown great potential in the biomedical fields, such as cancer diagnosis and therapy and tissue regeneration.[9-11] They are also good candidates for mimicking of cellular microenvironment since their size scale is similar to proteins.[12] Some biomimetic NPs with an uppermost layer similar to cell membrane have been reported, but ECM mimetic NPs have been rarely proposed.[13] To closely emulate the complexity and functionality of ECM, it is an attractive strategy to engineer NPs with surface ligands. NPs can serve as a core to construct ligand nanoclusters with tunable density. Arginine-glycine-aspartate (RGD) peptide derived from ECM proteins is a common used ligand that has a very high affinity to the integrin receptors on the cell membrane.[14] RGD motifs on NP surface are flexible and movable in biological liquid and should stimulate clustering of receptor-ligand complexes, therefore strengthening receptor-ligand mediated signal transduction. Furthermore, the ligand density on NP surface is tunable to control the receptor-ligand interaction. Design and construction of such ECM mimetic NPs is strongly desirable for investigation of the role of ECM on multipotent differentiation of stem cells.

In this study, RGD modified AuNPs were designed and prepared to mimic the ECM microenvironment. Although RGD density/spacing potentially has remarkable influence on cell adhesion, proliferation, migration and differentiation, it is very difficult to identify this effect in natural ECM.[15] To well understand this issue, biomimetic AuNPs with tunable RGD surface density were prepared. The inducibility of these biomimetic AuNPs on multiple differentiation of human bone marrow-derived mesenchymal stem cells (hMSCs), such as chondrogenesis, osteogenesis and adipogenesis was evaluated.

5.3 Materials and methods

5.3.1 Materials

Cyclic RGD peptide was obtained from Peptides international Inc. (Louisville, KY, USA). 1-ethyl-3-[3-dimethylaminopropyl] carbodiimide hydrochloride (EDC) was from Peptide Institute, Inc. (Osaka, Japan). N-hydroxysuccinimide (NHS), trisodium citrate, dimethyl sulfoxide (DMSO), 2-propanol and hydrogen tetrachloroaurate tetrahydrate **(**$HAuCl_4 \cdot 4H_2O$, 99.9%) were purchased from Wako Pure Chemical Industries, Ltd. (Tokyo, Japan). Methoxy-poly(ethylene glycol)-thiol (SH-*m*PEG, Mw = 2000) was from Yuka Sangyo Co., Ltd. (Tokyo, Japan). Poly(ethylene glycol) 2-mercaptoethyl ether acetic acid (SH-PEG-COOH, Mw = 2100), ascorbic acid (AA), penicillin, streptomycin, proline, sodium pyruvate, glutamine, nonessential amino acids, ascorbate-2-phosphate, ITS+1, Oil Red O, insulin, dexamethasone, β-glycerophosphate, 2-amino-2-methyl-1,3-propanediol, methyl-isobutylxanthine, indomethacin, naphthol AS-MX phosphate, fast blue RR salt, Dulbecco's modified Eagle's Medium (DMEM), papain, trypsin/EDTA, perchloric acid and DNA quantification kit were purchased from Sigma-Aldrich (St. Louis, MO, USA). All the chemical reagents were used as received without further purification. Fetal bovine serum (FBS) was purchased from Gibco Lab. (Grand Island, NY, USA). Sensolyte pNPP alkaline phosphatase assay kit was

purchased from AnaSpec (Fremont, CA, USA). 4'-6-diamidino-2-phenylindole (DAPI) solution and Cellstain live/dead double staining kit were obtained from Dojindo Lab. (Kumamoto, Japan). Alexa Fluor 488 goat anti-mouse IgG antibody and Alexa Fluor-594 phalloidin were purchased from Invitrogen (Grand Island, NY, USA). Mouse anti-vinculin primary antibody was purchased from Santa Cruz Biotechnology, Inc. (Santa Cruz, CA). WST-1 reagent was purchased from Roche Molecular Biochemicals (Mannheim, Germany). Milli-Q water with a resistivity of 18.2 MΩ.cm used in all the experiments was purified by a Q-POD Milli-Q water purification system (Millipore Corp., Billerica, MA, USA).

5.3.2 Synthesis of SH-PEG-RGD conjugate

SH-PEG-COOH (0.01 mmol, 21.00 mg), EDC (0.02 mmol, 3.83 mg) and NHS (0.02 mmol, 2.30 mg) was dissolved in 10.0 mL DMSO and the mixture solution was kept stirring at room temperature for 3 hours. The resulting solution of activated SH-PEG-NHS was dropwise added into 5.0 mL DMSO solution of RGD (0.02 mmol, 12.14 mg) under vigorous magnetic stirring at room temperature for 3 days. Afterwards, the reaction mixture was dialyzed against phosphate buffered saline (PBS) (3 times) and water (6 times) for 3 days using a dialysis membrane with molecular weight cut-off (MWCO) of 1000. After lyophilization, the product SH-PEG-RGD conjugate was obtained and stored at -20 °C for further use.

5.3.3 Synthesis of biomimetic AuNPs with different RGD density

Biomimetic AuNPs with different surface RGD density were synthesized through a seed-mediated method. The Au seed solution was prepared by the well-known Frens method employing the reduction of $HAuCl_4$.[16] The concentration of AuNPs in the seed solution was fixed at 2.0 nM by centrifugation for further use. The growth solution was prepared by successively adding $HAuCl_4$ solution (30.0 mg/mL, 0.6 mL), Au seed solution (2.0 nM, 12.0 mL) and AA solution (80.0 mg/mL, 0.2 mL) into 20 mL water under gently stirring. After the color of the growth solution turned to dark red, a mixture solution of SH-PEG-RGD/SH-*m*PEG at different ratios was added and the resultant solution was kept stirring at room temperature for 24 hours. The ratio of SH-PEG-RGD/SH-*m*PEG was adjusted to control the density of SH-PEG-RGD on Au NP surface. Subsequently, the obtained biomimetic AuNPs with different surface RGD density (defined as Au-RGDn NPs) were purified by 3 cycles of centrifugation/re-dispersion process and finally re-dispersed in water for further use.

5.3.4 Characterization techniques

^1H NMR spectra of the samples dissolved in D_2O were collected by using a FT-NMR system (300 MHz, JEOL, Tokyo, Japan). Transmission electron microscopy (TEM) images were obtained from a JEOL 2100F analytical electron microscope (JEOL, Tokyo, Japan) with operating voltage of 200 kV. The AuNPs were dispersed in water and TEM samples were prepared by dropping AuNP solution onto a carbon-covered copper grid, followed by air-drying at room temperature. ImageJ software was used to to assess the size and size distribution of the particles. The zeta potential and hydrodynamic size were measured by using a zeta-potential & particle size analyzer (ELSZ-2000, Otsuka Electronics Co., Ltd, Tokyo, Japan). The element concentration of Au and S was assessed by a Leeman Prodigy Inductively Coupled Plasma-Optical Emission

Spectroscopy (ICP-OES, SPS3520UV-DD) system (SII nano technology Inc., Tokyo, Japan).

5.3.5 Cell culture

The hMSCs at passage 4 (P4) were used for further experiments. The growth medium was DMEM supplemented with 10% heat-inactivated FBS, 4500 mg/L glucose, 4 mM glutamine, 100 U/mL penicillin, 100 μg/mL streptomycin, 0.1 mM nonessential amino acids, 0.4 mM proline, 1 mM sodium pyruvate and 50 μg/mL ascorbic acid. The basic medium was DMEM supplemented with 10% heat-inactivated FBS, 1000 mg/L glucose, 4 mM glutamine, 100 U/mL penicillin, 100 μg/mL streptomycin, 0.1 mM nonessential amino acids, 0.4 mM proline, 1 mM sodium pyruvate and 50 μg/mL ascorbic acid. The incomplete chondrogenic induction medium was DMEM supplemented with 1000 mg/L glucose, 584 mg/L glutamine, 100 U/mL penicillin, 100 μg/mL streptomycin, 0.1 mM nonessential amino acids, 1 mM sodium pyruvate, 0.4 mM proline, 50 μg/mL ascorbic acid, 100 nM dexamethasone, 150 μg/mL ascorbate-2-phosphate and 1% ITS+1. The osteogenic induction medium was DMEM supplemented with 10% heat-inactivated FBS, 1000 mg/L glucose, 584 mg/L glutamine, 100 U/mL penicillin, 100 μg/mL streptomycin, 0.1 mM nonessential amino acids, 50 μg/mL ascorbic acid, 100 nM dexamethasone and 10 mM β-glycerophosphate. The adipogenic induction medium was DMEM supplemented with 10% heat-inactivated FBS, 4500 mg/L glucose, 4 mM glutamine, 100 U/mL penicillin, 100 μg/mL streptomycin, 0.1 mM nonessential amino acids, 0.4 mM proline, 1 mM sodium pyruvate, 50 μg/mL ascorbic acid, 1 μM dexamethasone, 0.5 mM methyl-isobutylxanthine, 10 μg/mL insulin and 200 μM indomethacin.

5.3.6 Cytotoxicity assay

The hMSCs were seeded into 96-well plates with 200 μL fresh cell culture growth medium at a density of 0.5×10^4 cells/cm^2. After 24 hours of culture to allow cell adhesion, the medium in each well was replaced with 200 μL fresh growth medium containing PBS buffer (control) or Au-RGDn NPs at an Au concentration of 0.025, 0.050 or 0.100 mM. The cells were incubated with the Au-RGDn NPs for 1, 3, 7 and 10 days with the medium being changed every 3 days. After the treatments, the cells were washed with PBS, supplemented with fresh medium containing WST-1 reagent and further cultured for another 3 hours. A plate reader (Benchmark Plus, Bio-Rad, Hercules, CA, USA) was used to measure the absorbance of each well at 440 nm, which was used to calculate cell viability (n = 3).

5.3.7 Cellular uptake assay

The hMSCs were seeded in 6-well plates at a density of 0.5×10^4 cells/cm^2 in 2 mL serum-free growth medium and cultured for 24 hours to allow cell adhesion and spreading. For comparison, the hMSCs were also cultured in serum-free growth medium containing 2 μg/mL free RGD for 30 minutes to block cell membrane $\alpha_v\beta_3$ integrin of hMSCs (RGD blocking group). After that, the hMSCs were cultured in fresh serum-free growth medium containing PBS (control) or Au-RGDn NPs at an Au concentration of 0.05 mM for 3 days. After discarding the cell culture medium, the cells were washed twice with PBS carefully to remove the free NPs. Subsequently, the hMSCs were detached by trypsin solution, collected by centrifugation, counted by hemocytometer and lysed with aqua regia solution. And then the samples were

diluted with water for ICP-OES measurement (n = 3).

5.3.8 Influence of biomimetic AuNPs on focal adhesion and cytoskeleton

The hMSCs suspended in fresh cell culture growth medium were seeded into 24-well plates (0.5×10^4 cells/cm^2) and cultured at 37 °C and 5% CO_2 for 12 hours. The medium was replaced with fresh growth medium containing PBS buffer (control) or Au-RGDn NPs at an Au concentration of 0.1 mM and the cells were cultured for another 24 hours. After that, the cells were washed twice with PBS, fixed with 4% paraformaldehyde at room temperature for 10 minutes, permeabilized with 1% Triton X-100 and then blocked with 2% bovine serum albumin (BSA) solution for 30 minutes, followed by washing with PBS. Next, the samples were incubated with anti-vinculin primary antibody (1:100) at 37 °C for 1.5 hours and further washed three times with PBS. The cells were then incubated with Alexa Fluor 488 goat anti-mouse IgG antibody (1:800) at 37 °C for 1 hour and Alexa Fluor 594 phalloidin (1:40) at room temperature for 30 minutes. The nuclei were stained with DAPI (1:800) at room temperature for 10 minutes. The fluorescence images were captured by using an inverted fluorescence microscope.

5.3.9 Chondrogenic differentiation of hMSCs

3D cell pellet culture was performed to induce chondrogenic differentiation of hMSCs. Cell suspension solution containing 2×10^5 hMSCs was placed into a 15-mL polypropylene tube (Corning, NY, USA). The cells were collected by centrifugation and re-suspended in incomplete chondrogenic induction medium containing PBS (control) or Au-RGDn NPs at an Au concentration of 0.05 mM. The cell suspension was gently shook at 37 °C for 30 minutes. After being centrifuged again (1100× rpm, 5 minutes) to achieve aggregation, the cell pellets were cultured in incomplete chondrogenic induction medium containing Au-RGDn NPs (0.05 mM) for 21 days and the medium was changed every 3 days.

After culture, the morphologies of cell pellets were observed using an optical microscope and the size of cell pellets was measured by ImageJ software. Then the cell pellets were washed with PBS, collected and then digested in papain solution for 8 hours at 60 °C. DNA content in each pellet was measured by using Hoechst 33258-based DNA quantification kit according to our previously reported process.[7]

For immunohistochemical analysis, the cell pellets were washed with PBS, fixed with 10% formalin, dehydrated in a series of ethanol solution, embedded in paraffin and then cut into 5 μm thick sections. The sections were treated with proteinase K (Dako, Carpinteria, CA) for 5 minutes for antigen retrieval after deparaffinized and then incubated with primary antibodies of collagen I, collagen II and aggrecan. After that, the samples were immersed in peroxidase-conjugated secondary antibody (Dako, Carpinteria, CA) at room temperature for 1 hour. Finally the color of the samples was developed with 3,3'-diaminobenzidine (DAB) substrate-chromogen to visualize peroxidase-labeled antibody. An optical microscope was used to observe the stained sections at a magnification of 400×.

To investigate gene expression level of collagen I, aggrencan and Sox 9 after 21 days of pellet culture. RNA from the cell pellets was extracted using the RNAeasy Minikit (Qiagen, Netherlands) according to the manufacturer's instructions and the RNA concentration was measured using Thermo Scientific NanoDrop ND-1000 spectrophotometer (Thermo Fisher Scientific, Wilmington, DE). The RNA was converted to cDNA

by MuLV reverse transcriptase (Applied Biosystems, Foster City, CA, USA). Real-time polymerase chain reaction (PCR) was performed on a 7500 Real-Time PCR system (Applied Biosystems, USA) and the relative gene expression was calculated using the $2^{\Delta\Delta Ct}$ formula (n = 3). The primers and probes used for real-time PCR are listed in Table 5.1.

Table 5.1. The primers and probes for real-time PCR.

mRNA	Oligonucleotide
Collagen I	Forward 5'-TGGCAAAGACGGTCGCAT-3' Reverse 5'-CCTTGGGTCTGAGAGAAGTTGGT-3' Probe 5'-GTAACCACCACCACTTG-3'
Sox 9	Forward 5'-CACACAGCTCACTCGACCTTG-3' Reverse 5'-TTCGGTTATTTTTAGGATCATCTCG-3' Probe 5'-CCCACGAAGGGCGACGTTGG-3'
Aggrecan	Forward 5'- TCGAGGACAGCGAGGCC-3' Reverse 5'- TCGAGGGTGTAGCGTGTAGAGA-3' Probe 5'-ATGGAACACGATGCCTTTCACCACGA-3'
LPL	Hs00173425_m1
PPARG	Hs01115510_m1

5.3.10 Osteogenic differentiation of hMSCs

The hMSCs suspended in growth medium were seeded into cell culture plates at a density of 0.5×10^4 cells/cm^2 and cultured at 37 °C and 5% CO_2 for 24 hours. After that, the growth medium was discarded carefully and fresh osteogenic induction medium containing PBS buffer (control) or Au-RGDn NPs at an Au concentration of 0.03 mM was added into each well. The cells were incubated with Au-RGDn NPs in osteogenic induction medium for 21 days and the medium was changed every 3 days.

Alkaline phosphatase (ALP) staining and ALP activity assay were performed to investigate the osteogenic differentiation of hMSCs after incubation with Au-RGDn NPs for 21 days. The washed cells were fixed with 4% paraformaldehyde at room temperature for 10 minutes. After being further washed with PBS, the cells were incubated with 0.1% naphthol AS-MX phosphate and 0.1% fast blue RR salt in 56 mM 2-amino-2-methyl-1,3-propanediol working solution (pH = 9.9) at room temperature for 10 minutes. Afterwards, the cells were washed with PBS to remove unbound dyes and the stained images were captured by using an optical microscope. Quantitative ALP activity assay (n = 3) was carried out by using the Sensolyte pNPP alkaline phosphatase assay kit according to our previously reported protocol.[18]

For Alizarin Red S (ARS) staining, the fixed cells were incubated with 0.1% ARS solution at room temperature for 30 minutes. And then the cells were washed with PBS and observed under an optical microscopy. After that, the stained cells were dried in the air for quantitative calcium deposition assay. Perchloric acid (5%) was added into each well to dissolve the staining at room temperature for 20 minutes. The dissolved solution was transferred into 96-well plates and a plate reader was used to measure their absorbance at 405 nm (n = 3).

After 21 days of culture, the expression of osteogenic related marker genes including ALP, runt-related transcription factor 2 (Runx2), bone sialoprotein 2 (IBSP) and secreted phosphoprotein I (SPPI) was assayed by quantitative real-time PCR according to the protocols as above described (n = 3). The primers and probes used for real-time PCR are listed in Table 3.1.

5.3.11 Adipogenic differentiation of hMSCs

To investigate the influence of Au-RGDn NPs on adipogenic differentiation of hMSCs, the cells were seeded into cell culture plates at a density of 2×10^4 cells/cm^2 and cultured in growth medium overnight. After that, the cells were incubated with Au-RGDn NPs at an Au concentration of 0.03 mM in adipogenic induction medium for 21 days and the medium was changed every 3 days.

Oil Red O staining was carried out to visualize the oil droplet accumulation after 21 days of culture. The cells were washed with PBS, fixed with 4% paraformaldehyde and washed again with water. And then the fixed cells were soaked in 60% 2-propanol for 5 minutes and subsequently soaked in Oil Red O working solution at room temperature for 5 minutes. After being further washed with water, the cells were observed under an optical microscope. The stained cells were dried in the air and the Oil Red O dye was extracted using 2-propanol at room temperature for 30 minutes. The absorbance of Oil Red O dye in each well was measured by a plate reader at 540 nm (n = 3).

Real-time PCR was performed as above described to quantify the gene expression level of adipogenic related genes such as lipoprotein lipase (LPL), fatty acid binding protein 4 (FABP4), fatty acid synthase (FASN), peroxisome proliferator-activated receptor gamma (PPARG) and CCAAT/enhancer binding protein (CEBPA) (n = 3). The primers and probes used for real-time PCR are listed in Table 4.1 and Table 5.1.

5.3.12 Statistical analysis

All data were reported as mean ± standard deviation (SD) with experiments repeated in triplicate (n = 3). One-way ANOVA statistical analysis was performed to evaluate the significance of the experimental data. 0.05 was selected as the significance level and the data were indicated with (*) for $p < 0.05$, (**) for $p < 0.01$ and (***) for $p < 0.001$, respectively.

5.4 Results and discussion

5.4.1 Preparation and characterization of biomimetic AuNPs with different RGD density

A series of ECM mimetic AuNPs with different surface RGD density (Au-RGDn NPs) were designed

and prepared to induce the multiple differentiation of hMSCs. AuNPs were chosen due to their overwhelming advantages such as superior physicochemical features, good biocompatibility, facile synthesis method and versatile surface chemistry.[19] Biocompatible PEG was used as a spacer and stabilizer and cross-linked with RGD to form the SH-PEG-RGD conjugate. AuNPs prepared by a seed-mediated growth method were modified with PEG at different molar ratio of SH-PEG-RGD/SH-*m*PEG through Au-S bond, which resulted in the formation of Au-RGDn NPs.

^{1}H NMR spectroscopy confirmed the successful synthesis of SH-PEG-RGD conjugate (Figure 5.1). The characteristic peaks of RGD at 7.3 and 7.4 ppm (aromatic proton peaks) could be clearly observed in the spectrum of SH-PEG-RGD. For comparison, SH-PEG-COOH without RGD modification showed no peaks in these ranges. Based on the NMR integration, the average number of RGD conjugated to each PEG was estimated to be 0.49.

The well-known Frens method was employed to synthesize the Au seeds. Subsequently, the Au seeds were developed into Au-RGDn NPs in the growth solution in the presence of SH-PEG-RGD/SH-*m*PEG. To confirm the RGD number on the surface of AuNPs, ICP-OES was used to quantify the Au and S element content in the particle suspension. The results indicated that each Au NP was bound with 9830 ± 1140 total molecules of PEG on the surface. The surface coverage (0.51 nm^2/PEG) was slight higher than a footprint area of ～0.35 nm^2 per PEG molecule adsorbed on colloidal Au in a brush conformation.[20] The slightly high surface coverage of SH-*m*PEG and SH-PEG-RGD molecules could avoid too compact stacking of the molecules, which should be beneficial for the interaction with integrin and nanoclustering of receptor-ligand complexes. It was assumed that SH-*m*PEG and SH-PEG-RGD had a similar efficiency to bind with AuNPs according to a previous work.[21] By adjusting the feed ratio of SH-PEG-RGD and SH-*m*PEG (0/40000, 400/39600, 2000/38000, 10000/30000 and 40000/0), AuNPs with 0, 90, 513, 2848 and 8519 molecules of SH-PEG-RGD on their surface were prepared. The corresponding surface RGD number was estimated to be 0, 44, 251, 1395 and 4174, respectively. Hence, these biomimetic AuNPs with different RGD density were defined as Au-RGD0 NPs, Au-RGD50 NPs, Au-RGD250 NPs, Au-RGD1250 NPs and Au-RGD5000 NPs.

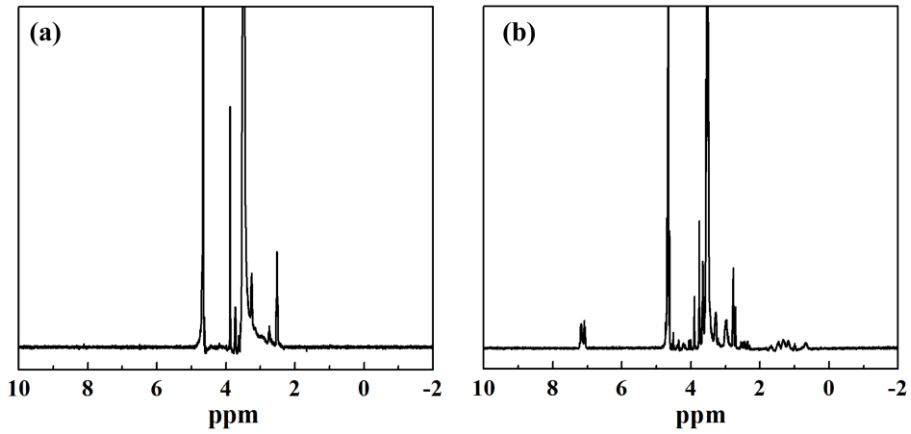

Figure 5.1 ^{1}H NMR spectroscopy of SH-PEG-COOH (a) and SH-PEG-RGD (b).

TEM observation showed that all the prepared AuNPs were spherical with a homogeneous distribution (Figure 5.2a). The size was determined to be 39.4 ± 7.7, 39.7 ± 7.6, 39.8 ± 7.8, 39.7 ± 6.3 and 41.9 ± 7.7 nm

for Au-RGD0, Au-RGD50, Au-RGD250, Au-RGD1250 and Au-RGD5000 NPs, respectively.

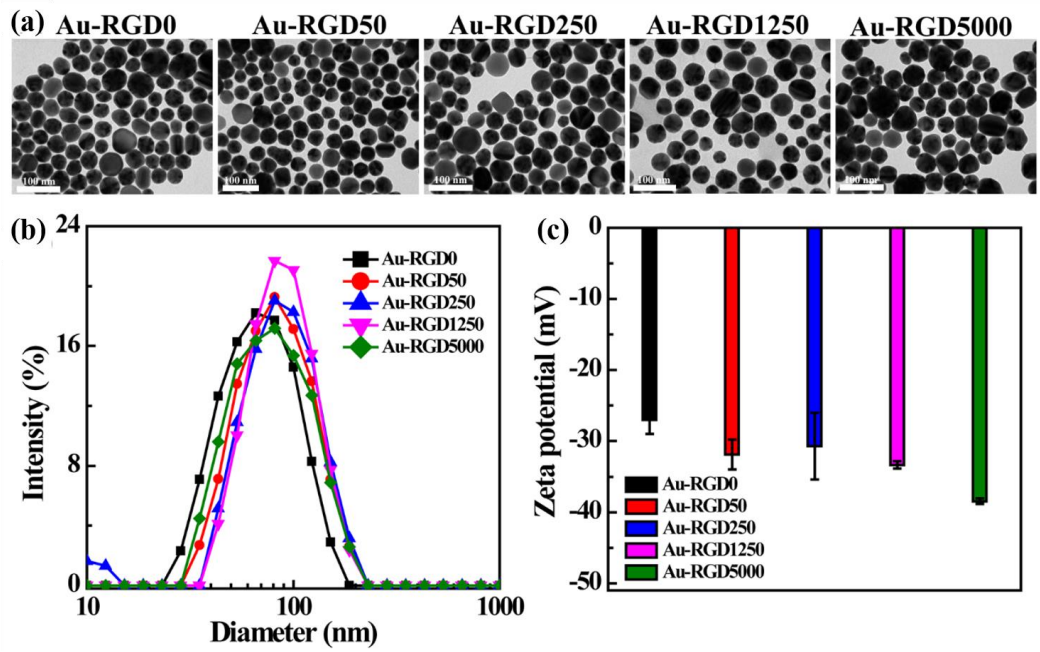

Figure 5.2 TEM images (a), hydrodynamic size (b) and zeta potential (c) of various Au-RGDn NPs.

Dynamic light scattering (DLS) measurement showed the hydrodynamic size of Au-RGD0, Au-RGD50, Au-RGD250, Au-RGD1250 and Au-RGD5000 NPs dispersed in water was 55.9 ± 1.1, 74.7 ± 2.1, 68.1 ± 2.4, 76.5 ± 2.1 and 65.4 ± 2.1 nm, respectively (Figure 5.2b). The hydrodynamic size was slightly bigger than the size measured from the TEM images for all the AuNPs. The surface zeta potential of the Au-RGDn NPs was also measured (Figure 5.2c). Their surface potential was -27.0 ± 2.0 mV (Au-RGD0), -31.9 ± 2.1 mV (Au-RGD50), -30.7 ± 4.7 mV (Au-RGD250), -33.3 ± 0.5 mV (Au-RGD1250) and -38.5 ± 0.4 mV (Au-RGD5000). The results indicated that the designed biomimetic AuNPs had similar diameter, hydrodynamic size and zeta potential, which should help to elucidate the influence of RGD density on cell functions without disturbance from other parameters.

5.4.2 Cytotoxicity assay and cellular uptake assay

It is necessary to evaluate the cytotoxicity of Au-RGDn NPs for stem cells before their potential biomedical applications. Cell viability of hMSCs after incubation with Au-RGDn NPs at an Au concentration of 0.025, 0.05 or 0.1 mM for 1 day was assessed by WST-1 assay (Figure 5.3a). In the studied concentration range, viability of hMSCs after treatments with AuNPs was almost 100% as compared with the control cells, suggesting good biocompatibility of these biomimetic AuNPs. The long-term cytotoxicity of Au-RGDn NPs at an Au concentration of 0.05 mM was also checked after the cells were cultured with the AuNPs for 3, 7 and 10 days. It was clear that all the AuNPs showed negligible cytotoxicity to hMSCs during the culture time as compared with the control group (Figure 5.3b). The results indicated the biomimetic AuNPs had good long-term biocompatibility at an Au concentration not higher than 0.05 mM, which should enable them to well function as ECM-like microenvironment.

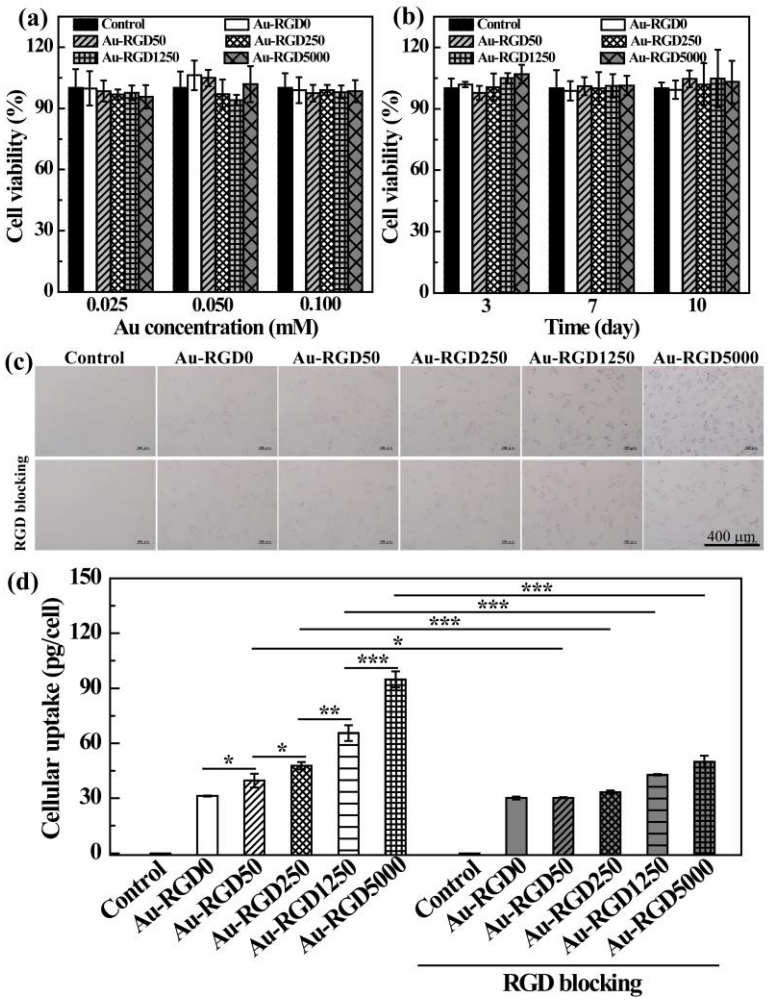

Figure 5.3 Cell viability of hMSCs incubated with the biomimetic AuNPs in growth medium at different Au concentrations (a) and different culture time (b); optical micrographs (c) and cellular uptake assay (d) of hMSCs or RGD-blocked hMSCs after incubation with the biomimetic AuNPs at an Au concentration of 0.05 mM for 3 days.

RGD peptide has a very high affinity to $\alpha_v\beta_3$ integrin that is expressed on the surface of hMSCs, which may mediate cellular uptake of Au-RGDn NPs. Herein, internalization of the Au-RGDn NPs into hMSCs after 3 days of culture in serum-free medium was evaluated (Figure 5.3c). Compared with the control cells without treatment, the treated cells showed obvious cellular uptake of AuNPs. More importantly, high RGD density led to increased cellular uptake, as more and more AuNP clusters were observed inside the cells or on the ECM of cells. For each kind of AuNPs, the particle clusters in the RGD-blocked cells were obviously less than those in the unblocked cells, except for the Au-RGD0 NPs. The cellular uptake of NPs into hMSCs was further quantified by ICP-OES (Figure 5.3d). It was clear that cellular uptake increased in the order of Au-RGD0 NPs, Au-RGD50 NPs, Au-RGD250 NPs, Au-RGD1250 NPs and Au-RGD5000 NPs. The free RGD blocking did not affect the cellular uptake of Au-RGD0 NPs, but significantly reduced the uptake of RGD-modified AuNPs. Internalization of biomimetic AuNPs into hMSCs was significantly inhibited by the free RGD blocking, which should be because the integrin receptors were partially occupied by the free ligands. These results indicated that RGD play a very important role in mediating the cellular uptake of biomimetic AuNPs into hMSCs.

5.4.3 Biomimetic AuNPs affected the focal adhesion and cytoskeleton of hMSCs

Immunofluorescence staining was performed to study the focal adhesion and cytoskeleton of hMSCs after incubation with biomimetic AuNPs (Figure 5.4). Au-RGD250, Au-RGD1250 and Au-RGD5000 NPs treated cells showed obviously less staining of vinculin than the control cells, while Au-RGD0 and Au-RGD50 NPs treated cells had a similar staining intensity as compared to the control cells. A similar tendency was observed for the F-actin staining. Incubation of hMSCs with Au-RGD250, Au-RGD1250 and Au-RGD5000 NPs resulted in a significant decrement in F-actin assembling. The results suggested that the binding between RGD on AuNP surface and integrin receptors on the cell membrane reduced the focal adhesion of cells, thus causing reorganization of actin microfilament network. Both focal adhesion and cytoskeleton have been reported to play an important role in regulation of the cell biological behaviors.[22]

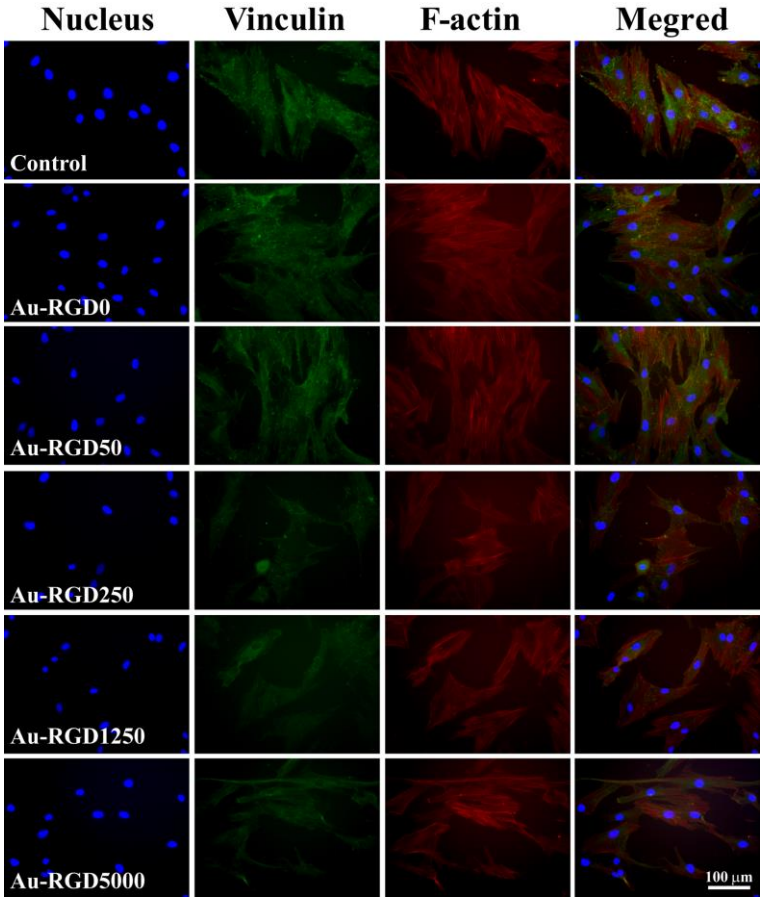

Figure 5.4 Immunofluorescence staining of vinculin and F-actin in hMSCs after treatments with the biomimetic AuNPs.

5.4.4 Influence of biomimetic AuNPs on chondrogenic differentiation of hMSCs

Cell pellet culture is usually to perform chondrogenic differentiation of stem cells.[23] Therefore, pellet culture was performed in this work to induce the chondrogenic differentiation of hMSCs. As shown in Figure 5.5a, the cell suspension was incubated with Au-RGDn NPs under shocking for 30 minutes at 37 °C to let the RGD on the AuNP surface bind to the cell membrane integrin and then centrifuged to form cell pellets. The cell pellets were cultured in incomplete chondrogenic induction medium containing Au-RGDn NPs for 21 days. Transforming growth factor β (TGFβ) is the most commonly used bioactive factor to induce

chondrogenesis of stem cells. However, TGFβ was not used in this system because of the following two reasons. Firstly, TGFβ may lead the differentiation toward a hypertrophic phenotype through the sustained high content;[24] secondly, the RGD influence on cell differentiation may be overwhelmed by the strong stimulatory effect of TGFβ. The macro pictures showed that all the cell pellets were spherical and their sizes were measured to be 832.4 ± 66.2, 797.3 ± 43.6, 873.0 ± 100.6, 806.8 ± 117.4, 758.9 ± 34.9 and 746.5 ± 58.6 μm for the control, Au-RGD0, Au-RGD50, Au-RGD250, Au-RGD1250 and Au-RGD5000 NPs treated group, respectively (Figure 5.5b and c). The treatment with biomimetic AuNPs did not evidently affect the morphologies and sizes of cell pellets. The quantified DNA amount in the cell pellets incubated with Au-RGDn NPs was almost the same as that in the control pellets (Figure 5.5d), suggesting the biomimetic AuNPs did not affect cell proliferation and viability after 21 days of culture in incomplete chondrogenic induction medium.

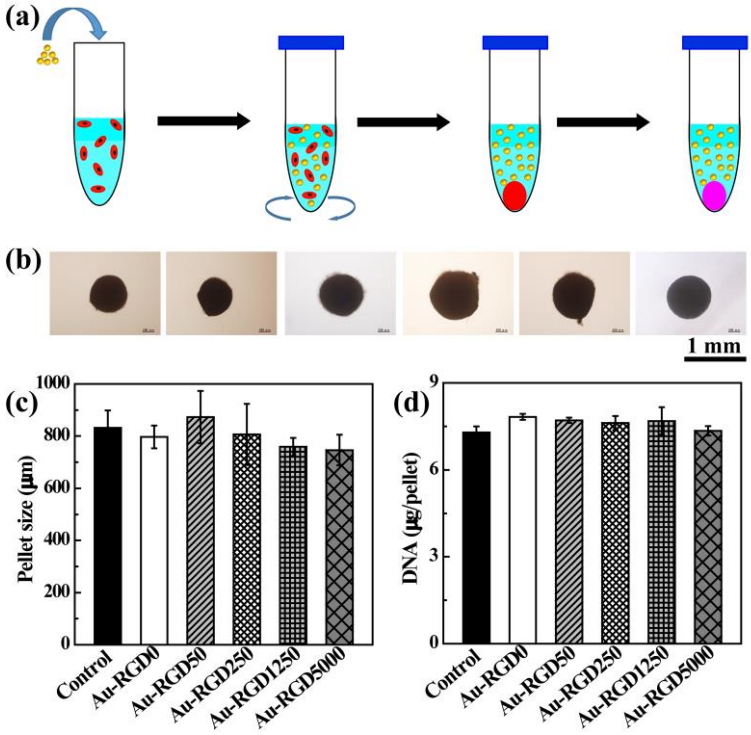

Figure 5.5 Schematic illustration of cell pellet formation and culture (a); optical micrographs (b), pellet size (c) and DNA amount (d) of cell pellets with different treatments in incomplete chondrogenic induction medium for 21 days.

Immunohistochemical staining was employed to analyze the expression of collagen II, aggrencan and collagen I in the cell pellets. During chondrogenic differentiation, the matrix dominant composition of MSCs was changed from collagen I to collagen II and aggrecan.[25] The staining intensity of collagen II was found to increase in the order of control < Au-RGD0 < Au-RGD50 < Au-RGD250 ≈ Au-RGD1250 ≈ Au-RGD5000 (Figure 5.6a). Similar trend was observed for the staining of aggrencan (Figure 5.6b). Au-RGD250, Au-RGD1250 and Au-RGD5000 NPs treated groups showed almost the same staining intensity of aggrencan and the staining intensity in these three groups was much stronger than that in the other groups. For the collagen I, the control group had the strongest staining intensity (Figure 5.6c). The Au-RGD0 NPs treated group showed stronger staining than the Au-RGD50 NPs treated group and almost no positive staining was

observed in the Au-RGD250, Au-RGD1250 and Au-RGD5000 NPs treated groups.

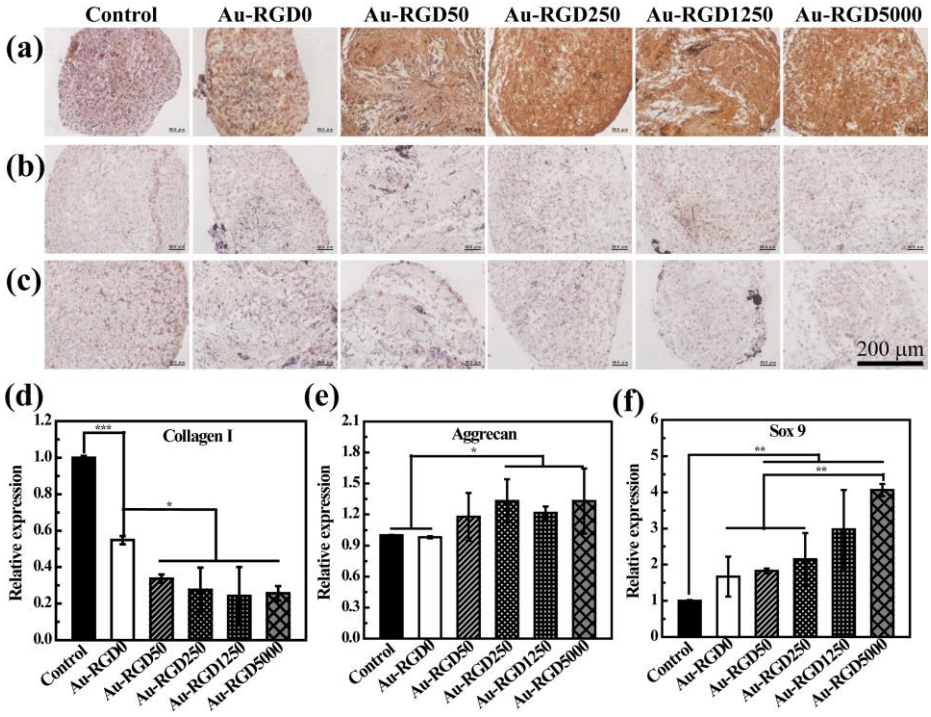

Figure 5.6 Immunohistochemical staining images of collagen II (a), aggrecan (b) and collagen I (c) and gene expression level of collagen I (d), aggrecan (e) and Sox 9 (f) in cell pellets after culture for 21 days.

The expression of chondrogenic related marker genes such as collagen I, aggrencan and Sox 9 in hMSCs was investigated by real-time PCR. Treatments with Au-RGDn NPs down-regulated gene expression of collagen I significantly as compared with control (Figure 5.6d). The Au-RGD50, Au-RGD250, Au-RGD1250 and Au-RGD5000 NPs treated groups showed much lower expression of collagen I than the Au-RGD0 NPs treated group. Expression of aggrecan in the Au-RGD250, Au-RGD1250 and Au-RGD5000 NPs treated groups was significantly higher than that in the control and Au-RGD0 NPs treated groups (Figure 5.6e). Expression of Sox 9 was found to increase in the order of control, Au-RGD0, Au-RGD50, Au-RGD250, Au-RGD1250 and Au-RGD5000 NPs (Figure 5.6f). Gene expression results indicated that the RGD density of the biomimetic AuNPs had obvious influence on the expression of chondrogenic related marker genes. Treatment with Au-RGD250, Au-RGD1250 and Au-RGD5000 NPs induced significant down-regulation of collagen I and up-regulation of aggrencan and Sox 9. Gene expression profile supported the GAG quantified analysis and immunohistochemical staining results, demonstrating the promotive effect of the biomimetic AuNPs with high RGD density on the chondrogenic differentiation of hMSCs. The inductive effect of Au-RGD250, Au-RGD1250 and Au-RGD5000 NPs had no obvious difference. This may be because the RGD density in this range was saturated and high enough to induce the chondrogenesis.

5.4.5 Influence of biomimetic AuNPs on osteogenic differentiation of hMSCs

ALP is thought to have a high expression during osteogenesis, so its production was evaluated after osteogenic induction culture. ALP staining images showed that Au-RGD0 NPs treated cells had a slightly higher staining intensity than the control cells, while Au-RGD50 and Au-RGD250 NPs treated cells

displayed a similar staining intensity to the control cells (Figure 5.7a). More interestingly, the ALP staining in the Au-RGD1250 and Au-RGD5000 NPs treated groups was much less than that in the other groups. Quantitative ALP activity assay showed that Au-RGD0 NPs increased the ALP activity in hMSCs, which was in agreement with our previous work.[18] However, Au-RGD1250 and Au-RGD5000 NPs treated cells had a significantly reduced ALP amount as compared with the control cells (Figure 5.7b).

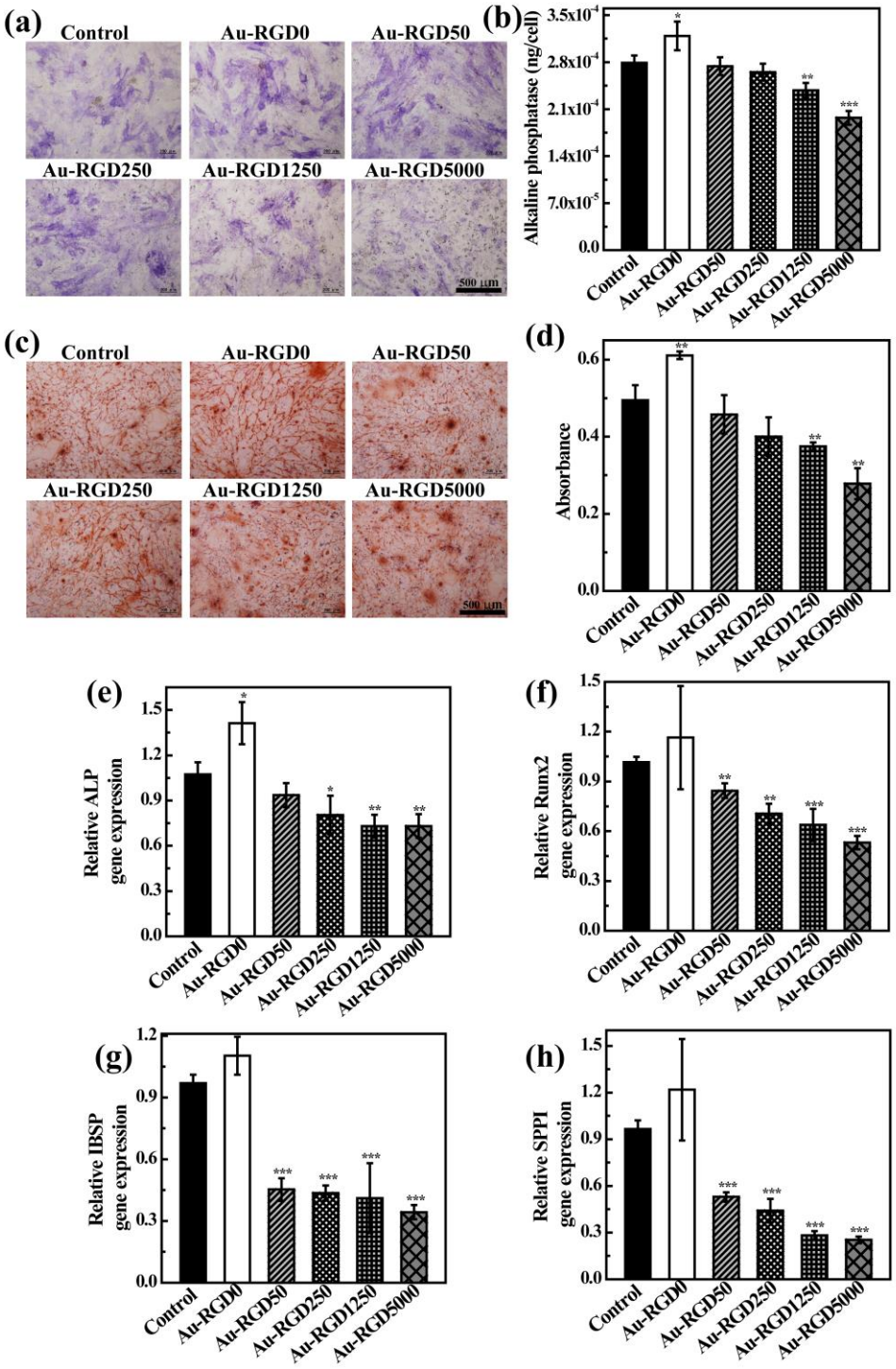

Figure 5.7 ALP staining (a), ALP activity assay (b), ARS staining (c), calcium deposition assay (d) and gene expression of ALP (e), Runx2 (f), IBSP (g) and SPPI (h) in hMSCs after incubation with PBS (control) or the biomimetic AuNPs in osteogenic induction medium for 21 days.

As another marker for osteogenic differentiation of stem cells, calcium deposition was evaluated to confirm the mineralization level of hMSCs. Red web-like staining was observed in all the groups and Au-RGD0 NPs treated group displayed the highest intensity of staining (Figure 5.7c). The cells treated with RGD-modified AuNPs had a reduced ARS staining intensity as compared with the control cells, especially for the Au-RGD1250 and Au-RGD5000 NPs treated groups. Quantitative analysis of calcium deposition showed that Au-RGD0 NPs treatment increased the calcium deposition (Figure 5.7d). However, treatment with the RGD-modified AuNPs reduced calcium deposition and the decrement was more significant with increasing RGD density.

Furthermore, expression of osteogenic related genes such as ALP, Runx2, IBSP and SPPI was investigated. The results of real-time PCR showed that Au-RGD0 NPs up-regulated the expression of osteogenic marker genes including ALP, Runx2, IBSP and SPPI (Figure 5.7e-h), which in accordance with our previous work.[18] However, the expression of these genes was significantly down-regulated after the cells were incubated with the RGD-modified AuNPs.

The results suggested that Au-RGD0 NPs promoted osteogenic differentiation of hMSCs while RGD-modified AuNPs had inhibitive effect on osteogenic differentiation of hMSCs which was dependent on the density of RGD modification. The Au-RGD1250 and Au-RGD5000 NPs remarkably reduced the ALP activity, calcium deposition and osteogenic marker genes expression. Recently, a number of researchers have incorporated RGD ligands into various biomaterials to evaluate their effects on cell behaviors.[26] Most of these works suggested that RGD motifs had a positive influence on the osteogenic differentiation of stem cells.[27] As an example, RGD-tethered poly(ethylene glycol) diacrylate (PEGDA) hydrogels has been reported to promote the osteogenesis of bone marrow-derived marrow stromal cells in a dose-dependent manner.[28] The influences of RGD on osteogenesis in this work seemed to be inconsistent with previous reports, which may be because of the different system and mechanism. Here, the designed biomimetic NPs could be uptaken by cells and promoted formation of nanoclusters of receptor-ligand complexes.

5.4.6 Influence of biomimetic AuNPs on adipogenic differentiation of hMSCs

The adipogenic differentiation of hMSCs after incubation with Au-RGDn NPs for 21 days was analyzed by using Oil Red O staining. The results showed that cells in all the groups cultured in adipogenic induction medium were positively stained (Figure 5.8a). The control group displayed a more intensive staining than did the other groups, which suggested the suppressive effect of AuNPs on adipogenic differentiation of stem cells that was in agreement with a previous report.[31] The staining was then dissolved for absorbance measurement to quantify the oil droplets formation (Figure 5.8b). The control cells had the highest level of oil droplets. It was interesting that oil droplets formation decreased from control to Au-RGD250 treated group and then increased from Au-RGD250 treated group to Au-RGD5000 treated group.

Expression of adipogenic related marker genes was investigated after the cells were incubated with the Au-RGDn NPs for 21 days. It was clear that the LPL gene expression in the treated cells was much lower than that in the control cells (Figure 5.8c). The expression of FABP4, FASN, PPARG and CEBPA displayed a same tendency dependent on the RGD density (Figure 5.8d-g). The treatment of Au-RGD0 and Au-RGD50 NPs down-regulated the expression of these genes as compared with control. The Au-RGD50 NPs treated

cells showed the lowest expression level of these genes. When the RGD density increased from 50 to 5000, the expression of these genes increased slightly.

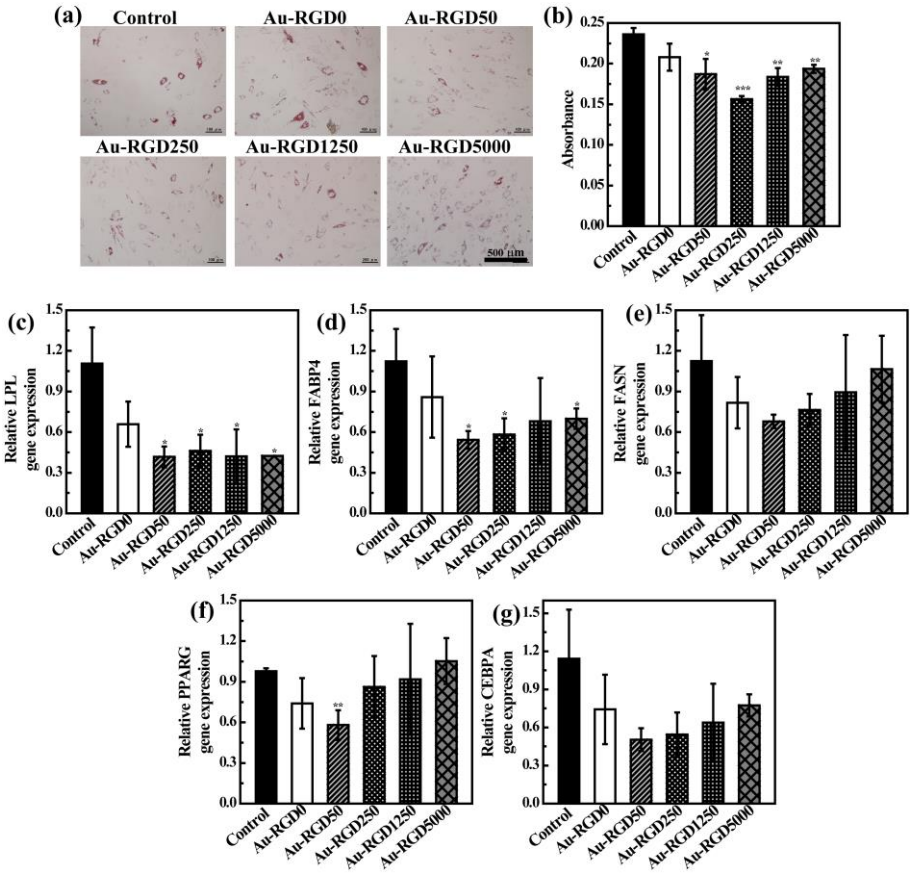

Figure 5.8 Oil Red O staining (a), quantitative oil droplets formation (b) and gene expression of LPL (c), FABP4 (d), FASN (e), PPARG (f) and CEBPA (g) in hMSCs after incubation with PBS (control) or the biomimetic AuNPs in adipogenic induction medium for 21 days.

As a whole, RGD motifs on the surface of biomimetic AuNPs had a positive influence on the adipogenic differentiation of hMSCs. But it is possible that this positive influence was weaker than the negative effects originated from the internalized AuNPs. Therefore the adipogenic differentiation activity of hMSCs treated with biomimetic AuNPs was not higher than that of the control cells. A previous work has shown that free RGD augmented the adipogenic differentiation of MSCs.[32] In another work, RGD-modified alginate hydrogels promoted adipogenesis of adipose-derived stromal cells (ASCs).[33] However, an opposite phenomenon has been reported in a recent work, where RGD-containing disintegrin inhibited adipogenesis of preadipocyte.[34] These researches indicated that RGD may induce inconsistent effects on adipogenesis in different systems. Our results indicated that the effect of RGD was dependent on its surface density. If surface density was high enough to overwhelm other inhibitive effects, RGD motifs could promote adipogenic differentiation of hMSCs.

Understanding the possible mechanism how the ECM mimetic AuNPs affected the multiple differentiation of stem cells is in urgent need. Different from the RGD on substrate surface or in the scaffolds, RGD ligands on the surface of NPs were movable and flexible when the NPs were uptaken by cells. Such a

culture system should be better to mimic the dynamic *in vivo* ECM microenvironment. Furthermore, the biomimetic AuNPs could function as multivalent ligands to form nanoclustering of receptor-ligand complexes.[35] A previous work has reported that RGD-modified polyamidoamin (PAMAM) was able to enhance formation of cell aggregation or spheroids probably through interacting with membrane integrin receptors of different cells.[36] The biomimetic AuNPs in this study should act as a "molecular glue" to bind massive cells together in the cell pellets. The enhanced cell-cell interaction has been found to be critical for chondrogenic differentiation progression and cartilage ECM production.[37] Meanwhile the formed nanoclustering of integrin-RGD complexes should play a pivotal role in triggering cellular signaling pathway. It has been reported that interaction between $\alpha_5\beta_1$ integrin and fibronectin potentially activated the internal signaling to induce the conversion of mesenchyme to chondroblasts.[38] Therefore, we speculated that the integrin binding and nanoclustering should be responsible for the activation of integrin signaling pathway to promote the chondrogenic differentiation of stem cells. Through the RGD-integrin bindings, RGD motifs with high density on the AuNP surface enhanced the cell-cell interactions and activated the integrin signaling pathway to promote the chondrogenic differentiation of hMSCs.

It is a reciprocal relationship between osteogenic differentiation and adipogenic differentiation, which is balanced by some factors in the cell culture.[39] Cytoskeleton structure and focal adhesion of hMSCs were reduced by the biomimetic AuNPs. The low focal adhesion and cytoskeletal tension were found to impair the osteogenic differentiation of stem cells.[22] Theefore, the cell surface RGD-integrin binding and subsequent cellular uptake led to reduced focal adhesion and actin fiber in the Au-RGD250, Au-RGD1250 and Au-RGD5000 NPs treated groups. The decrement in cytoskeletal tension resulted in inhibition on osteogenic differentiation while promotion on adipogenic differentiation of hMSCs.

The influence of RGD on osteogenic, adipogenic and chondrogenic differentiation of stem cells has been widely studied, but these works have been restricted to substrate surface and scaffolds/hydrogels and the RGD motifs were fixed, failing to well mimic the dynamic ECM microenvironment.[41, 42] This is the first time to mimic flexible and movable ECM in 3D microenvironment by using ligand-modified NPs and to investigate their influence on multiple differentiation of hMSCs. The biomimetic AuNPs were found to have a positive effect on chondrogenic differentiation while a negative effect on osteogenic differentiation of hMSCs. Their effect on MSC adipogenic differentiation was balanced by the internalized NPs and surface RGD density. This proof-of-concept study provided a new insight into the influence of ECM-cell interaction in the RGD-integrin formation on cell differentiation. Maybe future efforts should be made to fully understand the biological mechanism involved in the influence of biomimetic NPs on cell functions and cell fates, but our study should be useful in designing suitable nanoplatforms for various biomedical applications.

5.5 Conclusions

This work presented the preparation of ECM mimetic AuNPs with tunable RGD density and their influence on osteogenic, adipogenic and chondrogenic differentiation of hMSCs. RGD was conjugated onto AuNPs through PEG as a spacer and their surface density was well controlled. The biomimetic AuNPs had good biocompatibility in the studied concentration range and were internalized into the cells in a ligand

density-dependent manner. The biomimetic AuNPs promoted chondrogenic differentiation but inhibited osteogenic differentiation of hMSCs, especially for the Au-RGD1250 and Au-RGD5000 NPs. The influence of biomimetic AuNPs on MSC adipogenic differentiation was complicated that was dependent on the surface RGD density. RGD-mediated cell-cell interaction and integrin activation should be responsible for the promotive effects of biomimetic AuNPs on chondrogenic differentiation of hMSCs. These NPs affected the cytoskeletal tension of cells in 2D culture, which subsequently regulated the MSC osteogenic and adipogenic differentiation. Benefited from the finding in this present work, more and more useful nanoplatforms will be designed for different biomedical applications.

5.6 References

1. C. Frantz, K. M. Stewart and V. M. Weaver, *J Cell Sci*, 2010, 123, 4195-4200.
2. C. A. Buck and A. F. Horwitz, *Annu. Rev. Cell Biol.*, 1987, 3, 179-205.
3. M. Lutolf and J. Hubbell, *Nat. Biotechnol.*, 2005, 23, 47-55.
4. M. B. Rahmany and M. Van Dyke, *Acta Biomater.*, 2013, 9, 5431-5437.
5. T. Hoshiba, N. Kawazoe, T. Tateishi and G. Chen, *Adv. Mater.*, 2010, 22, 3042-3047.
6. L. Cai and S. C. Heilshorn, *Acta Biomater.*, 2014, 10, 1751-1760.
7. R. Cai, T. Nakamoto, N. Kawazoe and G. Chen, *Biomaterials*, 2015, 52, 199-207.
8. M. Goktas, G. Cinar, I. Orujalipoor, S. Ide, A. B. Tekinay and M. O. Guler, *Biomacromolecules*, 2015, 16, 1247-1258.
9. H. H. Yoon, S. H. Bhang, T. Kim, T. Yu, T. Hyeon and B. S. Kim, *Adv. Funct. Mater.*, 2014, 24, 6455-6464.
10. Z. Zhao, Z. Zhou, J. Bao, Z. Wang, J. Hu, X. Chi, K. Ni, R. Wang, X. Chen and Z. Chen, *Nat. Commun.*, 2013, 4, 2266.
11. J. Liu, W. Bu, L. Pan and J. Shi, *Angew. Chem. Int. Ed.*, 2013, 52, 4375-4379.
12. J. Shi, A. R. Votruba, O. C. Farokhzad and R. Langer, *Nano Lett.*, 2010, 10, 3223-3230.
13. A. M. Carmona-Ribeiro, *Int. J. Nanomed.*, 2010, 5, 249.
14. S. Desseaux and H.-A. Klok, *Biomaterials*, 2015, 44, 24-35.
15. X. Wang, C. Yan, K. Ye, Y. He, Z. Li and J. Ding, *Biomaterials*, 2013, 34, 2865-2874.
16. J. E. J. Li, N. Kawazoe and G. Chen, *Biomaterials*, 2015, 54, 226-236.
17. M. J. Akhtar, M. Ahamed, S. Kumar, M. Khan, J. Ahmad and S. A. Alrokayan, *Int J Nanomedicine*, 2012, 7, 845-857.
18. J. Li, J. Zhang, X. Wang, N. Kawazoe and G. Chen, *Nanoscale*, 2016, 8, 7992-8007.
19. M. Shevach, S. Fleischer, A. Shapira and T. Dvir, *Nano Lett.*, 2014, 14, 5792-5796.
20. X. Qian, X.-H. Peng, D. O. Ansari, Q. Yin-Goen, G. Z. Chen, D. M. Shin, L. Yang, A. N. Young, M. D. Wang and S. Nie, *Nat. Biotechnol.*, 2008, 26, 83-90.
21. D. Arosio, L. Manzoni, E. M. Araldi and C. Scolastico, *Bioconjugate Chem.*, 2011, 22, 664-672.
22. Y. Hou, K. Cai, J. Li, X. Chen, M. Lai, Y. Hu, Z. Luo, X. Ding and D. Xu, *Int. J. Nanomed.*, 2013, 8, 3619-3630.

23. K.-C. Hung, C.-S. Tseng, L.-G. Dai and S.-h. Hsu, *Biomaterials*, 2016, 83, 156-168.
24. J. Xu, J. Li, S. Lin, T. Wu, H. Huang, K. Zhang, Y. Sun, K. W. Yeung, G. Li and L. Bian, *Adv. Funct. Mater.*, 2016, 26, 2463-2472.
25. I. Sekiya, J. T. Vuoristo, B. L. Larson and D. J. Prockop, *Proc. Natl. Acad. Sci. U. S. A.*, 2002, 99, 4397-4402.
26. C. Chun, H. J. Lim, K.-Y. Hong, K.-H. Park and S.-C. Song, *Biomaterials*, 2009, 30, 6295-6308.
27. N. M. Moore, N. J. Lin, N. D. Gallant and M. L. Becker, *Acta Biomater.*, 2011, 7, 2091-2100.
28. F. Yang, C. G. Williams, D.-a. Wang, H. Lee, P. N. Manson and J. Elisseeff, *Biomaterials*, 2005, 26, 5991-5998.
29. A. Chompoosor, K. Saha, P. S. Ghosh, D. J. Macarthy, O. R. Miranda, Z. J. Zhu, K. F. Arcaro and V. M. Rotello, *Small*, 2010, 6, 2246-2249.
30. F. Atashi, A. Modarressi and M. S. Pepper, *Stem Cells Dev.*, 2015, 24, 1150-1163.
31. C. Yi, D. Liu, C.-C. Fong, J. Zhang and M. Yang, *ACS Nano*, 2010, 4, 6439-6448.
32. Q. Chen, P. Shou, L. Zhang, C. Xu, C. Zheng, Y. Han, W. Li, Y. Huang, X. Zhang and C. Shao, *Stem Cells*, 2014, 32, 327-337.
33. S. W. Kang, B. H. Cha, H. Park, K. S. Park, K. Y. Lee and S. H. Lee, *Macromol. Biosci.*, 2011, 11, 673-679.
34. Y.-T. Lin, C.-H. Tang, W.-J. Chuang, S.-M. Wang, T.-F. Huang and W.-M. Fu, *Biochem. Pharmacol.*, 2005, 70, 1469-1478.
35. W. Jiang, B. Y. Kim, J. T. Rutka and W. C. Chan, *Nat. Nanotechnol.*, 2008, 3, 145-150.
36. L.-Y. Jiang, B. Lv and Y. Luo, *Biomaterials*, 2013, 34, 2665-2673.
37. R. Tuli, S. Tuli, S. Nandi, X. Huang, P. A. Manner, W. J. Hozack, K. G. Danielson, D. J. Hall and R. S. Tuan, *J. Biol. Chem.*, 2003, 278, 41227-41236.
38. A. DeLise, L. Fischer and R. Tuan, *Osteoarthritis Cartilage*, 2000, 8, 309-334.
39. D. Liu, C. Yi, D. Zhang, J. Zhang and M. Yang, *ACS Nano*, 2010, 4, 2185-2195.
40. H. Qin, C. Zhu, Z. An, Y. Jiang, Y. Zhao, J. Wang, X. Liu, B. Hui, X. Zhang and Y. Wang, *Int. J. Nanomed.*, 2014, 9, 2469.
41. F.-Y. Cao, W.-N. Yin, J.-X. Fan, L. Tao, S.-Y. Qin, R.-X. Zhuo and X.-Z. Zhang, *ACS Appl. Mater. Interfaces*, 2015, 7, 6698-6705.
42. M. You, G. Peng, J. Li, P. Ma, Z. Wang, W. Shu, S. Peng and G.-Q. Chen, *Biomaterials*, 2011, 32, 2305-2313.

Chapter 6

Concluding remarks and future prospects

6.1 Concluding remarks

This research focused on the development of functional AuNPs with suitable properties for cancer therapy and tissue engineering. Firstly, star-shaped AuNPs were functionalized with BSA-FA conjugates (BSA-FA-AuNSs) for targeting photothermal therapy of cancer cells. Secondly, BSA-coated AuNPs with different sizes and shapes were synthesized to investigate their influence on cell viability, cell proliferation, cellular uptake and osteogenic differentiation of hMSCs. Furthermore, the influence of sub-10 nm AuNPs on cytotoxicity, osteogenic differentiation and adipogenic differentiation of hMSCs were explored. Finally, RGD peptides modified AuNPs with tunable surface ligand density were synthesized to mimic the ECM. The inducibility of these biomimetic AuNPs on multiple differentiation of hMSCs including chondrogenesis, osteogenesis and adipogenesis was evaluated.

Chapter 1 briefly introduces the background of this study. The potential applications of nanomaterials for biomedical applications were introduced. The interaction between nanomaterials and cells was also summarized. The advantages of AuNPs for biomedical applications and their representative candidates were reviewed. Development of functional AuNPs with suitable properties for different biomedical applications were motivated.

Chapter 2 describes the synthesis of BSA-FA-AuNSs as agents for targeting photothermal ablation of cervical cancer cells (HeLa). The BSA-FA-AuNSs were star-like with a mean size about 100 nm and had a strong absorption property in near-infrared (NIR) regions. Benefited from the surface coating, BSA-FA-AuNSs showed good dispersibility and colloidal stability in different medium. The temperature of particle solution increased rapidly under NIR laser irradiation, suggesting their good photothermal convention efficiency. The synthesized BSA-FA-AuNSs had good biocompatibility in the studied concentrations and high targeting specificity to FA receptors-overexpressed cancer cells, HeLa cells. In addition, the BSA-FA-AuNSs displayed a much better therapeutic efficiency to HeLa cells under the NIR

laser compared with BSA-AuNSs without FA modification. The BSA-FA-AuNSs should have a great potential as photothermal conversion agents for the receptor-mediated treatment of cancer cells.

Chapter 3 describes the synthesis of BSA-coated AuNPs with different shapes (Au nanospheres, Au nanostars and Au nanorods) and different diameters (40, 70 and 110 nm) and the investigation of their influence on osteogenic differentiation of hMSCs. Osteogenic differentiation of hMSCs was dependent on the size and shape of AuNPs. The sphere-40, sphere-70 and rod-70 significantly increased the alkaline phosphatase (ALP) activity, calcium deposition and osteogenic marker gene expression in hMSCs, while rod-40 reduced the ALP activity, calcium deposition and gene expression. Au nanostars (star-40, star-70 and star-110) and bigger AuNPs (sphere-110, star-110 and rod-110) showed negligible effects on osteogenic differentiation of hMSCs. The results suggested that the size and shape of NPs have obvious influence on MSC osteogenic differentiation, which will provide some useful information for the design of various NPs for different tissue engineering and biomedical applications.

Chapter 4 describes the preparation of methoxy-poly(ethylene glycol) coated sub-10 nm AuNPs with a size of 4 nm (Au4-*m*PEG NPs) and their influence on osteogenic and adipogenic differentiation of hMSCs with 40-nm counterparts (Au40-*m*PEG NPs) as a comparison. The influence of Au4-*m*PEG NPs and Au40-*m*PEG NPs on hMSC differentiation was opposite. Au4-*m*PEG NPs reduced the ALP activity, calcium deposition and osteogenic marker gene expression while increased the oil droplets formation and adipogenic marker gene expression in hMSCs. It is highly possible that Au4-*m*PEG NPs inhibited the osteogenic differentiation while promoted the adipogenic differentiation because they induced high ROS level without significantly affecting the mechanical properties. This study provides some insights on the influence of sub-10 nm AuNPs on stem cell differentiation and their applications for tissue engineering.

Chapter 5 describes the preparation of ECM mimetic AuNPs with tunable surface RGD density and their influence on chondrogenic, osteogenic and adipogenic differentiation of hMSCs. The biomimetic AuNPs had good biocompatibility without significantly affecting cell proliferation. The AuNPs were taken up by hMSC through integrin-mediated endocytosis. The biomimetic AuNPs were found to have positive influence on the chondrogenesis of hMSCs in 3D cell pellet culture. In addition, these AuNPs regulated the osteogenic and adipogenic differentiation of hMSCs through affecting the cytoskeletal tension. Overall, the results demonstrated that ECM mimetic AuNPs had a significant influence on the differentiation of hMSCs and this influence became more evident with increase of ligand density. The results should provide a strategy for fabricating biomimetic AuNPs to regulate cell differentiation, which holds great potentials in tissue engineering applications.

In conclusion, AuNPs with suitable size, shape and surface modification were synthesized and used for targeting photothermal therapy of cancer cells and stem cell differentiation. The properties and functions of AuNPs could be easily controlled according to different requirements. Targeting ligand surface modification was a good strategy to enhance the cellular uptake of star-shaped AuNPs into cancer cells and improve the therapeutic efficiency. In addition, AuNPs could well mimic the ECM and regulate the fates and differentiation of stem cells. The osteogenic, adipogenic and chondrogenic differentiation of hMSCs was

significantly affected by AuNPs with different properties including size, shape and surface ligand density, which may be because of the different cellular interactions between stem cells and AuNPs. Investigating the influence of NP properties on stem cell differentiation will help us to elucidate the roles of ECM on cell fates and functions. The insights of this study should inspire the design of nanomaterials with defined size, shape or surface chemistry for cancer therapy and tissue engineering.

6.2 Future prospects

Cancer has become a leading cause of death around the world, the early-stage diagnosis and therapy of cancer is a big challenge. Current therapies such as chemotherapy, radiation therapy and surgery usually have some disadvantages including side effects and tumor recurrence. Therefore, development of non-traditional approaches for cancer treatments is very important. Various AuNPs have showed great potential in cancer therapy, while their development and applications still need more and more improvements. Firstly, it is highly desirable to perform the cancer treatments under the guidance of molecular imaging for the accurate location of cancer tissues. Secondly, signal therapeutic model in general fails to achieve effective therapeutical effect, so multifunctional nanoplatforms based on AuNPs may be necessary for the combined treatments of cancers. Finally, to improve the therapeutical efficiency of cancer but reduce the side effects to normal tissues, more novel approaches for the modifications and functionalizations of AuNPs should also be further considered.

AuNPs have showed their great potential in regulating stem cell fates and their influence on multipotent differentiation of stem cells have been found to be different dependent on their properties, as shown in this study. More endeavors will be devoted to explore the molecular mechanism regarding the influence of nanomaterial size, shape and surface chemistry on stem cell differentiation. These findings will motivate us to fabricate novel nanomaterials for different applications of tissue repair. For example, loading drugs or genes in 40-nm AuNPs with suitable surface modifications for enhanced osteogenic differentiation of stem cells. However, increasing research works still should be proceeded to explore some unknown phenomenon. Firstly, how about the influence of other shaped nanomaterials on stem cell differentiation, such as rice-shaped, wire-shaped and cube-shaped nanomaterials. Secondly, the synergetic influence of nanomaterial size, shape and surface chemistry should be investigated to optimize the condition for tissue engineering. Finally, it is necessary to confirm the cell fates change and corresponding mechanisms after the AuNPs enter into the cell nucleus.

After evaluating the functions of AuNPs *in vitro*, it is possible to expand their applications in living animals. The prepared BSA-FA-AuNSs in this study may have a very high therapeutic efficiency for the ablation of xenografted tumor model *in vivo*. It is generally thought that AuNPs are biocompatible, while their potential menaces in hemolysis, immune response and genotoxicity after the intravenous injection into living body should be investigated before the final clinical applications. We all known that the injected nanomaterials often have a very high accumulation in the reticuloendothelial system (RES). For the cancer therapy, how to reduce these unwanted uptake but increase the accumulation into tumors is still a big

problem, and more endeavors should be made to engineer the nanomaterials. In addition, AuNPs bave been widely used for molecular imaging because of their unique optical properties, therefore it will be an excellent idea to use functional AuNPs for stem cell labeling and tracking *in vivo*. The stimulative influence of AuNPs on osteogenic differentiation of stem cells will enable their treatments of bone defects *in vivo*. The ECM mimetic AuNPs with RGD modifications promote the chondrogenic differentiation of stem cells, which will enable their applications for cartilage engineering after transplant. However, how to deliver and maintain the AuNPs in the defects is still a big difficulty that should be settled.

List of publications

[1] **Jingchao Li**, Rong Cai, Naoki Kawazoe and Guoping Chen. Facile preparation of albumin-stabilized gold nanostars for the targeted photothermal ablation of cancer cells. J. Mater. Chem. B 2015, 3: 5806-5814.

[2] **Jingchao Li**, Jia'En Jasmine Li, Jing Zhang, Xinlong Wang, Naoki Kawazoe and Guoping Chen. Gold nanoparticle size and shape influence on osteogenesis of mesenchymal stem cells. Nanoscale 2016, 8: 7992-8007.

[3] **Jingchao Li**, Ying Chen, Yingjun Yang, Naoki Kawazoe and Guoping Chen. Sub-10 nm gold nanoparticles promote adipogenesis and inhibit osteogenesis of mesenchymal stem cells. J. Mater. Chem. B 2017, 5: 1353-1362.

[4] Jing Zhang, **Jingchao Li**, Shangwu Chen, Naoki Kawazoe and Guoping Chen. Preparation of gelatin/Fe_3O_4 composite scaffolds for enhanced and repeateable cancer cell ablation. J. Mater. Chem. B 2016, 4: 5664-5672.

[5] Jing Zhang, **Jingchao Li**, Naoki Kawazoe and Guoping Chen. Composite scaffolds of gelatin and gold nanoparticles with tunable size and shape for photothermal cancer therapy. J. Mater. Chem. B 2017, 5, 245-253.

[6] Jianmin Yang, **Jingchao Li**, Xinlong Wang, Xiaomeng Li, Naoki Kawazoe and Guoping Chen. Single mammalian cell encapsulation by in situ polymerization. J. Mater. Chem. B 2016, 4: 7662-7668.

[7] Hongli Mao, **Jingchao Li**, Ida Dulińska-Molak, Naoki Kawazoe, Yoshihiko Takeda, Hiroaki Mamiya and Guoping Chen. Cellular effects of magnetic nanoparticles explored by atomic force microscopy. Biomater. Sci. 2015, 3, 1284-1290.

[8] Xinlong Wang, Xiaohong Hu, **Jingchao Li**, Adriana C. Mulero Russe, Naoki Kawazoe, Yingnan Yang and Guoping Chen. Influence of cell size on cellular uptake of gold nanoparticles. Biomater. Sci. 2016, 4, 970-978.

[9] **Jingchao Li**, Xiaomeng Li, Ying Chen, Jing Zhang, Naoki Kawazoe and Guoping Chen. Biomimetic gold nanoparticles with tunable RGD density regulate multipotent differentiation of human mesenchymal stem cells. Submitted.

Acknowledgements

At the end of my thesis, I would like to express the sincerest appreciations to all those who gave me selfless help during my PhD program.

I would like to be deeply grateful to my supervisor Prof. Guoping Chen for his valuable guidance on the research plan and generous concerns on my life in Japan. During my three years PhD program, Prof. Chen shares me his vast knowledge, skills and ideas in science, which helps me so much in the research. In the daily life, he usually gives me some generous advices and tells me how to deal with difficulties.

I would like to give my warm gratitude to Dr. Naoki Kawazoe. He helps me so much in arranging and assisting my research works. His modest character, hard-working spirit and friendly manner impressed me deeply.

I would also like to express my thanks to the thesis committee members: Prof. Hee Young Kim, Prof. Tetsushi Taguchi and Prof. Mitsuhiro Ebara for their precious comments, suggestions and supports.

I really appreciate the kind help form Mr. Toshiaki Takei and Mr. Makito Nakatsu. Their supports in characterization technique help me so much in the research works. I also appreciate the warm assistance from Mrs. Fusako Hidaka and Mrs. Akemi Tateno. Their great efforts make my life in Japan much easier and more enjoyable.

I also want to thank all the members in our group, Prof. Gang Wu, Prof. Shujun Dong, Dr. Tomoko Nakamoto, Dr. Jia'En Jasmine Li, Dr. Lingfeng Guo, Dr. Himansu S. Nanda, Dr. Hongli Mao, Dr. Rong Cai, Dr. Shangwu Chen, Dr. Xinlong Wang, Dr. Jianmin Yang, Ms. Jing Zhang, Ms. Xiaohong Hu, Ms. Jia Hui NG, Mr. Xiaomeng Li, Ms. Ying Chen, Ms. Nur Rofiqoh, Mr. Yingjun Yang and Ms. Xiuhui Wang. I appreciate their contribution and accompaniment in these three years in Japan.

I would like to give the acknowledgements to the financial support from the Doctoral Program in Materials Science and Engineering of Graduate School of Pure and Applied Science, National Institute for Materials Science and University of Tsukuba, Japan.

Finally, I must express my gratitude and love to my family. Their encouragement and support conduces to my meaningful and blissful life.

Thank all of you very much and I wish you have a very bright future.